In-Flight Nitrogen Oxide Measurements for Different Settings of a Lean Burn Engine

Luca Leon Stremming

Delft University of Technology

TU Delft

In-Flight Nitrogen Oxide Measurements for Different Settings of a Lean Burn Engine

by

Luca Leon Stremming

in partial fulfillment of the requirements for the degree of

Master of Science
in Aerospace Engineering

at the Delft University of Technology,
to be defended publicly on Monday February 26, 2024 at 09:00 AM.

Student number:	5513952	
Project Duration:	March, 2023 - January, 2024	
Thesis Committee:	Prof. dr. Volker Grewe,	TU Delft, DLR
	Prof. dr. Arvind Gangoli Rao,	TU Delft
	Dr. Feijia Yin,	TU Delft
	Dr. Tiziana Bräuer,	DLR

Cover: CFM LEAP-1A during emission measurements - adapted from internal source.

TU Delft

Preface

This master's thesis is written to obtain the degree Master of Science in Aerospace Engineering. Throughout my studies within the Flight Performance and Propulsion track at Delft University of Technology, I continuously gained interest in understanding aviation's complex impact on our environment. Therefore, I am extremely happy that I got the opportunity to actively contribute to this research field as a part of my graduation work at the German Aerospace Center. Performing in-flight nitrogen oxide measurements during two aircraft emission test campaigns in Europe and North America not only introduced me to the stunning world of airborne, experimental research, but also showed me how important cooperation between science and industry is to reduce climate effects of aviation. I am really grateful that with this thesis, I can add a little piece to a more sustainable future of air travel to enable later generations to explore the fascination of flying and to fall in love with aviation like I did.

During this research work, I had the chance to exchange ideas with wonderful colleagues at the German Aerospace Center. Especially, I would like to express my gratitude towards Tiziana, Theresa and Volker. It has been a pleasure to work together on this topic and without your guidance, this thesis would not have been possible. Finally, I would like to thank my family and friends for their continuous support during my master's program in Delft.

Luca Leon Stremming
Delft, February 2024

Abstract

Aviation is an important contributor to anthropogenic climate change. As indirect greenhouse gases, nitrogen oxides (NO_x = NO + NO_2) add to the Effective Radiative Forcing (ERF) induced by aircraft emissions. This work addresses a better understanding of emission mitigation by investigating dependencies between engine parameters and emitted nitrogen oxides as a part of the campaign VOLCAN. In-flight near field measurements are conducted using the DLR research aircraft Falcon, chasing an Airbus A321neo equipped with CFM LEAP-1A engines featuring lean combustion through staged fuel injection. Nitrogen oxide concentrations are measured applying the well-established chemiluminescence method. Emission indices are quantified for different fuels including Jet A-1, Sustainable Aviation Fuel (SAF) and two SAF blends with different levels of aromatics. Four combustor inlet temperature settings are tested and staged (lean) combustion is compared to unstaged (rich) combustion. Emissions are measured for two different but technically identical engines, deviating in terms of exhaust gas temperature margin. As expected, results indicate no significant differences in emitted nitrogen oxides for the investigated fuels. Measurements confirm that nitrogen oxide emission indices increase exponentially with combustor inlet temperature. Due to the forced nature of the analyzed rich burn mode, a reduction in nitrogen oxide emissions through lean combustion cannot be confirmed. Based on presented data, a relationship between engine degradation and nitrogen oxides is likely. Near field observations agree with well-established far field measurements and lead to lower uncertainties. Preliminary results of the ECO-Demonstrator campaign are in line with VOLCAN measurements. The performed research is a highly valuable contribution to extremely rare empirical in-flight emission data. Established nitrogen oxide dependencies support technical decision making to reduce aviation's climate impact.

Contents

List of Figures

List of Tables

Nomenclature

Abbreviations

Abbreviation	Definition
ATC	Air Traffic Control
CFD	Computational Fluid Dynamics
DLR	German Aerospace Center
EGTM	Exhaust Gas Temperature Margin
EI	Emission Index
ENG	Engine
ERF	Effective Radiative Forcing
FBN	Fuel Bound Nitrogen
GPT	Gas Phase Titration
HA	High Level of Mono-Aromatics
HEFA	Hydroprocessed Esters and Fatty Acids
HPC	High Pressure Compressor
HPT	High Pressure Turbine
ICAO	International Civil Aviation Organization
LA	Low Level of Mono-Aromatics
LPC	Low Pressure Compressor
LPT	Low Pressure Turbine
NASA	National Aeronautics and Space Administration
NMHC	Non-Methane Hydrocarbons
PAN	Peroxyacetyl Nitrate
RF	Radiative Forcing
RPK	Revenue Passenger Kilometers
RQL	Rich Quench Lean
SAF	Sustainable Aviation Fuel
SPK	Synthetic Paraffinic Kerosene
TAPS	Twin Annular Premixing Swirler
T3	Combustor Inlet Temperature
TRA	Temporary Reserved Airspace
VOLCAN	VOL avec Carburants Alternatifs Nouveaux
ZA	Zero Air

Symbols

Symbol	Definition	Unit
A	Plume Start Time	s
AFR	Air to Fuel Ratio	-
$AFR_{stoichiometric}$	Stoichiometric Air to Fuel Ratio	-
B	Plume End Time	s
CO_2	Measured Carbon Dioxide Concentration	ppm
$CO_{2,bgr}$	Interpolated Carbon Dioxide Background Concentration	ppm
ΔCO_2	Integrated Carbon Dioxide Concentration Enhancement	ppm s
$EGTM$	Exhaust Gas Temperature Margin	K
$EI(CO_2)$	Carbon Dioxide Emission Index	g CO_2 kg^{-1}
$EI(NO_x)$	Nitrogen Oxide Emission Index	g NO_2 kg^{-1}
$\Delta EI(NO_x)$	Nitrogen Oxide Emission Index compared to Reference Value	g NO_2 kg^{-1}
ERF	Effective Radiative Forcing	mW m^{-2}
$Error$	Error of individual Nitrogen Oxide Emission Indices	g NO_2 kg^{-1}
ΔFF	Fuel Flow compared to Reference Value	kg h^{-1}
FL	Flight Level	ft $(100ft)^{-1}$
k	Rate Coefficient	-
M	Mach Number	-
$M(C)$	Molar Mass of Carbon	g mol^{-1}
$M(CO_2)$	Molar Mass of Carbon Dioxide	g mol^{-1}
$M(H)$	Molar Mass of Hydrogen	g mol^{-1}
$M(NO_2)$	Molar Mass of Nitrogen Dioxide	g mol^{-1}
m	Sensitivity	Hz ppb^{-1}
m_{air}	Air Mass	kg
m_{fuel}	Fuel Mass	kg
n	Number of Plume Encounters or Samples	-
$NO_{y,bgr}$	Interpolated Nitrogen Oxide Background Concentration	ppb
$NO_{y,final}$	Measured Nitrogen Oxide Concentration corrected for Dilution	ppb
$NO_{y,measured}$	Measured Nitrogen Oxide Concentration	ppb
ΔNO_y	Integrated Nitrogen Oxide Concentration Enhancement	ppb s
p	Static Pressure	Pa
p_T	Probability Value T-test	-
p_{MW}	Probability Value Mann-Whitney U Rank Test	-
$Q_{dilution}$	Dilution Volume Flow	l min^{-1}
Q_{total}	Total Volume Flow	l min^{-1}
R	Ideal Gas Constant	J K^{-1} mol^{-1}
R^2	Coefficient of Determination	-
RPK	Revenue Passenger Kilometers	km
S_D	Dark Current Signal	Hz
S_{in}	Chemical Interference Signal	Hz

Symbol	Definition	Unit
S_{main}	Main Chamber Signal	Hz
S_{NO}	Nitrogen Monoxide Signal	Hz
S_{pre}	Pre Chamber Signal	Hz
s	Standard Deviation	g CO_2 kg^{-1}
T	Static Temperature	K
t	Time	s
t	Test Statistic T-test	-
TAT	Total Air Temperature	K
$T3$	Combustor Inlet Temperature	K
$\Delta T3$	Combustor Inlet Temperature compared to Reference Value	K
U	Test Statistic Mann-Whitney U Rank Test	-
V_m	Molar Volume	m^3 mol^{-1}
α	Significance Level	-
α	Hydrogen to Carbon Molar Ratio	-
η_C	Converter Efficiency	-
ϕ	Equivalence Ratio	-

1 Introduction

1.1. Motivation

Aviation is a major contributor to anthropogenic climate change (Lee et al., 2021). Through the combustion of hydrocarbons (C_xH_y) several species are emitted by aircraft engines, leading to direct or indirect climate effects. Figure 1.1 summarizes the current understanding of aviation's impact on global warming in terms of Effective Radiative Forcing (ERF) for both carbon dioxide (CO_2) effects and non-CO_2 effects for the year 2018, considering emissions since 1940. ERF is a climate metric expressing the change in the earth's energy balance due to externally imposed changes in mW m^{-2} (Stocker et al., 2014). Positive values indicate warming, while negative contributions describe a cooling effect.

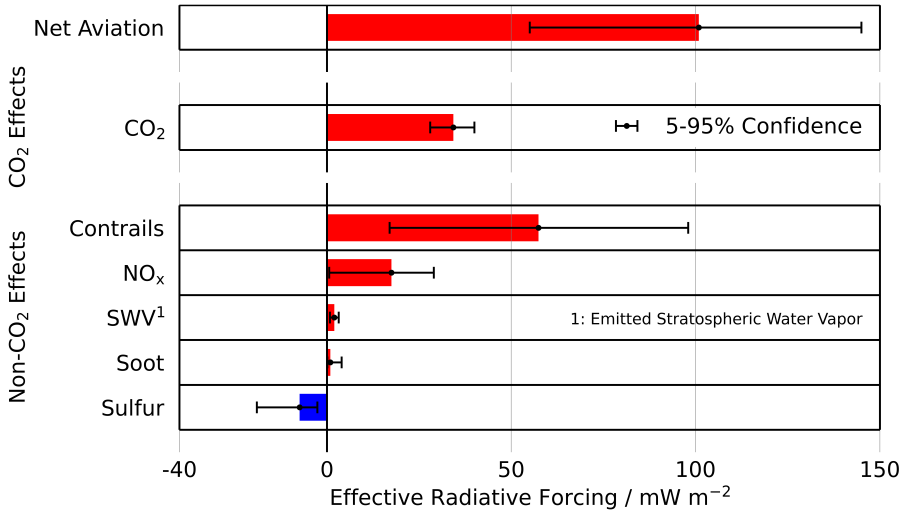

Figure 1.1: CO_2 and non-CO_2-induced ERF of aviation from 1940 to 2018 - adapted from Lee et al. (2021).

The data presented by Lee et al. (2021) illustrates that next to commonly discussed CO_2, a number of additional emissions lead to a net change in ERF. Contributions arise from contrails, nitrogen oxides, water vapor emitted into the stratosphere, soot and sulfur. Nitrogen oxides, referred to as NO_x, assuming that the main components are nitrogen monoxide (NO) and nitrogen dioxide (NO_2), are responsible for a major part. According to the estimate of 17.5 mW m^{-2}, NO_x is responsible for 17.4% of aviation-induced ERF and for 0.64% of the total anthropogenic ERF over the industrial era, when comparing to the assessment by Forster et al. (2023) for the period from 1750 to 2019. As indirect greenhouse gases, NO_x induce changes in the atmosphere leading to both warming and cooling. Warming is caused by an increase in short-term ozone production, while cooling results from methane depletion, as well as from reductions in log-term ozone and stratospheric water vapor formation. Current research on NO_x-caused ERF is subject to large uncertainties. While some studies are proposing a net

adverse contribution to global warming (Holmes, Tang and Prather, 2011), the current research by Lee et al. (2021) shows that a significant positive contribution is most likely. To increase the level of confidence, further research is required to enable a more accurate quantification of the climate impact of aviation's NO_x emissions.
Experimental measurements of aircraft emissions help to reduce uncertainties in the assumed climate effect of aviation-induced NO_x emissions (Schulte and Schlager, 1996). Emission inventories are an important input for climate models. Their determination requires an assumption for average emissions of the global aircraft fleet. Prediction methods solve this problem by quantifying aircraft emissions at cruise altitude based on published values for ground conditions. In-flight measurements (e.g., Schulte and Schlager, 1996; Schulte et al., 1997) allow for model validation and hence, an improved prediction of aviation-caused NO_x effects.
Confirming dependencies between engine settings and emissions at cruise conditions contributes to the reduction of uncertainties in future emission scenarios incorporating future technology. Saluja (2021) developed a method to investigate the sensitivity of aviation's climate impact in terms of near-surface temperature change to certain engine design parameters. Emissions for different design choices are determined using a simulation program for gas turbines in combination with prediction methods to derive respective emission inventories as an input for a climate model. An assessment of engine parameter changes' effect on aviation's climate impact is enabled. However, there is no publication yet, validating dependencies based on in situ measurements at cruise conditions. The research presented here addresses this gap by performing experimental measurements to confirm correlations between engine operating conditions and nitrogen oxide emissions. It is aimed to contribute to the simplification of design choices to meet future emission requirements set by the International Civil Aviation Organization (ICAO), reducing aviation's climate impact.

1.2. Objectives

This research intends to quantify differences in nitrogen oxide emissions for a variety of engine settings. Expected dependencies between emitted nitrogen oxides and several engine parameters are reported in literature (e.g., Lipfert, 1972; Gleason and Martone, 1980; Lukachko and Waitz, 1997; Foust et al., 2012). The presented study assesses these correlations based on in situ emission measurements. As a part of the test campaign VOL avec Carburants Alternatifs Nouveaux (VOLCAN) in March 2023, chase flights are performed using the airborne measurement platform Falcon of the German Aerospace Center (DLR). Investigated is a CFM LEAP-1A engine, powering an Airbus A321neo. Measurements are conducted in the so-called near field with plume ages below 1 s.

Two research questions are formulated to fulfill the objectives. The first question focuses on experimentally determined correlations between engine parameters and NO_x emissions:

1. Do in situ near field measurements confirm expected dependencies between engine parameters and NO_x emissions?

This research addresses four aspects, as stated in the following subquestions:

1.1 Does a change from Jet A-1 to Sustainable Aviation Fuel affect NO_x emissions?
1.2 Do measured NO_x emissions increase exponentially with combustor inlet temperature?
1.3 Does lean combustion reduce NO_x emissions?
1.4 Does engine degradation affect NO_x emissions?

The first subquestion investigates effects of a change in fuel type on nitrogen oxides. Three different blends of Hydroprocessed Esters and Fatty Acids (HEFA) Synthetic Paraffinic Kerosene (SPK) are compared with conventionally used Jet A-1: 100 % HEFA SPK without mono-aromatics, a HEFA SPK blend with a low level of mono-aromatics (HEFA SPK+LA) and a HEFA SPK blend with a high level of mono-aromatics (HEFA SPK+HA). According to Teoh et al. (2022), these so-called Sustainable Aviation Fuels (SAFs) are of fundamental interest to rapidly reduce aviation's climate impact. Hence, an experimental confirmation of the fuels' effect on pollutants introduced in Figure 1.1 is of high relevance.
The impact of combustor inlet temperature T3 on nitrogen oxide formation is addressed by the second subquestion. According to previous research, an exponential behavior is expected (e.g., Lipfert, 1972). As this behavior is not yet confirmed by in-flight measurements, this study aims to establish a correlation based on experimental data collected during conducted emission test flights.
Nitrogen oxide mitigation through lean combustion is investigated by the third subquestion. The assessed LEAP-1A engine aims to reduce NO_x emissions through a lean burn mode, being active in a dedicated part of it's operation envelope. For the first time, it is aimed to confirm the decrease in emissions by in situ measurements for two distinguished combustion modes at cruise conditions.
The effect of engine degradation on NO_x formation is analyzed by the fourth subquestion. To establish emission inventories, average emission indices are determined and assumed to be valid for the worldwide aircraft fleet. To reduce uncertainties, it is important to quantify how aging affects emissions to estimate possible variations among engines of the same type. Thus, both engines of the chased source aircraft, deviating in terms of their exhaust gas temperature margin, are compared.

The second research question evaluates obtained near field results:

2. Do near field measurements agree with observations in the far field?

Currently, there is no publicly available research analyzing nitrogen oxide emissions based on near field measurements. To evaluate conducted near field analyses, a comparison with well-established far field measurements is performed. As reflected in the formulated subquestions, data is collected during two distinguished campaigns:

2.1 Do emission indices derived from near and far field measurements during the VOLCAN campaign agree?

2.2 Are NO_x dependencies observed during VOLCAN confirmed by far field emission measurements during the ECO-Demonstrator campaign?

The first subquestion compares near and far field measurements obtained during VOLCAN. It is aimed to assess if results of the two setups agree. In addition, it is analyzed if near field measurements lead to expected reductions in uncertainties.
The second subquestion addresses far field measurements conducted during the campaign ECO-Demonstrator in October 2023. Emissions of a CFM LEAP-1B engine, powering a Boeing 737-10, are tested using the research aircraft DC-8 of the National Aeronautics and Space Administration (NASA). It is aimed to assess whether dependencies between NO_x emissions and engine parameters derived from VOLCAN near field measurements can be confirmed.

The following report is divided into four chapters. Chapter 2 summarizes relevant background information, focusing on effects of aviation-caused nitrogen oxide emissions and

their formation as a by-product of combustion. The conducted measurement flights and the applied data analysis procedure are introduced in Chapter 3. Chapter 4 presents and discusses obtained results. Conclusions regarding the research questions are provided in Chapter 5 together with recommendations for future work.

2
Background

This chapter provides scientific background information relevant to this work. It is divided into two sections. Section 2.1 summarizes current research on aviation-induced nitrogen oxide effects on our climate. Section 2.2 covers gas turbine combustion, outlining formation mechanisms of nitrogen oxides and explaining engine parameter dependencies. Selected mitigation technologies are introduced.

2.1. Climate Effects of Aviation's Nitrogen Oxide Emissions

This section focuses on climate effects induced by aviation's nitrogen oxide emissions. Subsection 2.1.1 summarizes the current understanding in terms of ERF. Underlying atmospheric chemistry is outlined in Subsection 2.1.2.

2.1.1. Effective Radiative Forcing

The effects of nitrogen oxides emitted by aviation on our global climate are complex (Lee et al., 2021). As NO_x are indirect greenhouse gases, the interaction with other species lead to the caused change in the earth's radiation balance. Positive contributions (warming) and negative contributions (cooling) are distinguished. While a short-term increase in the production of the greenhouse gas ozone (O_3) causes positive RF, depletion of methane (CH_4), a decrease in the production rate of long-term O_3 and a decrease in Stratospheric Water vapor production lead to a negative impact, since the concentration of these greenhouse gases is reduced accordingly. Holmes, Tang and Prather (2011) claim that a strong correlation exists between the contributing effects.

Figure 2.1 presents the ERF resulting from the respective NO_x effects for the years 2000 to 2018, published by Lee et al. (2021). The indicated net effects and their uncertainties are obtained using a Monte Carlo sampling method. The shown data covers a variety of models, as 20 studies are considered. Since models differ especially in their way of treating long-term effects, several assumptions are applied.

It is shown that the net ERF of NO_x emitted by aviation almost constantly increased between the years 2000 and 2018 from 12.2 mW m^{-2} to 17.5 mW m^{-2}. As mentioned in the introduction, for 2018 the value makes up for about 17.4% of the ERF caused by global aviation and for about 0.64% of the total anthropogenic ERF. The development reflects the strong increase in Revenue Passenger Kilometers (RPK) in the same period from $3.2 \cdot 10^{12}$ km $\cdot$ yr^{-1} to $8.3 \cdot 10^{12}$ km $\cdot$ yr^{-1}. This increase involves a rising global fuel consumption from 217 Tg to 327 Tg within the same period. However, the development of NO_x emissions shows that the amount of consumed fuel is not the only factor determining how much NO_x is emitted, since the mass of NO_x released to the atmosphere increases disproportionately with fuel. The reason is that NO_x emissions depend on the engine's load condition, additionally influenced by the internal combustion process (Deidewig, Doepelheuer and Lecht, 1996). Dependencies between engine parameters and NO_x emissions are introduced in Subsection 2.2.2.

It is expected that the presented trend of the increasing warming effect of aviation-caused

NO_x emissions continues. According to Airlines for America (2023), RPKs are again increasing since the drop caused by the Covid pandemic in 2020. No major propulsion technology breakthroughs aiming to reduce NO_x emissions entered service since 2018 apart from the continuous modernization of the worldwide aircraft fleet. Hence, rising fuel consumption along with rising NO_x emissions are expected in the near future, resulting in a progressing shift in the earth's radiation balance due to aviation-caused NO_x.

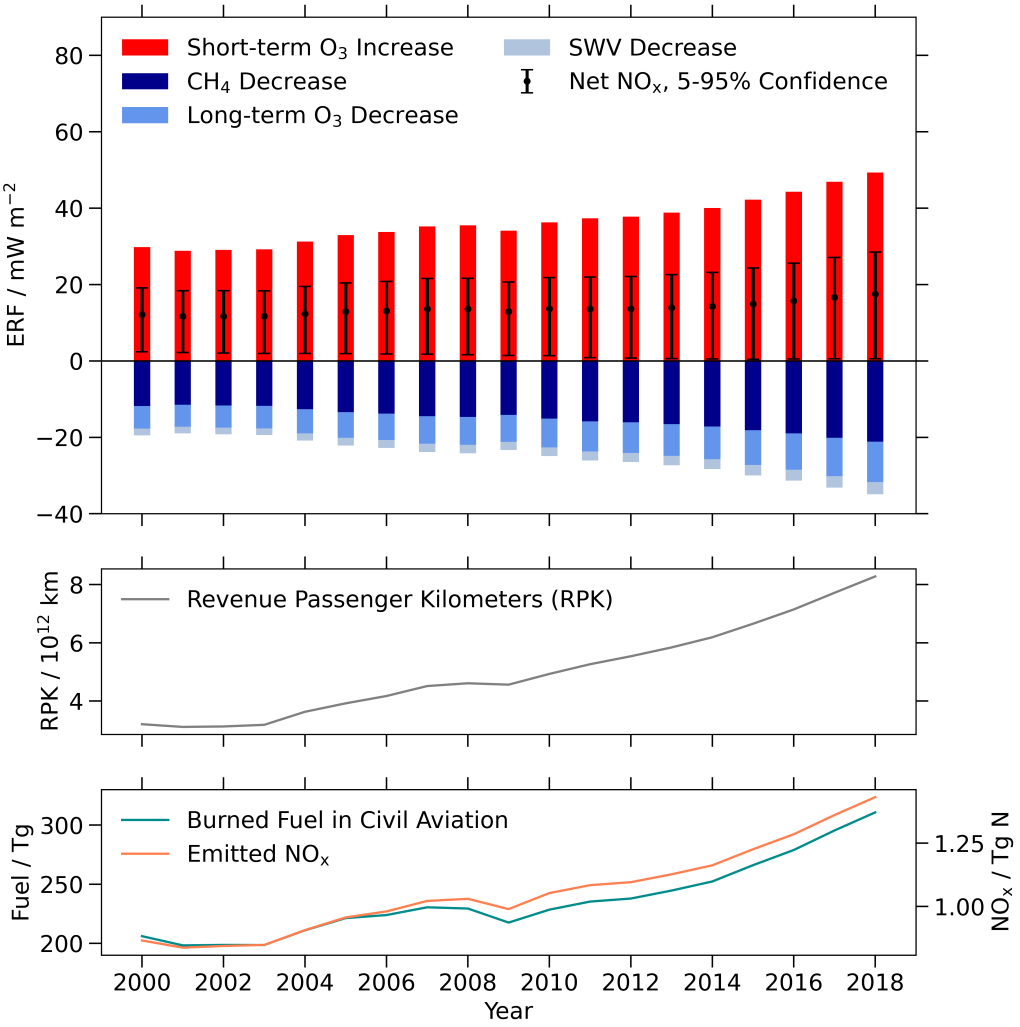

Figure 2.1: ERF of effects induced by aviation's NO_x emissions from 2000 to 2018 and related parameters, including revenue passenger kilometers *RPK*, burned fuel and emitted nitrogen oxides - adapted from Lee et al. (2021).

The work by Pitari et al. (2017) shows that additional effects not directly indicated in Figure 2.1 exist. The study investigates the effect of nitrate-, sulfur- and organic aerosol formation due to NO_x emissions. Aerosols can interact with radiation and clouds, affecting radiative forcing. However, uncertainties of NO_x-induced aerosol effects are comparably high (Lee et al., 2021).

Depending on the objective, other metrics might be more suitable than radiative forcing as illustrated by Grewe and Stenke (2008). The linear response model AirClim is applied for different emission scenarios. Results are presented in terms of both radiative forcing and near-surface temperature change. Subject to the scientific question, different results can be obtained for the metrics. Hence, a careful choice is required. Grewe and Dahlmann (2015) highlight that a precise formulation of the research question is essential for choosing the right

metric and to avoid ambiguity.

2.1.2. Atmospheric Chemistry

This subsection outlines the atmospheric processes leading to the previously introduced indirect effects of nitrogen oxide emissions.

Short-Term Ozone Increase

Increased nitrogen oxide concentrations due to aircraft emissions result in a short-term increase in ozone production within the troposphere (Penner, 1999). In general the production of ozone in the troposphere depends on the concentrations of nitrogen oxides (NO + NO_2), hydroxyl (OH) and hydroperoxyl (HO_2), as the simplified process in Figure 2.2 illustrates.

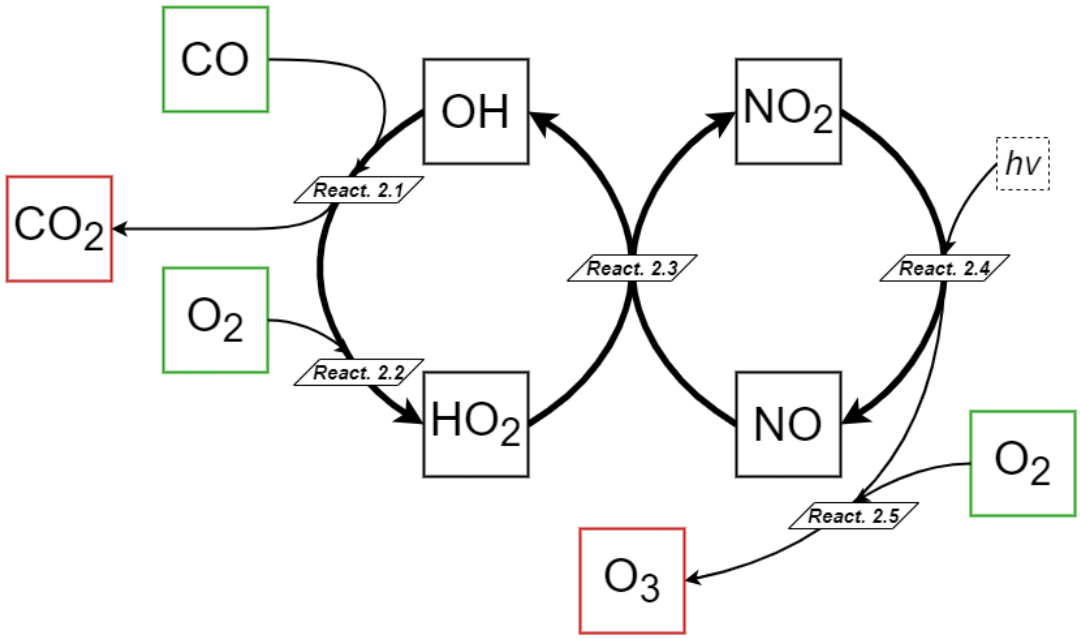

Figure 2.2: Simplified process of ozone production - adapted from Grewe (2009).

Reaction 2.1 to Reaction 2.6, described in the following, are taken from Fishman and Crutzen (1978): Carbon monoxide reacts with hydroxyl, forming carbon dioxide and atomic hydrogen according to Reaction 2.1. HO_2 is formed following Reaction 2.2, where M represents a gaseous third body. HO_2 reacts with NO, resulting in NO_2 and OH as stated in Reaction 2.3. The photolysis of NO_2 leads to NO and atomic oxygen as Reaction 2.4 indicates. Atomic oxygen and an oxygen molecule produce ozone according to Reaction 2.5. Net, as shown in Reaction 2.6, CO and two O_2 molecules (marked in green) result in CO_2 and O_3 (marked in red). According to Fishman and Crutzen (1978), also methane or Non-Methane Hydrocarbons (NMHC) can serve as an input for the ozone production within the troposphere, replacing carbon monoxide. However, in the troposphere the reaction path via CO is most likely to occur, depending on local background concentrations and reaction rates.

$$OH + CO \rightarrow H + CO_2 \tag{2.1}$$

$$H + O_2 + M \rightarrow HO_2 + M \tag{2.2}$$

$$NO + HO_2 \rightarrow NO_2 + OH \tag{2.3}$$

$$NO_2 + hv \rightarrow NO + O \tag{2.4}$$

$$O + O_2 + M \rightarrow O_3 + M \tag{2.5}$$

$$\text{Net} : CO + 2O_2 \rightarrow CO_2 + O_3 \tag{2.6}$$

Local changes in the NO_x concentration due to emissions shift the balance between species and hence, lead to a higher O_3 production rate, increasing radiative forcing (Fishman, Solomon and Crutzen, 1979; Isaksen and HOV, 1987). If the NO concentration rises, the rate of Reaction 2.3 increases. Consequently, the ratio between HO_2 and OH is shifted towards OH. As a result, more CO, CH_4 and NMHC are oxidized, increasing the ozone production rate following the reaction path introduced above. As ozone is an important greenhouse gas, contributing about 5 % to the background greenhouse effect as stated by Grewe (2009), a warming effect as described in Subsection 2.1.1 is obtained.
Depletion of ozone limits its lifetime within the troposphere to about 1-2 months in summer (Fishman and Crutzen, 1978). Within the troposphere, ozone is destroyed photochemically following Reaction 2.7. This reaction appears in pair with the hydroxyl-producing Reaction 2.8. An additional path of ozone depletion is Reaction 2.9. Grooß, Brühl and Peter (1998) also state that a reduction in ozone concentration occurs via Reaction 2.10. However, obtained OH through ozone depletion might again lead to ozone production according to the mechanism explained above.

$$O_3 + hv \rightarrow O_2 + O^* \tag{2.7}$$

$$O^* + H_2O \rightarrow 2OH \tag{2.8}$$

$$O_3 + HO_2 \rightarrow OH + 2O_2 \tag{2.9}$$

$$O_3 + OH \rightarrow HO_2 + O_2 \tag{2.10}$$

An increase in the local NO_x concentration must not necessarily lead to a higher ozone production (Grooß, Brühl and Peter, 1998). The background NO_x concentration is an important ambient factor, influencing the effect of NO_x emissions as Figure 2.3 illustrates. For very low NO_x background concentrations, when the ratio between NO and O_3 is very low, Reaction 2.9 competes against Reaction 2.3. Hence, ozone is depleted, and the effective production is slowed down. With rising background concentrations the increment in ozone formation due to additional NO_x increases until a maximum is reached. Beyond this point NO_2 is reacting with OH or HO_2 according to Reaction 2.11 and Reaction 2.12. The production of ozone and the lifetime of nitrogen oxides are reduced. Obtained HNO_3 can be washed out (Grewe, 2009). Also, a reaction of nitrogen oxides with hydrocarbons to Peroxyacetyl Nitrate (PAN) is possible (I. Köhler, 1997). In general, the photochemical oxidant production in Reaction 2.4 is not linear dependent on precursor concentration and UV radiation (Stevenson and Derwent, 2009).

However, a linear relation between aircraft induced changes in NO_x and O_3 integrated over the troposphere of the northern hemisphere and total aviation NO_x emissions is found by Grewe et al. (1999).

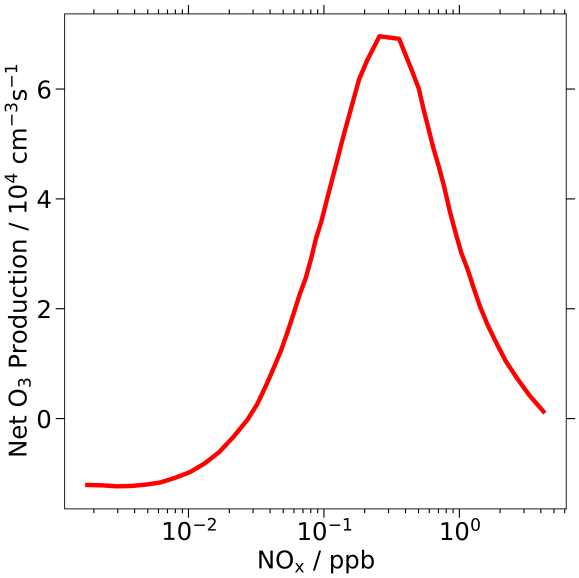

Figure 2.3: O_3 production with NO_x background concentration - adapted from Grooß, Brühl and Peter (1998).

$$NO_2 + OH + M \rightarrow HNO_3 + M \tag{2.11}$$

$$NO_2 + HO_2 + M \rightarrow HNO_4 + M \tag{2.12}$$

Methane Depletion

Such as the concentration of ozone, also the concentration of methane is sensitive to changes in NO_x (Fuglestvedt, 1999). The main sink of methane is stated in Reaction 2.13.

$$CH_4 + OH \rightarrow CH_3 + H_2O \tag{2.13}$$

As Reaction 2.3 indicates, NO_x emissions result in an increased concentration of hydroxyl. Thus, the sink of methane is fed, and its lifetime is reduced. Since CH_4 is a greenhouse gas, the reduction in its concentration reduces radiative forcing, contributing negatively to ERF (Berntsen et al., 2005). While the lifetime of methane is 8.9 years (Prinn et al., 1995), the concentration changes have a lifetime of about 12 years (Forster et al., 2007). According to Lee et al. (2009), a possible way to express the coupling between the depletion of methane and the short-term ozone increase in models is to scale changes in methane-induced RF with changes in ozone-induced RF, ignoring non-linearities.

Long-Term Ozone Decrease

Emissions of nitrogen oxides lead to a decrease in the production of long-term ozone (Stevenson and Derwent, 2009). As introduced before, the short-term O_3 production rate increases due to emitted NO_x along with a shift of the ratio between HO_2 and OH towards OH. If methane is

oxidized through OH following Reaction 2.13, the ratio shifts back towards HO_2, considering Reaction 2.14 to Reaction 2.17, being taken from Grooß, Brühl and Peter (1998). Therefore, a reduction in the lifetime of methane due to emitted nitrogen oxides lowers the production of ozone. The expression long-term ozone is used, since the decrease in production rate has a long lifetime, being coupled with methane depletion.

$$CH_4 + OH \rightarrow CH_3 + H_2O \tag{2.14}$$

$$CH_3 + O_2 + M \rightarrow CH_3O_2 + M \tag{2.15}$$

$$CH_3O_2 + NO \rightarrow CH_3O + NO_2 \tag{2.16}$$

$$CH_3O + O_2 \rightarrow CH_2O + HO_2 \tag{2.17}$$

Stratospheric Water Vapor Decrease

Depletion of methane leads to a reduction in stratospheric water vapor (Nicolet, 1964). As a precursor, the concentration of methane affects the production of stratospheric water vapor. Atomic oxygen obtained through photochemistry leads to oxidation of methane, as stated in Reaction 2.18. Consequently, H_2O is formed. This production of stratospheric water is dependent on the methane exchange between troposphere and stratosphere, resulting from turbulence. Thus, if less methane is available due to depletion, less methane can be transported into the stratosphere and the production of H_2O within the stratosphere is slowed down.

$$CH_4 + O \rightarrow CH_2 + H_2O \tag{2.18}$$

Emission Altitude Dependencies

Ozone production is most efficient at typical cruise altitudes of subsonic aircraft (Penner, 1999). In the upper troposphere and lower stratosphere the background concentrations of NO_x and HO_x are relatively low. In addition, the NO to NO_2 ratio is high. These factors promote a high increase in ozone production due to nitrogen oxide emissions.

Decreasing cruise altitude leads to lower NO_x effects through a decrease in residence time of O_3 precursors (Grewe et al., 2002; Frömming et al., 2012). The work by Grewe et al. (2002) compares the increase in ozone production due to aircraft NO_x emissions for a base case and a case with a 1 km lower cruise altitude, applying the coupled climate-chemistry model E39/C. A for increased fuel consumption corrected reduction of about 10% in ozone production is reported for decreased flight level operation. Frömming et al. (2012) additionally consider water vapor, contrails, methane and carbon dioxide emissions for trading-off the effects for changes in cruise altitude. For lower altitudes decreasing non-CO_2 effects dominate compared to increasing CO_2 effects. However, accounting for different time frames shows that increasing CO_2 effects remain for a significantly longer time than relatively short-living non-CO_2 effects. This dependency must be considered when choosing mitigation strategies. For aiming a reduction in non-CO_2 effects, aerodynamic design for lower cruise altitudes is suggested.

The forcing of ozone produced due to emitted oxides of nitrogen is sensitive to altitude (Dahlmann, 2012). The temperature difference between the absorption layer and the ground is

an influencing factor. Hence, ozone's forcing is increasing accordingly towards the poles and with height. Additionally, its background concentration affects the forcing of concentration changes due to emissions.
Grewe and Stenke, 2008 show that differences between NO_x effects of subsonic and supersonic aircraft exist. Due to changing background concentrations, there is a turning point within the stratosphere at which NO_x emissions lead to O_3 depletion instead of increasing O_3 production rates. As UV radiation is increased as a result of ozone depletion, more hydroxyl is produced and an increase in methane depletion is obtained. According to Penner (1999), the depletion of stratospheric ozone due to nitrogen oxide emissions results, among others, from Reaction 2.19 to Reaction 2.21. This catalytic depletion through NO_x is enabled due to the high background concentration of O_3 along with the low pressure at these altitudes.

$$O_3 + hv \rightarrow O_2 + O \tag{2.19}$$

$$O + NO_2 \rightarrow NO + O_2 \tag{2.20}$$

$$NO + O_3 \rightarrow NO_2 + O_2 \tag{2.21}$$

Latitude, Longitude and Seasonal Dependencies
The latitude of the NO_x emission location influences their effect (M. O. Köhler et al., 2013; Grewe and Stenke, 2008). It is observed that at lower latitudes nitrogen oxide emissions cause stronger effects on ozone production and methane depletion rates than at higher latitudes. According to Grewe and Stenke (2008), the strongest effect of ozone in terms of near-surface temperature change is observed for emissions in the upper tropical troposphere. The impact of methane concentration changes is highest in the middle tropical troposphere. The southern hemisphere is more sensitive to NO_x emissions, as the background concentration is lower than in the northern hemisphere (M. O. Köhler et al., 2013).
Photochemistry varies throughout the year, leading to seasonal changes in NO_x effects (Stevenson, 2004). For instance, in the northern hemisphere, the largest change in ozone concentration is obtained for NO_x emissions in October due to its longer lifetime in the following months. As a consequence of the reduced lifetime, the smallest ozone increase is obtained for NO_x emissions in July. Nevertheless, the change in radiative forcing due to an ozone increment is largest in April and smallest in January. Methane anomalies are highest in July and lowest in October, depending on changes in hydroxyl concentrations. OH concentrations are influenced by sunlight, as well as by changes in NO_x and O_3 concentrations. The net radiative forcing due to NO_x emissions can change between positive and negative throughout the year.

2.2. Combustion and Nitrogen Oxide Emissions

This section focuses on nitrogen oxides as a product of combustion. After providing an overview on gas turbine emissions, Subsection 2.2.1 outlines distinguished nitrogen oxide formation paths and Subsection 2.2.2 discusses dependencies between nitrogen oxide emissions and engine parameters. Mitigation techniques relevant to this work are presented in Subsection 2.2.3.

A turbofan engine consists of several components. Air enters the engine at the inlet. Behind the fan within the core engine, air is compressed by the Low Pressure Compressor (LPC) and the High Pressure Compressor (HPC). Compressed air is directed into the combustor. Hydrocarbons are injected and the mixture ignites. Obtained combustion products propel both the High Pressure Turbine (HPT) and the Low Pressure Turbine (LPT). HPT and LPT in turn drive Fan, LPC and HPC by the means of shafts. Behind the duct, the exhaust gases are accelerated through the nozzle and emitted into the ambient atmosphere.
Products of complete combustion and combustion by-products are distinguished, as shown in Figure 2.4. According to Saravanamuttoo et al. (2017), complete combustion is taking place following Reaction 2.22. All carbon and all hydrogen of the injected fuel react with oxygen to CO_2 and H_2O respectively. Both are greenhouse gases directly contributing to the ERF of aviation.

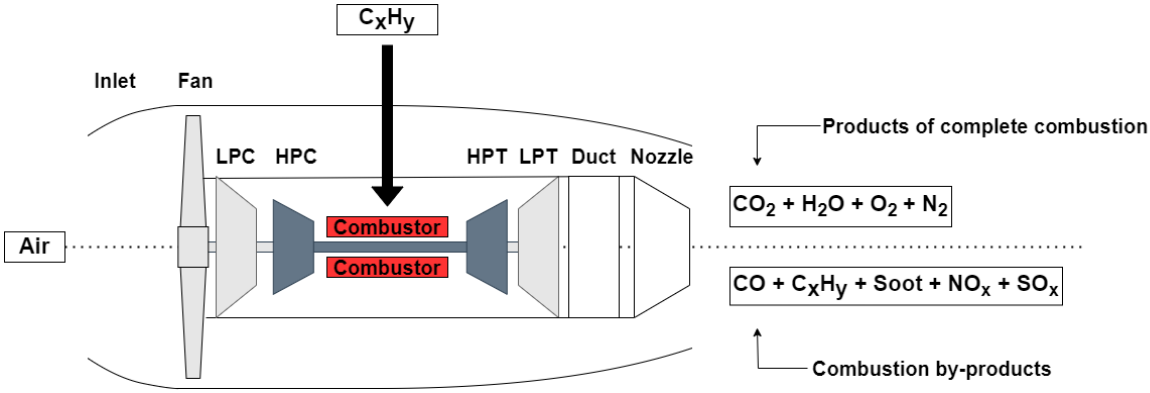

Figure 2.4: Combustion products of a gas turbine - adapted from Wuebbles, Gupta and Ko (2007).

In addition to products of complete combustion, combustion by-products are obtained (Lefebvre and Ballal, 2010). Carbon monoxide (CO), soot and unburned hydrocarbons (C_xH_y) are obtained due to incomplete combustion. Fuel impurities cause the formation of sulfur oxides (SO_x) and NO_x. However, the major part of emitted NO_x is produced due to high temperatures. While emitted CO_2 and H_2O scale with the amount of consumed fuel, the additional combustion by-products are influenced by a number of different engine parameters. Due to the importance of NO_x to this work, the underlying principles of their formation and driving parameters are introduced in more detail in Subsection 2.2.1 and Subsection 2.2.2.

$$C_xH_y + \left(x + \frac{y}{4}\right) O_2 \rightarrow xCO_2 + \frac{y}{2}H_2O \tag{2.22}$$

Apart from the direct greenhouse effects of CO_2 and H_2O, also the by-products influence the climate (Lee et al., 2010). The effects of NO_x emissions on the atmosphere's composition are outlined in detail in Section 2.1. SO_x, C_xH_y, as well as Soot affect aerosols, contrails and clouds through microphysical processes. Thus, a change in radiative forcing is obtained.
An important parameter to describe the amount of emitted species is the so-called Emission

Index EI. It describes which amount in terms of mass of a certain species is emitted per amount of burned fuel. It is typically provided in g kg^{-1}. Table 2.1 provides an overview of average EI values of the global aircraft fleet. Regarding NO_x emissions it must be mentioned that the emission index is expressed in terms of g NO_2 per kg of consumed fuel (Schulte and Schlager, 1996). It avoids additional uncertainties through incorporation of the NO to NO_2 ratio and makes values comparable.

Table 2.1: Mean emission indices and typical ranges for combustion products of gas turbines - adapted from Lee et al. (2010).

Combustion Product	EI / g kg^{-1}
CO_2	3160
H_2O	1240
NO_x	14 (12-17)
SO_2	0.8 (0.6-1.0)
Soot	0.025 (0.01-0.05)
CO	3 (2-3)
C_xH_y	0.4 (0.1-0.6)

Legislative regulations aim to reduce the amount of aviation induced emissions to limit the climate effect and to control the impact on air quality (Ballal and Zelina, 2004). The Committee on Aviation Environmental Protection (CAEP) of the ICAO assesses the current and future impact of aviation's noise and emissions to provide data to assist the organization in policy decision-making. Aviation standards are introduced and participating states of the Chicago Convention aim to follow them. Nevertheless, these regulations are not legally biding. Yet, manufacturers follow them, as local legislative bodies implement ICAO guidelines.
The air to fuel ratio AFR and the equivalence ratio ϕ are relevant combustion parameters (Çengel and Boles, 1989). The air to fuel ratio is defined in Equation 2.23, where m_{air} and m_{fuel} are the masses of air and fuel of the mixture respectively. If the amount of air matches the amount of fuel such that Reaction 2.22 is fulfilled, the combustion is just complete. This condition is called stoichiometric combustion. The equivalence ratio expresses the ratio between the actual air to fuel ratio and the air to fuel ratio of stoichiometric combustion, as stated in Equation 2.24. The equivalence ratio is 1 for stoichiometric combustion. If it is smaller than 1, there is excess air and the combustion is lean. If it is higher than 1, there is excess fuel and the combustion is rich. In the latter case, the combustion is incomplete.

$$AFR = \frac{m_{air}}{m_{fuel}} \tag{2.23}$$

$$\phi = \frac{AFR_{stoichiometric}}{AFR} \tag{2.24}$$

2.2.1. Formation of Nitrogen Oxides

This subsection introduces relevant reaction pathways of NO production and addresses NO_2 formation. Dependencies between engine parameters and nitrogen oxide emissions are outlined.

Nitrogen Monoxide Formation

Nitrogen monoxide is produced due to five distinguished mechanisms of NO formation (Gokulakrishnan and Klassen, 2013). These are the thermal mechanism, the prompt mechanism, the nitrous oxide mechanism, the NNH mechanism and the Fuel Bound Nitrogen (FBN) mechanism.

Thermal NO is predominant for flame temperatures above 1800 K (Gokulakrishnan and Klassen, 2013) and especially of relevance for non-premixed combustors (Correa, 1998). According to Warnatz (2001), molecular nitrogen is reacting with atomic oxygen and NO is obtained together with atomic nitrogen, as stated in Reaction 2.25. Additionally, NO results from the following reaction of atomic nitrogen with molecular oxygen or OH, as shown in Reaction 2.26 and Reaction 2.27. The mechanism, first observed by Zeldovich (1992), is limited by the high activation energy required for breaking the strong bond of the N_2 molecule in Reaction 2.25. The work by Correa (1998) states that this energy is achieved through the high temperatures at stoichiometric interfaces between air and fuel, which are present in non-premixed combustors. According to Warnatz (2001), the NO production rate is given by the expression in Equation 2.28, where k is the rate coefficient. Hence, the formation of NO can be reduced by decreasing the rate coefficient through reduced temperature. Gokulakrishnan and Klassen (2013) outline that due to the exponential relationship between flame temperature and atomic oxygen concentration, a similar relationship is found between flame temperature and thermal NO formation.

$$N_2 + O \rightarrow NO + N \tag{2.25}$$

$$N + O_2 \rightarrow NO + O \tag{2.26}$$

$$N + OH \rightarrow NO + H \tag{2.27}$$

$$\frac{d[NO]}{dt} = 2k[O][N_2] \tag{2.28}$$

Rich flames support the formation of prompt NO (Gokulakrishnan and Klassen, 2013). Reaction 2.29 indicates that atomic nitrogen and hydrocyanic acid (HCN) result from the reaction between the hydrocarbon radical CH and N_2, further reacting to NO. The work by Warnatz (2001) states that as CH is formed at the flame front due to its precursor C_2H_2, especially present under rich conditions, fat mixtures support this path of NO production. It is first observed by Fenimore (1971). The activation energy required for Reaction 2.29 is lower than for Reaction 2.25. Thus, prompt NO is produced at lower temperatures than thermal NO. According to Gokulakrishnan and Klassen (2013), quantum chemists propose that Reaction 2.29 requires intermediate steps to account for electron spin conservation.

$$CH + N_2 \rightarrow HCN + N \tag{2.29}$$

Nitrous NO formation is predominant for lean premixed combustion (Correa, 1993). As for thermal NO formation, molecular nitrogen and atomic oxygen react. However, as Reaction 2.30 shows, instead of NO and N, nitrous oxide (N_2O) results from the reaction involving a gaseous third body. N_2O reacts with O and NO is obtained following Reaction 2.31. Warnatz (2001) explains that under stoichiometric or rich conditions the production rate of NO via this path is very low compared to the thermal and prompt mechanism, respectively. Nevertheless, under lean conditions the low temperatures limit thermal NO and missing C_2H_2 reduces prompt NO. Thus, nitrous NO is significant to the total NO production rate for lean conditions, since comparably low activation energy along with high pressure is sufficient for Reaction 2.30. The mechanism is based on findings by Wolfrum (1972) and Malte and Pratt (1975).

$$N_2 + O + M \rightarrow N_2O + M \tag{2.30}$$

$$N_2O + O \rightarrow NO + NO \tag{2.31}$$

Nitrogen contained in fuel due to impurities can be responsible for the formation of NO (Warnatz, 2001). During the gasification process of nitrogen containing compounds NO is formed in the gas phase according to Reaction 2.32. Also, the reaction to N_2 is possible as stated in Reaction 2.33. The respective production rates are influenced by the equivalence ratio. The analysis of a model system using propane doped with methylamine as a fuel showed the formation of NO is reduced towards rich mixtures with a minimum for $\phi \approx 1.4$. Thus, the production rate of N_2 is maximum at this point. The FBN pathway is especially relevant for the combustion of coal.

$$N + OH \rightarrow NO + H \tag{2.32}$$

$$N + NO \rightarrow N_2 + O \tag{2.33}$$

At low flame temperatures NO is formed via the intermediate species NNH (Gokulakrishnan and Klassen, 2013). NNH is formed through the Reaction 2.34 and can increase the NO production rate within the combustor. The reaction with atomic hydrogen then results in NO according to Reaction 2.35. The NO production rate induced by this pathway increases with equivalence ratio. However, at high temperatures close to an equivalence ratio of $\phi = 1$ NNH and O react to N_2 and OH or to N_2O and H. Hence, the NO production rate along the NNH pathway is reduced at high flame temperatures. The NNH mechanism was initially proposed by Bozzelli and Dean (1995).

$$N_2 + H \rightarrow NNH \tag{2.34}$$

$$NNH + O \rightarrow NO + NH \tag{2.35}$$

Nitrogen Dioxide Formation
Further downstream in the combustor and especially within the aging exhaust plume, obtained NO oxidizes to NO_2 following certain mechanisms.

NO_2 is formed in not significant quantities through oxidization processes (Feitelberg and Correa, 1999). While mixing of the hot gas with dilution air, atomic hydrogen is obtained through oxidization of CO according to Reaction 2.36. HO_2 is formed through Reaction 2.37. Reaction 2.38 states how NO_2 is produced. This pathway is dependent on the temperature of the hot gas. In general, lower temperatures result in a lower NO_2 production rate. This pathway is less relevant for lean combustion due to lower temperatures and less dilution air in the downstream zones of the combustor.

$$CO + OH \rightarrow CO_2 + H \tag{2.36}$$

$$H + O_2 + M \rightarrow HO_2 + M \tag{2.37}$$

$$NO + HO_2 \rightarrow NO_2 + OH \tag{2.38}$$

Another production mechanism of NO_2 is the reaction of NO with unburned fuel downstream of the combustor (Feitelberg and Correa, 1999). The effectiveness of this pathway varies among hydrocarbons and is therefore fuel-dependent.
In the exhaust plume a reaction between emitted NO and ambient O_3 can cause NO_2 as described by Reaction 2.39 (Schulte and Schlager, 1996). The production rate depends on the degree of mixing between the exhaust and ambient air. Experimental measurements of Schulte and Schlager (1996) in a young exhaust plume indicate fractions of NO_2 within NO_x of 6 to 23%. According to Schlager et al. (1997), the final ratio between NO_2 and NO in an aged plume is reached when the production rate of NO_2 via Reaction 2.39 and photolysis of NO_2 are in equilibrium.

$$NO + O_3 \rightarrow NO_2 + O_2 \tag{2.39}$$

2.2.2. Engine Parameters versus Nitrogen Oxide Emissions

Previously introduced mechanisms of NO formation show that especially the flame temperature determines the amount of emitted nitrogen oxides through the production of thermal NO. Several parameters affect the flame temperature and therefore also NO_x emissions. The fundamentals are discussed in this section.

Thrust Setting
The emission index of NO_x changes with thrust setting as Figure 2.5 illustrates (Lefebvre and Ballal, 2010). It is shown that the emission index of NO_x is low for low thrust settings and that a maximum is obtained for take-off power setting. Simplified, this behavior is obtained due to higher flame temperatures required for increments in thrust along with higher thermal NO formation rates. The increase in flame temperature leads to a rise in compression ratio and is

therefore coupled to the combustor inlet temperature $T3$. Figure 2.6 presents the exponential relationship between nitrogen oxide emissions and $T3$ established by Lipfert (1972), based on ground-based emission tests.

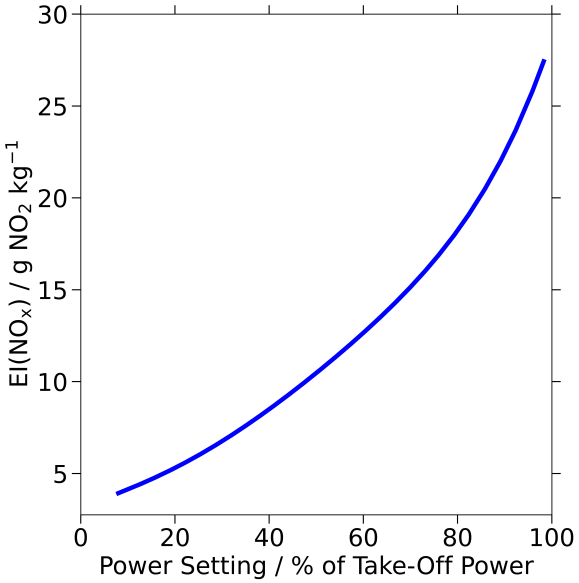

Figure 2.5: NO_x emission index with power setting - adapted from Lefebvre and Ballal (2010).

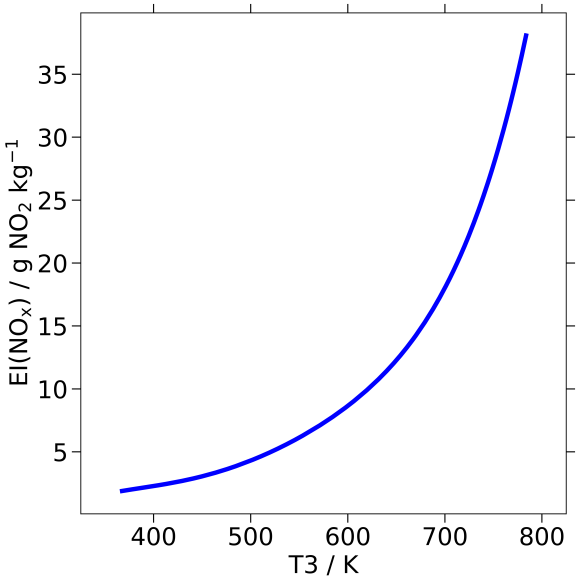

Figure 2.6: NO_x emissions with combustor inlet temperature - adapted from Lipfert (1972).

Equivalence Ratio

The amount of emitted NO_x depends heavily on the equivalence ratio due to the associated change in flame temperature (Saravanamuttoo et al., 2017). As explained in Subsection 2.2.1, the thermal NO formation mechanism is responsible for the major part of emitted NO_x at sufficiently high flame temperatures. Since this is the case for gas turbines of aircraft, a change in flame temperature has a strong impact on NO_x emissions. One way of controlling the flame temperature is adjusting the equivalence ratio, because there is a strong dependence between

these two parameters as shown in Figure 2.7. It is illustrated that the flame temperature is maximum close to the stoichiometric ratio. Towards rich and lean mixtures the flame temperature decreases rapidly. The maximum lays slightly on the rich side, as the cooling effect of the air's nitrogen is reduced (Glaude et al., 2014). Figure 2.7 indicates that NO_x emissions follow this pattern. However, the peak in NO_x emissions lays slightly on the lean side even if the maximum flame temperature is obtained slightly on the rich side. The reason is that both C_xH_y and N compete for the available O atoms (Lefebvre and Ballal, 2010). As oxygen is preferably consumed by hydrocarbons, the peak in NO_x is obtained on the lean side. It can be inferred that neither the prompt NO formation mechanism, nor the nitrous NO formation mechanism can compensate for the decrease in thermal NO towards more rich or more lean mixtures, respectively.

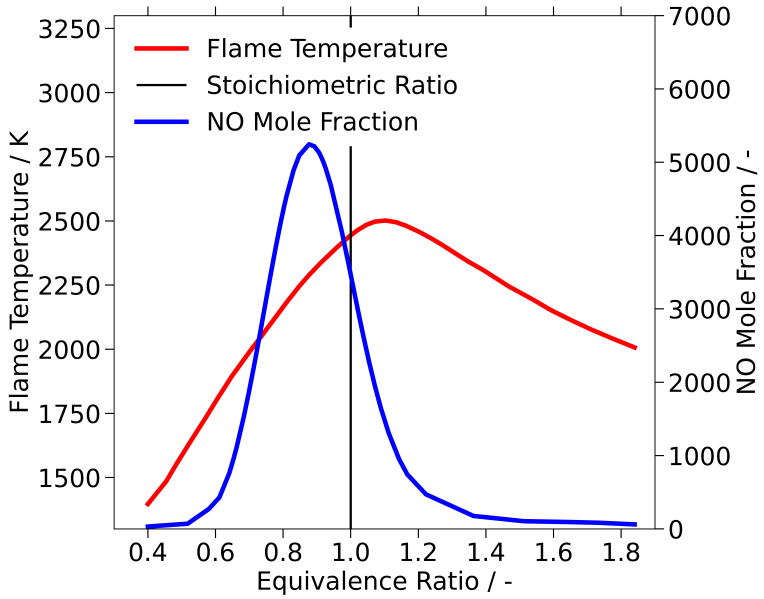

Figure 2.7: NO_x emissions and flame temperature with equivalence ratio - adapted from Glaude et al. (2014).

Premixing

To achieve a lean flame along with a successful reduction in NO_x emissions, sufficient atomization of injected fuel and sufficient premixing are required (Leonard and Stegmaier, 1994). Figure 2.8 compares NO_x emissions with flame temperature on a logarithmic scale for different degrees of premixing. It is shown that emissions are reduced with improved premixing. Good premixing is associated with sufficient atomization of fuel. If fuel is not atomized accordingly, the mean fuel droplet size is too high promoting envelop flames (Lefebvre and Ballal, 2010). These envelope flames surround large drops and burn close to the stoichiometric ratio, resulting in regions of high temperatures and promoting the formation of thermal NO. Hence, increasing the degree of premixing though sufficient atomization reduces NO_x emissions of lean mixtures.

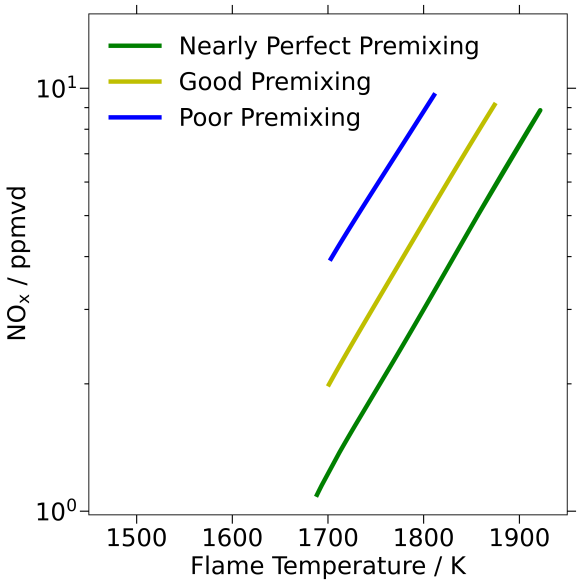

Figure 2.8: NO_x emissions with flame temperature and degree of premixing - adapted from Leonard and Stegmaier (1994).

Residence Time

Another parameter potentially influencing the formation of NO_x is the residence time. A study by Anderson (1975) indicates that a reduction in residence time results in lower NO_x emissions. Nevertheless, this effect is only present for sufficiently high equivalence ratios. This is confirmed by Leonard and Stegmaier (1993), as no dependence between the amount of emitted NO_x and residence time is found for the analysis of a lean premixed combustor. According to Anderson (1975), the reason is that NO_x is formed more rapidly for lean mixtures.

Pressure

As pressure affects several combustion parameters, it also affects the formation of NO_x (Gokulakrishnan and Klassen, 2013). Studies suggest that the effect of pressure on the production rate of NO_x depends on the equivalence ratio and thus, on the flame temperature. While the investigation of a lean premixed combustor by Leonard and Stegmaier (1993) does not indicate a significant dependence, Maughan, Luts and Bautista (1994) identify that NO_x emissions increase with pressure for equivalence ratios closer to 1. It is suggested that the reason is an increased sensitivity of thermal NO to pressure compared to other NO formation mechanisms, remembering that thermal NO is dominant at high temperatures being present closer to the stoichiometric ratio.

Fuel

There are two fuel parameters potentially affecting emitted nitrogen oxides: FBN and hydrogen to carbon ratio. It is explained previously that FBN can contribute to NO formation within the combustor. However, according to Blakey, Rye and Wilson (2011) the amount of nitrogen contained in aviation fuels such as Jet A-1 is practically zero. This is also the case for SAFs such as HEFA SPK. These alternative fuels have the advantage that additionally, trace amounts of nitrogen can be removed through hydroprocessing. Hence, no significant differences in emitted nitrogen oxides due to FBN are likely for aviation applications.
Increasing hydrogen content leads to a reduction in nitrogen oxide emissions. Gleason and Martone (1980) report ground based emissions measurements for thirteen different fuels. A correlation between hydrogen content and NO_x is identified and a reduction in $EI(NO_x)$ from

28.3 to 25.5 g NO_2 kg^{-1} is presented for an increase in hydrogen content from 12 to 14%. The effect is related to to the impact of fuel hydrogen to carbon ratio on flame temperature and hence, on thermal NO formation. Since the hydrogen to carbon ratio varies between conventional Jet A-1 and alternative fuels (Blakey, Rye and Wilson, 2011), a difference in the amount of emitted nitrogen oxides is possible.

Engine Degradation

Engine degradation can affect nitrogen oxide emissions. Lukachko and Waitz (1997) investigate the effect of turbofan engine component aging on nitrogen oxides. Based on emission modelling, it is found that depending on the component, positive or negative impacts on NO formation are possible. The change in formation rates are related to flame temperature variations due to component efficiencies being affected by distortion and contamination. According to presented data, deterioration of fan HPC, LPC and LPT results in increased nitrogen oxide formation, while HPT deterioration leads to a decrease in emissions. According to Apostolidis and Stamoulis (2021), the exhaust gas temperature margin, describing the difference between an averaged exhaust gas temperature value and the operational limit, can be an indicator for the degree of engine aging. The lower the value, the more degradation can be expected.

2.2.3. Nitrogen Oxide Mitigation in Turbofan Engines

Subsection 2.2.2 shows that due to the high significance of the thermal NO production path, reducing the flame temperature is efficient to reduce NO_x emissions. In aeronautic applications, solutions aim to achieve this by combustion control through suitable adaptation of the equivalence ratio, as this section shows. Other methods to reduce flame temperature such as water/steam injection or post-combustion control to reduce NO_x emissions are less suitable for aerospace applications due to their impact on weight and thus, not considered in this section (Saravanamuttoo et al., 2017).

Rich Quench Lean Combustion

The Rich Quench Lean (RQL) principle combines sequences of rich and lean combustion to reduce NO_x emissions while limiting the amount of other combustion products (Liu et al., 2017). Equivalence ratios of 1.2 to 1.8 result in a rich flame in the primary zone and are associated with a lower flame temperature. Hence, the NO production is reduced in this zone. Nevertheless, dilution downstream of the combustion chamber is necessary to enable oxidation of CO, hydrogen and hydrocarbon intermediates, resulting from the rich primary zone. Consequently, the mixture becomes lean, crossing an equivalence ratio of 1 in the secondary zone and leading to increased NO production rates. Therefore, rapid mixing is required to minimize this area. Once a sufficiently lean mixture is achieved, lower flame temperatures result again in limited NO production rates within the so-called dilution zone.

Lean Premixed Combustion

The principle of lean premixed combustion aims to reduce NO_x on the lean side by limiting the formation of thermal NO through a reduction in temperature (Lefebvre and Ballal, 2010). The corresponding combustor is divided into three zones. In the so-called premixing zone fuel is injected, evaporated and mixed with air to obtain a homogeneous, lean mixture. The degree of homogeneity and evaporation is of high importance to avoid envelope flames and to achieve a constantly low flame temperature. Thus, it is of high importance that evaporation and mixing do not exceed the autoignition delay time to ensure that only the fully premixed mixture is ignited. This is especially important for high power settings associated with high combustor inlet temperatures and pressures. Downstream of the premixing zone, the actual combustion is taking place in the so-called secondary zone. A dilution zone follows.

While NO_x emissions are reduced through lowered flame temperatures, CO emissions increase (Warnatz, 2001). Due to the strong temperature dependence of the OH production rate, the oxidization rate of CO is reduced for lean combustion. Hence, CO emissions are increased, bounding the equivalence ratio such that unacceptable CO values are not exceeded. However, since residence time is not affecting NO_x emissions at low equivalence ratios, as introduced in Subsection 2.2.2, the reduced rate in oxidization of CO can be counteracted by increasing residence time without affecting NO_x emissions (Lefebvre and Ballal, 2010). Additional challenges include acoustic resonance due to coupling between the combustion process and combustor acoustics, flashback (Lefebvre and Ballal, 2010), as well as lean blowout (Saravanamuttoo et al., 2017).

Example: CFM LEAP Engine

An example for nitrogen oxide mitigation is the Twin Annular Premixing Swirler (TAPS) combustor as implemented in CFM's LEAP engine, investigated in the presented research. Applying lean burn technology, it aims to reduce nitrogen oxide emissions by reducing flame temperature through adaptation of the equivalence ratio (Foust et al., 2012).
Fuel staging enables operation of the engine at various power settings, as outlined by Stickles and Barrett (2013). Figure 2.9 illustrates that two flame zones are distinguished: a lean premixing zone and a rich pilot zone. At low power settings only the pilot injector is active, since the mixture is too lean for stable premixed combustion. With increasing power, the so-called main injector starts to operate and fuel is split between main and pilot. At high power settings, most fuel is injected through the main injectors resulting in a lean mixture for about 70% of the total air flow.

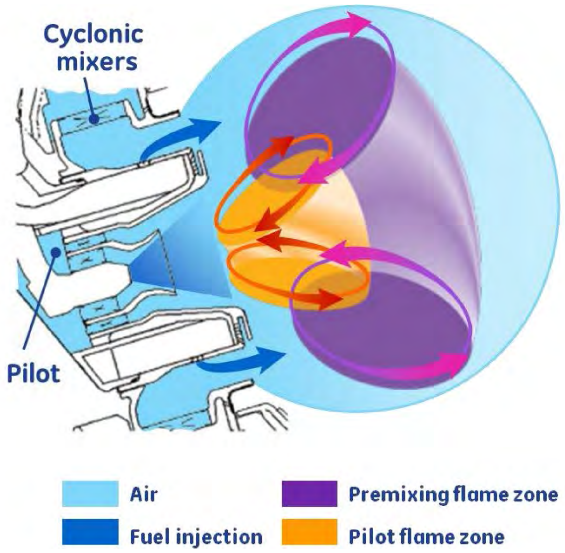

Figure 2.9: Pilot and main injectors with the respective flame zones of the TAPS combustor (Foust et al., 2012).

Figure 2.10 shows how fuel staging of the TAPS combustor affects nitrogen oxide emissions in comparison to a RQL combustor. For low thrust settings, similar emissions are predicted for both designs. At approach thrust, the curves start to deviate with slightly lower nitrogen oxide emission indices for the TAPS combustor. The distinct effect of fuel staging is visible at low cruise thrust settings, resulting in a sharp drop in emitted NO_x for the TAPS design, while the trend of the RQL combustor stays constant. The difference in nitrogen oxide emissions between the designs decreases towards maximum thrust.
Comparing obtained emissions for pilot-only and staged operation indicates significant

differences. Stickles and Barrett (2013) analyzes total nitrogen oxide emissions for a typical 500 nm mission. The reported value for staged combustion is about 35 % lower than for pilot-only injection, considering climb, cruise and descent phases. Hence, a reduction in emitted nitrogen oxides is expected for staged operation of the LEAP engine.

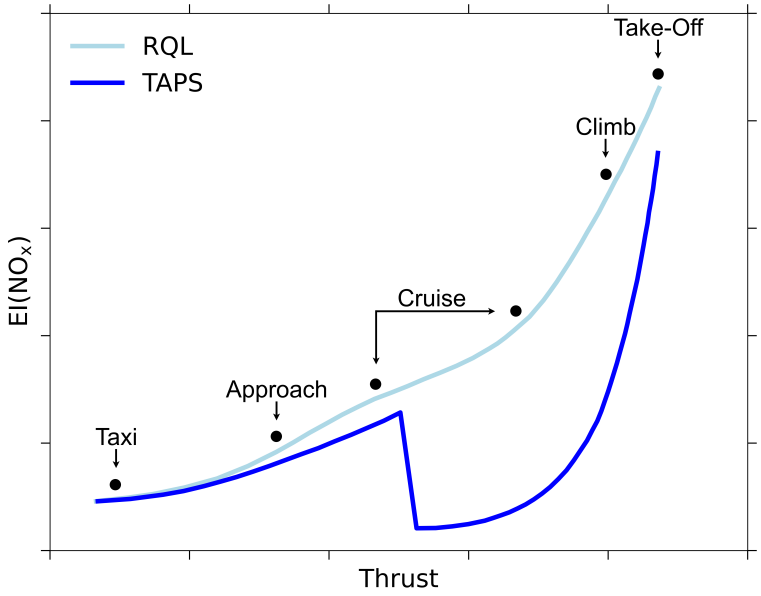

Figure 2.10: Schematic NO_x emission index with thrust setting for an RQL and the TAPS combustor - adapted from Foust et al. (2012).

3
In-Flight Nitrogen Oxide Measurements

This chapter outlines the methodology applied to investigate the posed research questions. Section 3.1 provides an overview on performed experimental near field flights, while Section 3.2 explains the applied measurement principles. Section 3.3 presents the adapted analysis routine to derive experimental emission indices and Section 3.4 introduces far field measurements conducted for comparative analyses.

3.1. Experimental Setup and Near Field Sampling Strategy VOLCAN

This section provides an overview on near field measurements performed as a part of the emission test campaign VOLCAN - a cooperation between DLR, Airbus, Safran and GE Aerospace. The overall experimental setup is presented and the chasing procedure is illustrated. The strategies followed to derive dependencies between experimentally determined nitrogen oxide emissions and the respective engine parameter are introduced. A summary for each of the four conducted emission test flights is given.

Nitrogen oxide emissions are determined experimentally by performing chase flights. The involved aircraft are shown in Figure 3.1. A Dassault Falcon 20-E5, depicted in Figure 3.1 (a), is modified as a measurement platform to determine NO_y and CO_2 concentrations, both required to calculate nitrogen oxide emission indices as introduced below in this section. The Falcon is chasing a source aircraft, an Airbus A321-251NX equipped with two CFM LEAP-1A35 engines illustrated in Figure 3.1 (b). For each test point, different engine settings are selected on the source aircraft and the respective emissions are measured. The combustion technology of the investigated engine is introduced in Subsection 2.2.3.

(a) (b)

Figure 3.1: (a) Measurement platform Dassault Falcon 20-E5 (Registration: D-CMET) and (b) source aircraft Airbus A321-251NX (Registration: D-AVZO), equipped with two CFM LEAP-1A engines - adapted from internal source.

Temporary Reserved Airspace (TRA) is required for the emission test flights. Measurements are conducted in the so-called near field. The near field describes the area behind an aircraft, where the engines' exhaust is not yet mixed with the wake vortices. For the outlined research the distance between measurement platform and source aircraft ranges from 55 to 180m with a mean of 98m. As this is far below the minimum safety distance, conventional, controlled airspace is not suitable to perform the experiment. Therefore, a suitable TRA is selected for each flight. Criteria are airspace availability and weather forecast. The latter is of high importance, since contrail formation must be avoided to ensure visibility at low aircraft separation. The respective flight routes of the Falcon above the north-eastern part of the Mediterranean are provided in Figure 3.2. Tests are carried out between February 28 and March 27, 2023.

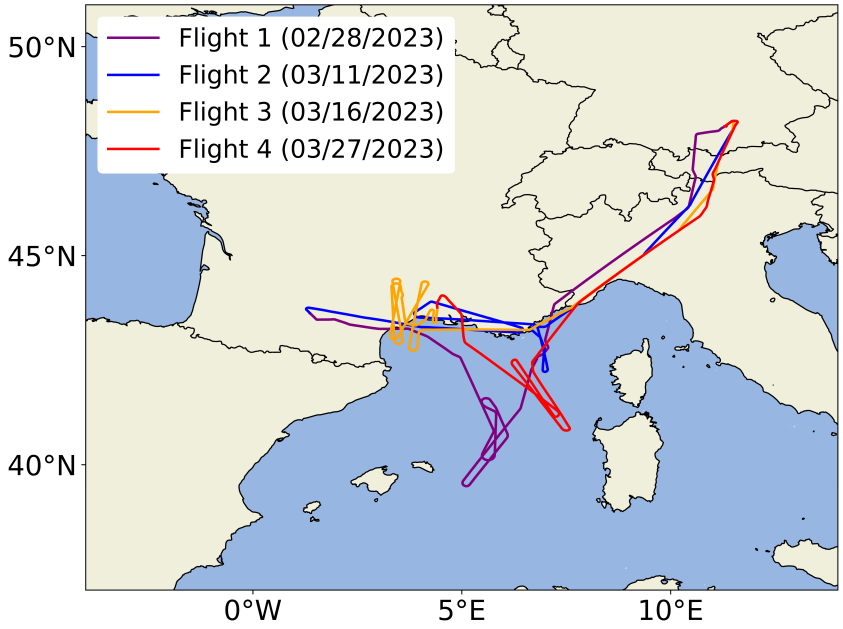

Figure 3.2: Falcon flight routes for the four near field emission test flights conducted in February and March 2023.

The chasing procedure itself is illustrated in Figure 3.3. At the beginning of the measurements, the two aircraft are guided by Air Traffic Control (ATC) until visual contact is established. Starting from this point, coordination is managed by the flight crews of both aircraft via radio communication. In the start position, indicated with number one, the Falcon is flying at the same altitude as the Airbus. When the tested engine is stabilized in the right configuration according to the respective test point, the Falcon is going into a short dive to cross the wake vortex from below. Once it is flying between both wake vortices, it is pulling up to enter the exhaust plume of the engine at the position indicated as number two. It is desired that the emission inlets illustrated in Figure 3.1 are directly laying within the exhaust plume. A plume encounter time of about 60 s is intended. After this time the Falcon is diving out of the plume to measure a short sequence of NO_y and CO_2 background concentrations. The Falcon is pulling up again for another sample and the procedure is repeated until sufficient data is collected for the respective test point. The measurement area is left by again crossing the wake vortex from below and the Falcon is waiting at position 1 until the source aircraft is on condition for the next test point.

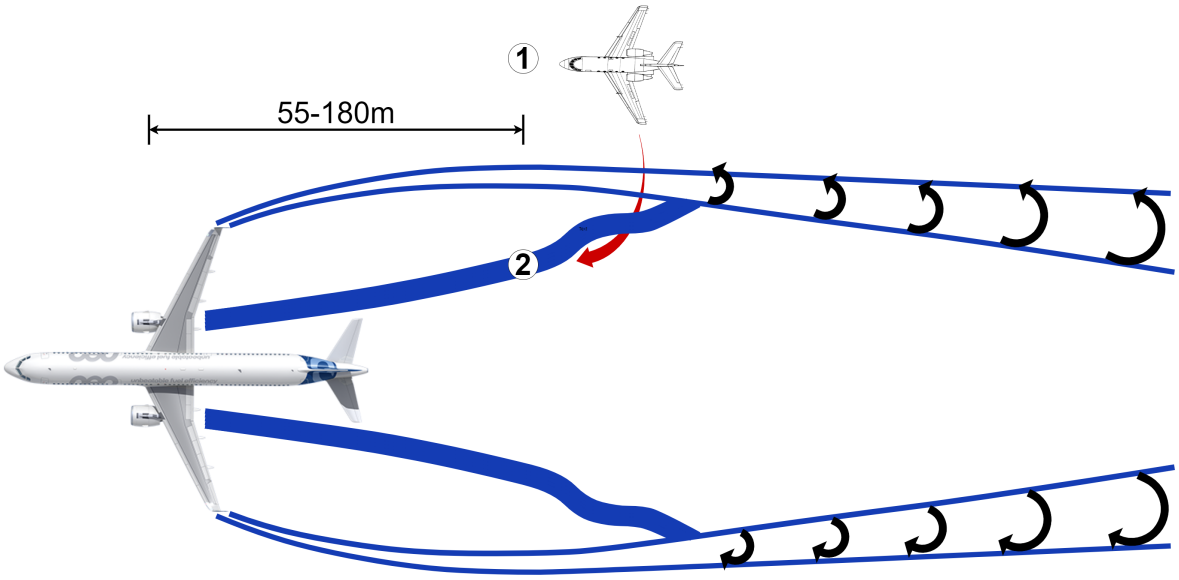

Figure 3.3: Near field chasing procedure applied during emission test flights - adapted from internal source.

NO_x emission indices are determined using simultaneously measured concentrations of both nitrogen oxides and carbon dioxide to quantify emissions for each test point. The concept of emission indices is introduced in Section 2.2. The determination is enabled by Equation 3.1 (Schulte and Schlager, 1996). $EI(NO_x)$ and $EI(CO_2)$ are the emission indices of NO_x and CO_2 respectively, where the latter is known and quantified based on the fuel's hydrogen content as explained below. The ratio $\frac{46}{44}$ relates the molar masses of NO_2 and CO_2. ΔNO_y and ΔCO_2 describe the change in volume mixing ratio of the respective species compared to the background concentration. Section 3.3 outlines in detail how these terms are determined based on measured NO_y and CO_2 concentrations. The value of $EI(NO_x)$ is determined using NO_y concentrations to avoid neglecting HNO_2 and HNO_3, formed from NO_x within the aging plume (Schumann, 1997). Hence, it is ensured that all NO_x emitted at the engine's exit plane is detected.

$$EI(NO_x) = EI(CO_2) \cdot \frac{46}{44} \cdot \frac{\Delta NO_y}{\Delta CO_2} \tag{3.1}$$

As introduced above, the value of $EI(CO_2)$ is estimated based on the fuel composition. Equation 3.2 states the according relation (Moore et al., 2017). Required parameters include the ideal gas constant R, molar masses of carbon $M(C)$, hydrogen $M(H)$ and carbon dioxide $M(CO_2)$, the hydrogen-to-carbon molar ratio α, as well as the values of the static temperature T, the static pressure p and the molar volume V_m at mid sea level standard conditions. The equation assumes complete combustion. Determined carbon dioxide emission indices for the tested fuels are provided below in this section.

$$EI(CO_2) = \frac{R \cdot T \cdot M(CO_2)}{P \cdot V_m \cdot (M(C) + \alpha \cdot M(H))} \tag{3.2}$$

Dependencies between experimentally determined nitrogen oxide emissions and four distinguished engine parameters are investigated in this research, according to the subquestions of the first research question formulated in Section 1.2. In the following the respective sampling

strategies are outlined and a summary for each of the four performed near field emission test flights is provided.

Fuels tested during VOLCAN

For the first subquestion it is analyzed whether a change in fuel type can result in different amounts of emitted nitrogen oxides. Three different Synthetic Paraffinic Kerosene (SPK) blends are tested and compared to Jet A-1. SPK fuels differ from Jet A-1 in terms of their feedstocks and production. While Jet A-1 is obtained from crude oils through a refining process, SPK fuels are made from coal or biomass by applying Fischer Tropsch Synthesis or hydrotreating of oils (Blakey, Rye and Wilson, 2011). SPK used in this research is obtained from Hydroprocessed Esters and Fatty Acids (HEFA). According to Undavalli et al. (2023) the feedstock includes waste oils, vegetable oils, animal fats, non-edible crops, and algae.
The three investigated HEFA SPK blends are distinguished in their aromatic content. While 100% HEFA SPK has practically no aromatics, HEFA SPK with low aromatic content (HEFA SPK+LA) and HEFA SPK with high aromatic content (HEFA SPK+HA) are mixed with different levels of mono aromatics as so-called drop-in fuels. Table 3.1 specifies the total volume content of mono aromatics in the fuels. Aromatic hydrocarbons are needed to achieve sufficient fuel density and to ensure elastomer swell in aircraft fuel systems (Shahabuddin et al., 2020). Hence, drop-ins are of interest on the road map to certification of 100% HEFA SPK.
Tested fuels differ in terms of their hydrogen to carbon ratio . Table 3.1 provides the fuels' composition specifying hydrogen and carbon mass contents. Hydrogen values are provided by a co-worker and determined based on low resolution nuclear magnetic resonance spectrometry according to the ASTM D3701 method. Measurements are characterized by a reproducibility of 0.11%. It is assumed that carbon adds up to the total mass. Carbon dioxide emission indices are computed according to Equation 3.2.

Table 3.1: Relevant quantities of investigated fuels during VOLCAN, including aromatic content, hydrogen content, carbon content and assumed CO_2 emission index.

Fuel Type	Aromatic Content / vol %	Hydrogen Content / mass %	Carbon Content / mass %	EI(CO_2) / g CO_2 kg^{-1}
Jet A-1	12.8	13.97	86.03	3152
HEFA SPK	<1	15.29	84.71	3104
HEFA SPK+LA	8.4	14.84	85.16	3121
HEFA SPK+HA	17.6	14.29	85.71	3141

To identify potential discrepancies, all HEFA SPK blends are compared to Jet A-1 at different engine settings. These engine settings are defined in terms of selected combustor inlet temperature T3 and combustion mode, according to the specifications in Table 3.3 and Table 3.4. HEFA SPK is tested during Flight 1 (02/28/2023), as well as during Flight 4 (03/27/2023), HEFA SPK+LA is investigated as a part of Flight 2 (03/11/2023) and HEFA SPK+HA is analyzed during Flight 3 (03/16/2023). The flights and the respective test points are summarized in Table 3.6 to Table 3.9. It must be noted that due to contamination during Flight 1, different blends of Jet A-1 and HEFA are compared instead of the pure fuels. Table 3.2 specifies the compositions burned for test points denoted as Jet A-1 and HEFA. $EI(CO_2)$ values of the blends are provided.

Table 3.2: CO_2 emission indices of investigated blends during Flight 1 with fuel composition in terms of Jet A-1 and HEFA SPK.

Blend	Jet A-1 / %	HEFA SPK / %	EI(CO_2) / g CO_2 kg^{-1}
Jet A-1 dominant	81	19	3143
HEFA dominant	47	53	3127

Combustor Inlet Temperature Settings during VOLCAN

Dependencies between measured nitrogen oxide emissions and combustor inlet temperature T3 are investigated to answer the second subquestion. Four different combustor inlet temperature settings are defined: very low, low, mid and high. These settings are specified in Table 3.3. Since the combustor inlet temperature is proprietary, values relative to mid T3 setting are provided. It is not distinguished between the fuel types, as the results of the first subquestion do not indicate significant differences. All measurements to determine dependencies between nitrogen oxide emissions and T3 are performed in forced pilot-only combustion mode, defined in Table 3.4.

Table 3.3: Investigated combustor inlet temperature settings.

Setting	ΔT3 / K
Very low	-52
Low	-28
Mid	0
High	28

Combustion Modes tested during VOLCAN

The effect of staged combustion on nitrogen oxides is analyzed to answer the third subquestion. As outlined in Table 3.4, two different combustion modes are analyzed as a part of this research project: a forced pilot-only mode and the conventional pilot+main mode. As described in Section 2.2, the modes differ in their active fuel injectors. While for pilot+main mode both main and pilot injectors are active, initiating lean and rich flames simultaneously, 100% of the fuel is injected through the pilot injector when pilot-only mode is active, resulting in rich combustion. In this research the pilot-only mode is denoted as forced, since it is activated manually at a power setting at which normally the pilot+main mode would be active. Hence, it does not lay within the engine's standard operation envelope and is tested to investigate particle emission dependencies, not covered in this thesis. In general, both combustion modes are tested during all of the four conducted near field test flights described in Table 3.6 to Table 3.9. Measurements are performed at mid T3 setting and as motivated before, it is not distinguished between the fuels.

Table 3.4: Investigated combustion modes in terms of fuel split between pilot and main injectors during VOLCAN.

Combustion Mode	Fuel injected by Pilot / %	Fuel injected by Main / %
Forced Pilot-Only	100	0
Pilot+Main	<100	>0

Engines investigated during VOLCAN

Dependencies between engine degradation and emitted nitrogen oxides are investigated to answer the fourth subquestion. Table 3.5 specifies the condition of Engine 1 (ENG 1) and Engine

2 (ENG 2) during the test campaign in terms of Exhaust Gas Temperature Margin (EGTM). As explained in Subsection 2.2.2, exhaust gas temperature margin is an engine performance indicator, affected by deterioration (Apostolidis and Stamoulis, 2021). ENG 1 is the source aircraft's left engine and ENG 2 is the source aircraft's right engine in direction of flight. ENG 2 is the standard engine investigated in this research. Only during Flight 4 (03/27/2023) emissions of ENG 1 are measured additionally to enable a comparison between the two. This comparison is performed at mid T3 setting for both forced pilot-only and pilot+main combustion mode.

Table 3.5: Investigated engines and their respective exhaust gas temperature margin $EGTM$ during VOLCAN.

Engine	EGTM / K
ENG 1 (left)	x-15
ENG 2 (right)	x

Overview of VOLCAN Near Field Flights

As mentioned before, a total of four near field emission test flights is performed to cover all test points. Table 3.6 to Table 3.9 summarize each individual emission test flight. Flight conditions are provided covering mean Mach Number (M), mean Flight Level (FL) and mean Total Air Temperature (TAT) during the plume encounters. The respective standard deviation is indicated. It can be inferred from the tables that the flight conditions are very similar for all flights. Thus, emissions obtained for all flights are comparable, considering accuracy and precision of the measurements.
Several parameters are defining the test points of each flight. The column Tested Engine specifies if ENG 1 or ENG 2 is investigated. The column Tested Fuel describes which fuel is burned by the tested engine and the column Combustion Mode specifies which of the previously introduced combustion modes is active. The selected T3 setting is indicated and for each test point mean values of the Fuel Flow ΔFF are provided. As introduced previously, $\Delta T3$ describes the absolute change in combustor inlet temperature compared to mid T3 setting. ΔFF specifies the absolute change in fuel flow compared to a representative value at mid T3 setting. The parameter n specifies the number of plume encounter or samples for each test point.

Table 3.6: Flight conditions in terms of Mach number M, flight level FL and total air temperature TAT, as well as test points in terms of tested engine, tested fuel, combustion mode, T3 setting, mean normalized combustor inlet temperature $\Delta T3$, mean normalized fuel flow ΔFF and number of samples n during Flight 1 - 02/28/2023.

Flight	Flight Conditions	Tested Engine	Tested Fuel	Combustion Mode	T3 Setting	Δ T3 / K	Δ FF / kg h^{-1}	n / -
Flight 1	M=0.62±0.011 FL=320±33 ft TAT=242±1 K	ENG2	Jet A-1	Pilot only	Low	-28.6±1	-208.5±14	3
					Mid	-0.4±0	-31.8±10	4
					High	-	-	-
				Pilot+Main	Mid	0.5±1	20.2±24	6
			HEFA SPK	Pilot only	Low	-27.7±0	-192.7±4	3
					Mid	0.2±0	18.8±13	3
					High	-	-	-
				Pilot+Main	Mid	0.4±0	9.3±5	4

Table 3.7: Flight conditions in terms of Mach number M, flight level FL and total air temperature TAT, as well as test points in terms of tested engine, tested fuel, combustion mode, T3 setting, mean normalized combustor inlet temperature $\Delta T3$, mean normalized fuel flow ΔFF and number of samples n during Flight 2 - 03/11/2023.

Flight	Flight Conditions	Tested Engine	Tested Fuel	Combustion Mode	T3 Setting	Δ T3 / K	Δ FF / kg h^{-1}	n / -
Flight 2	M=0.59±0.002 FL=300±4 ft TAT=246±1 K	ENG2	Jet A-1	Pilot-Only	Low	-28.0±0	-188.1±4	4
					Mid	-0.5±0	18.6±9	4
					High	27.2±0	236.5±1	4
				Pilot+Main	Mid	-0.3±0	2.3±4	6
			HEFA SPK+LA	Pilot-Only	Low	-28.3±0	-178.4±7	4
					Mid	-0.5±0	3.7±2	4
					High	27.9±0	215.3±1	4
				Pilot+Main	Mid	0.1±0	-14.6±2	6

Table 3.8: Flight conditions in terms of Mach number M, flight level FL and total air temperature TAT, as well as test points in terms of tested engine, tested fuel, combustion mode, T3 setting, mean normalized combustor inlet temperature $\Delta T3$, mean normalized fuel flow ΔFF and number of samples n during Flight 3 - 03/16/2023.

Flight	Flight Conditions	Tested Engine	Tested Fuel	Combustion Mode	T3 Setting	Δ T3 / K	Δ FF / kg h^{-1}	n / -
Flight 3	M=0.59±0.001 FL=300±1 ft TAT=245±0 K	ENG2	Jet A-1	Pilot-Only	Low	-28.0±0	-174.9±1	5
					Mid	-0.1±0	13.3±4	4
					High	28.0±0	253.8±4	3
				Pilot+Main	Mid	0.0±0	29.1±3	4
			HEFA SPK+HA	Pilot-Only	Low	-27.8±0	-172.7±7	5
					Mid	-0.2±0	7.8±2	5
					High	28.1±0	256.0±3	4
				Pilot+Main	Mid	-0.3±0	13.8±9	6

Table 3.9: Flight conditions in terms of Mach number M, flight level FL and total air temperature TAT, as well as test points in terms of tested engine, tested fuel, combustion mode, T3 setting, mean normalized combustor inlet temperature $\Delta T3$, mean normalized fuel flow ΔFF and number of samples n during Flight 4 - 03/27/2023.

Flight	Flight Conditions	Tested Engine	Tested Fuel	Combustion Mode	T3 Setting	Δ T3 / K	Δ FF / kg h^{-1}	n / -
Flight 4	M=0.58±0.002 FL=290±3 ft TAT=242±0 K	ENG2	Jet A-1	Pilot-Only	Very Low	-52.0±0	-247.2±7	3
					Mid	-0.0±0	130.6±3	6
				Pilot+Main	Mid	0.3±0	124.0±2	7
			HEFA SPK	Pilot-Only	Mid	0.2±0	108.1±2	4
				Pilot+Main	Mid	-0.3±1	101.0±4	6
		ENG1	Jet A-1	Pilot-Only	Mid	0.7±0	215.7±12	4
				Pilot+Main	Mid	-0.1±0	180.7±6	6

3.2. Applied Measurement Techniques

This section outlines the measurement principles applied to determine NO_y and CO_2 concentrations required to quantify nitrogen oxide emission indices, as explained in Section 3.1. Subsection 3.2.1 introduces the measurement setup used to measure nitrogen oxides and Subsection 3.2.2 presents the utilized carbon dioxide instrument.

3.2.1. Nitrogen Oxide Measurements

A procedure outlined in Drummond, Volz and Ehhalt (1985) is applied for the presented in situ nitrogen oxide emission measurements. The well-established measurement principle is based on the chemiluminescence reaction of NO with O_3 and its applicability for aircraft emission measurements is proven in several studies (e.g., Schulte and Schlager, 1996; Schulte et al., 1997; Jurkat et al., 2011; Harlass et al., in preparation). The CLD 780 TR is a NO measurement instrument developed by Eco Physics applying this technique (Eco Physics, 2000). Figure 3.4 provides a simplified illustration of its working principle including adaptations to allow for the measurement of NO_y species at high concentrations. Figure 3.5 shows the instrument integrated in the research aircraft Falcon.

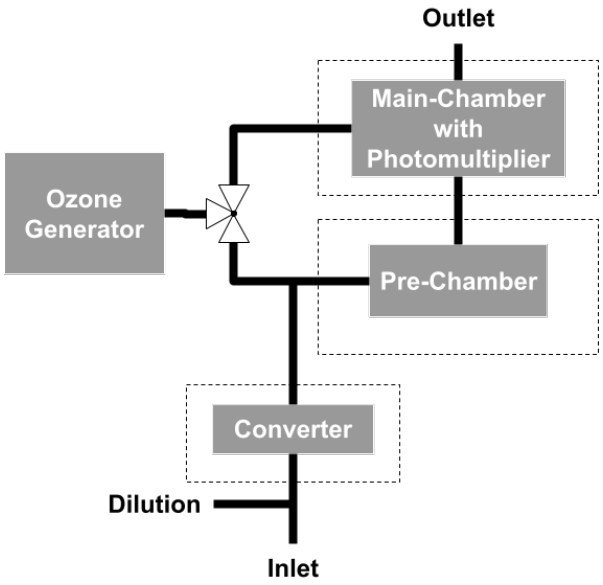

Figure 3.4: Simplified illustration of the CLD 780 TR working principle - adapted from Eco Physics (2000).

Figure 3.5: CLD 780 TR integrated in the research aircraft Falcon.

In general, sample air is directed into a main chamber and ozone generated within the instrument using a O_3 generator is added. Reaction 3.3 and Reaction 3.4 take place and NO_2 in

excited state is obtained. The excited NO_2 is deactivated spontaneously through Reaction 3.5 and Reaction 3.6. The emitted photon obtained from Reaction 3.5 is detected by a photomultiplier and a measurement signal is detected at a frequency of 1 Hz. A linear correlation between the photomultiplier signal and the NO concentration of the analyzed sample air exists. Calibrations are necessary to establish this relation (Ziereis, Stock and Schlager, 2012). The specific calibration procedure developed for this research is outlined in detail in Subsection 3.3.1. In the following, the need for so-called pre-chamber measurements is explained and instrument adaptations for this research through the integration of a converter and a dilution system are outlined.

$$NO + O_3 \rightarrow NO_2 + O_2 \tag{3.3}$$

$$NO + O_3 \rightarrow NO_2^* + O_2 \tag{3.4}$$

$$NO_2^* \rightarrow NO_2 + hv \tag{3.5}$$

$$NO_2^* + M \rightarrow NO_2 + M \tag{3.6}$$

Pre-Chamber Measurements

As previously explained a signal is detected by the photomultiplier. However, this signal S_{main} is not only caused by the chemiluminescence reaction of NO with O_3. Additionally to this desired NO signal S_{NO}, a dark current signal S_D and a chemical interference signal S_{in} exist, such that the superposition of all these three signals is measured, as described in Equation 3.7. To isolate the signal of interest, S_{NO}, a separate measurement of the sum of S_D and S_{in} is required. For this purpose, ozone is added to the pre-chamber such that the photon emission due to the NO concentration is taking place there. Consequently, the pre-chamber signal as stated in Equation 3.8 is measured in this case. The isolated NO signal is obtained according to Equation 3.9. Figure 3.6 schematically illustrates the signals for both pre-chamber and main-chamber measurements. During emission test flights, pre-chamber measurements are performed approximately every 10min.

$$S_{main} = S_{NO} + S_{in} + S_D \tag{3.7}$$

$$S_{pre} = S_{in} + S_D \tag{3.8}$$

$$S_{NO} = S_{main} - S_{pre} \tag{3.9}$$

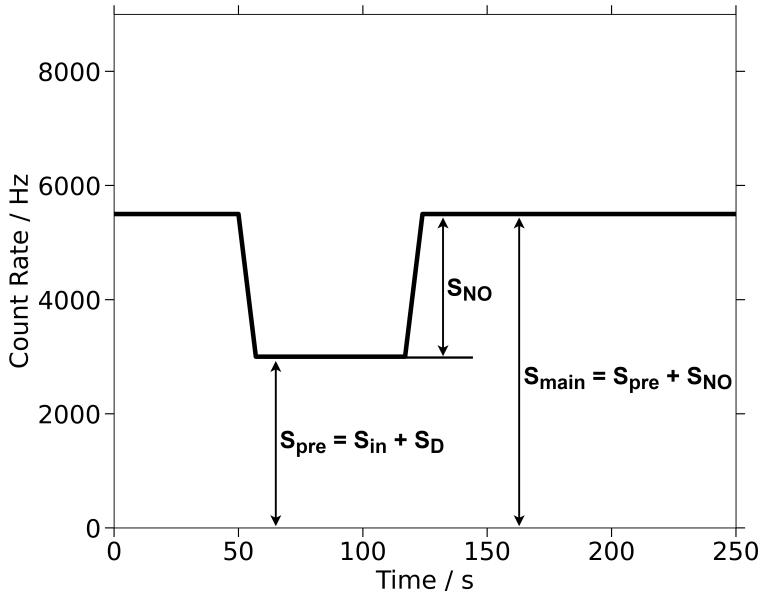

Figure 3.6: Pre-chamber and main-chamber signals for a schematic measurement sequence - adapted from Drummond, Volz and Ehhalt (1985).

Converter

A converter is implemented to allow for the measurement of nitrogen oxides different from NO. The described measurement principle does only allow for the measurement of nitrogen monoxide. Nevertheless, to quantify emitted nitrogen oxides also NO_2 must be measured, since NO oxidizes within the engine (Feitelberg and Correa, 1999), as well as within the aging plume (Schulte and Schlager, 1996), as described in Subsection 2.2.1. Section 3.1 explains that in addition, small amounts of HNO_2 and HNO_3 can be formed from NO_x (Schumann, 1997). Thus, a gold converter as described in Bollinger et al. (1983) serves to detect all these species called NO_y. Heated to about 300 °C, it converts NO_y to NO, which can then be measured using the chemiluminescence principle described above. It is important to regularly verify the efficiency of this conversion. The according procedure applied in this research work is outlined in Subsection 3.3.1.

Dilution System

Integrating a dilution system enables to raise the upper detection limit (Harlass et al., in preparation). The maximum detectable mixing ratio of the applied measurement instrument is ≈1000 ppb. This value is exceeded in this research due to very high concentrations in the near field plume. Diluting the sample air reduces the mixing ratio within the measurement chambers and hence, higher concentrations can be quantified. However, the uncertainty increases slightly, as outlined in Subsection 3.3.2. In the study presented here, the dilution ratio is increased from 1:1, as reported in Harlass et al. (in preparation), to a ratio of 3:1 to implement suggested improvements.

3.2.2. Carbon Dioxide Measurements

Non-dispersive infrared spectroscopy is applied to measure CO_2 concentrations in this research. The instrument used is the so-called LI-7000 (LI-COR, 2007). Sample air is directed into a sampling chamber. Infrared light of a wavelength suitable for absorption by CO_2 is passed through this chamber, as illustrated in Figure 3.7. The remaining radiation is directed to a detector, where it is measured to compute the absorption. Simultaneously, measurements

are performed using a reference chamber filled with gas of known CO_2 concentration. The CO_2 concentration of the sample air is then derived by determining the difference between the signals of the two chambers. Concentrations are obtained at a frequency of 10 Hz. Lenses are used to allow for maximized sensitivity by focusing the radiation.

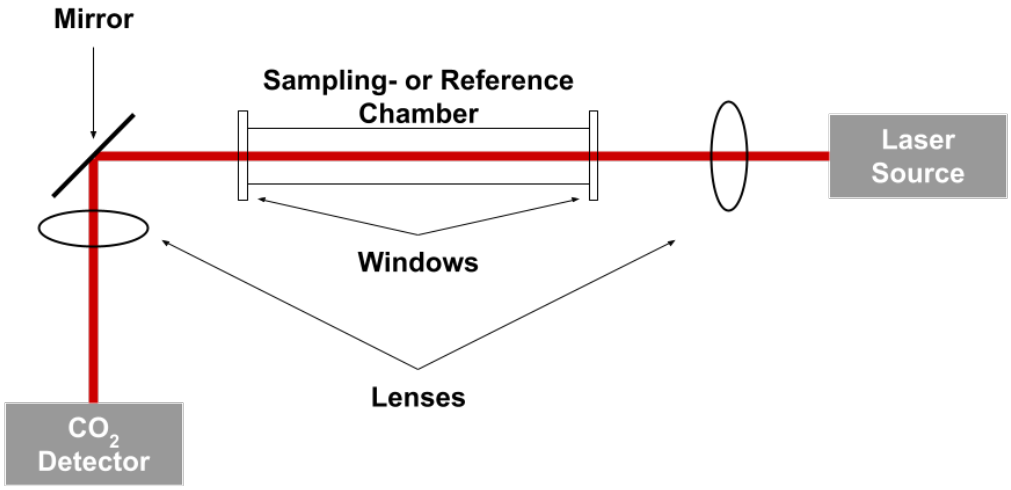

Figure 3.7: Simplified illustration of the LICOR 7000 working principle - adapted from LI-COR (2007).

3.3. Adapted Analysis Procedure

This section explains the adapted analysis procedure to determine nitrogen oxide emission indices. It is clearly indicated if an existing routine is implemented, adapted or improved to meet the research goals.

3.3.1. Emission Index Calculation

Several steps are necessary to derive experimental emission indices. As introduced in Section 3.1, both NO_y and CO_2 concentration enhancements relative to the background concentration in ambient air must be determined during a plume encounter. NO_y concentration time series are determined following the procedure outlined below. CO_2 concentration time series in 1 Hz resolution are provided by a co-worker. For both species background concentrations must be determined for plume encounter sequences, based on background measurements before and after entering the exhaust. Plume starting- and end times are specified and quantified concentration enhancements are integrated over the determined time interval to obtain values for ΔNO_y and ΔCO_2. The emission index for the respective plume is quantified according to Equation 3.1.

Nitrogen Oxide Concentration

As explained in Subsection 3.2.1, calibrations are necessary to establish the linear relation between the measured signal and the NO concentration of the sample air. These calibrations are performed on a regular basis during the time frame of the test campaign to obtain calibration parameters representative for all emission test flights. These calibration parameters comprise three values: one value expressing the sensitivity m, one value expressing the converter efficiency η_C for the conversion from NO_y to NO (see Subsection 3.2.1) and one value expressing the NO signal $S_{NO,ZA}$ at Zero Air (ZA) conditions, defining the systems offset. The mean of all calibrations is determined for each calibration parameter. Table 3.10 summarizes the calibrations performed as a part of this research to quantify the respective mean values. In the

following, it is outlined in detail how calibration parameters are obtained.

Table 3.10: Summary of performed nitrogen oxide measurement instrument calibrations during VOLCAN, including the offset signal $S_{NO,ZA}$, the sensitivity m and the converter efficiency η_C, as well as respective mean values.

Calibration Date	$S_{NO,ZA}$ / Hz	m / Hz ppb^{-1}	η_C / %
01/25/2023	26	887	100.0
02/14/2023	256	900	99.7
03/01/2023	99	882	99.6
03/08/2023	78	866	96.4
03/16/2023	24	897	98.8
03/23/2023	61	915	100.0
Mean	**91**	**891**	**99.1**

The mean sensitivity $\overline{m}$ is required to relate a measured signal enhancement to a NO concentration enhancement. The value for each calibration is established by performing measurements for a set of known concentrations. The tested concentration sequence is illustrated in Figure 3.8, presenting the measured time series for the calibration on March 16. It is shown that framed by ZA measurements, a set of seven concentrations is investigated, ranging from 3 ppb to 200 ppb. It is aimed to cover as much as possible of the concentration range expected during emission measurement flights. However, calibrations are limited by available reference gases, not allowing to generate concentrations close to the detection limit, as encountered during test flights. A linear regression through all test points is applied to derive the sensitivity m for the respective calibration. Figure 3.9 presents the curve obtained for March 16. A coefficient of determination R^2 of 1 is quantified, proving the linear relationship between NO concentration and measured count rate.

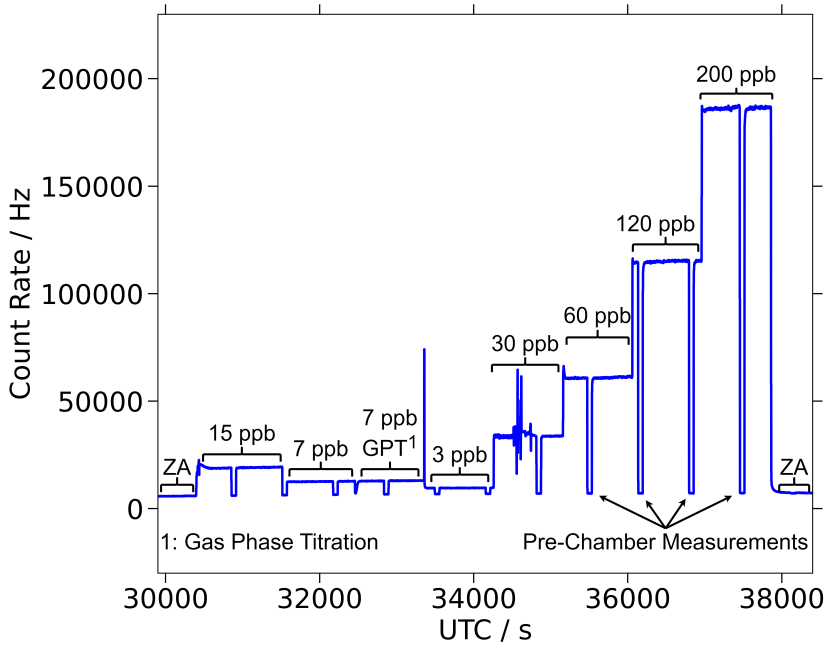

Figure 3.8: Time sequence of tested concentrations during calibration on March 16.

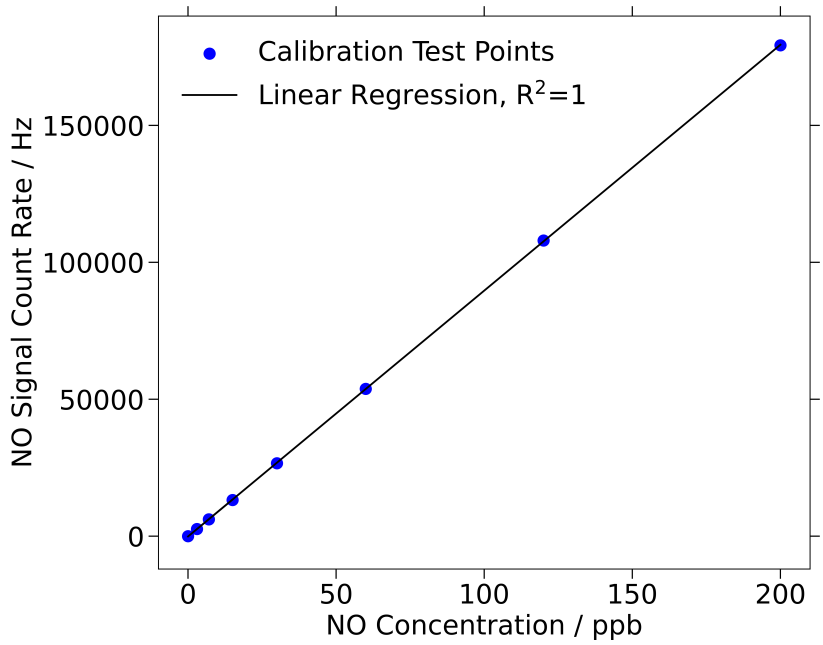

Figure 3.9: Obtained linear regression curve for calibration on March 16.

A gas phase titration during calibrations allows to specify the converter efficiency η_C applied in Equation 3.12 (Feigl, 1998). Figure 3.8 indicates that the NO concentration of 7 ppb is tested twice: once in normal calibration mode and once applying gas phase titration. During gas phase titration, ozone is generated to oxidize NO contained in the sample gas to NO_2. Hence, NO_2 must be converted back to NO by the converter. Based on the difference in received signal for both 7 ppb tests, the efficiency of the converter can be quantified as stated in Equation 3.10.

$$\eta_C = \frac{S_{main,7ppb,GPT} - S_{pre,7ppb,GPT} - \bar{S}_{NO,ZA}}{S_{main,7ppb} - S_{pre,7ppb} - \bar{S}_{NO,ZA}} \tag{3.10}$$

Both Equation 3.12 and Equation 3.10 require the term $\bar{S}_{NO,ZA}$ to correct the measured main-chamber signal for the offset of the system. As explained in Subsection 3.2.1, pre-chamber measurement signals S_{pre} must be subtracted from the main-chamber measurement signal S_{main} to determine the NO signal S_{NO}. Nevertheless, an offset is obtained for ZA measurements, meaning that for a sample without NO concentration there is still an offset signal $S_{NO,ZA} \neq 0$ received, as defined in Equation 3.11. Hence, this correction must be considered when computing S_{NO}. It is determined using the mean values for $S_{main,ZA}$ and $S_{pre,ZA}$ of the two ZA measurements indicated in Figure 3.8.

$$S_{NO,ZA} = \bar{S}_{main,ZA} - \bar{S}_{pre,ZA} \tag{3.11}$$

Obtained calibration parameters are applied to determine the concentration time series. For emission test flights the NO_y concentration $NO_{y,measured}$ at a certain time t can be obtained according to Equation 3.12. $S_{main}(t)$ is the measured signal in main-chamber mode. $S_{pre,int.}(t)$ is the pre-chamber signal at the same time obtained by interpolating through all pre-chamber sequences within the time series of the respective emission test flight, remembering that a

pre-chamber measurement of about 60 s is performed roughly every 10 min, as explained in Subsection 3.2.1. Different than for previous publications the interpolation is obtained through a polynomial fitting, applying the method of Least Squares to increase accuracy compared to the conventional, linear approach. Together with determined mean calibration values, the concentration time series can be established.

$$NO_{y,measured}(t) = \frac{\left(S_{main}(t) - S_{pre,int.}(t) - \overline{S_{NO,ZA}}\right)}{\overline{m} \cdot \overline{\eta_C}} \tag{3.12}$$

A dilution correction is required to obtain the final NO_y concentration. Subsection 3.2.1 outlines that a dilution system is integrated to increase the upper detection limit of the nitrogen oxide measurement instrument. To convert the measured concentration $NO_{y,measured}(t)$ to the final concentration $NO_{y,final}(t)$, the volume flow of the ZA used for dilution must be considered. Applying Equation 3.13, $NO_{y,final}$ is determined by calculating the reversed volume flow fraction of the sample air. Q_{total} is the total volume flow within the nitrogen oxide measurement instrument and $Q_{dilution}$ is the ZA volume flow added by the dilution system.

$$NO_{y,final}(t) = NO_{y,measured}(t) \cdot \frac{Q_{total}}{Q_{total} - Q_{dilution}} \tag{3.13}$$

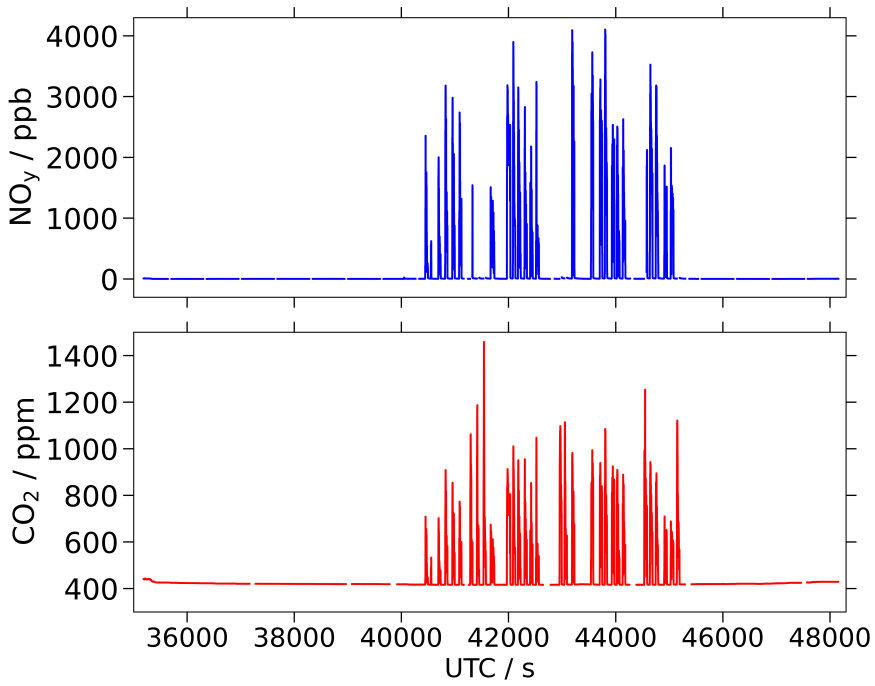

Figure 3.10: NO_y and CO_2 concentration time series of Flight 1 (02/28/2023).

The NO_y concentration time series obtained for Flight 1 (02/28/2023) by following the outlined procedure is shown in Figure 3.10. In addition, the according CO_2 concentration time series is provided. The figure contains a sequences for which CO_2 enhancements are visible without according NO_y values. Those values are taken out of the time series, as the maximum detection limit is exceeded. During this research this is the case for some plume encounters

for the high T3 setting, even if compared to a previous study the dilution system is adapted by increasing the dilution ratio. Received values are not representative and consequently, not considered.

Background Interpolation

Interpolating NO_y- and CO_2 background concentrations for plume encounters is necessary to determine experimental nitrogen oxide emission indices. Above, it is explained how concentration time series are obtained. According to Section 3.1, it is required to determine the concentration enhancements during exhaust plume encounters compared to the concentrations in ambient background conditions. While measuring the concentrations within the plume, no simultaneous measurements of background concentrations are possible. Thus, an interpolation using background sequences throughout the emission test flights is required. For the first time, a Least Squares polynomial fit is applied for this purpose, replacing the in previous studies applied linear approach. Better results with reduced background uncertainty are expected.

Plume Definition

Once the concentration time series of NO_y and CO_2, as well as their continuous background concentrations are known, the individual plume sequences are defined to determine the respective emissions index. As introduced in Section 3.1, the concentration enhancements within the exhaust plume must be determined. Hence, for each species, the background concentration time series, obtained as described above, is subtracted from the total concentration time series. The obtained enhancement is integrated over the respective plume sequence as described by Equation 3.14 and Equation 3.15, where A is the plume start and B the plume end. For this purpose, the numerical integration approach postulated by Simpson is applied (Cartwright, 2017). $NO_{y,bgr}(t)$ and $CO_{2,bgr}(t)$ are the background concentration time series of NO_y and CO_2, determined as described above.

$$\Delta NO_y = \int_A^B \left(NO_{y,final}(t) - NO_{y,bgr}(t)\right) dt \tag{3.14}$$

$$\Delta CO_2 = \int_A^B \left(CO_2(t) - CO_{2,bgr}(t)\right) dt \tag{3.15}$$

Plume start and plume end are selected for each plume encounter. The plume start is defined as a point at which the concentration time series of either NO_y or CO_2 starts to exceed the background level variation. The plume end is defined as a point at which both time series have returned to background level variations. This approach ensures that it is accounted for the full enhancement of both species, considering the different response times of the two instruments, the difference in tubing length and the difference in inlet position. Figure 3.11 illustrates three selected plume encounters during Flight 1 (02/28/2023) and their respective plume boundaries.

Specified conditions must be met by each plume to be considered for this research. A minimum encounter duration of 10 s is defined to ensure that accidental plume crossings do not contribute to the analysis. This is important as it must be guaranteed that the measurement instrument inlets depicted in Figure 3.1 are positioned fully within the plume. Further, it must be assured that the investigated engine is stabilized at the desired condition for the respective test point. A maximum combustor inlet temperature deviation of ± 3 K within the plume sequence is

chosen. However, this is not the case for any encounter of the four flights.

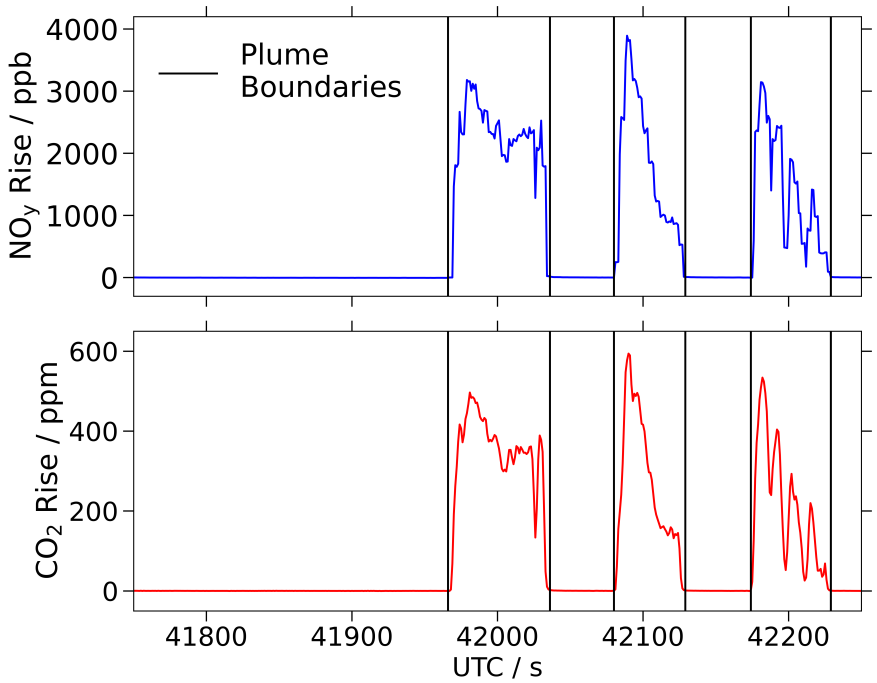

Figure 3.11: NO_y and CO_2 concentration enhancements with defined plume boundaries during a selected sequence of Flight 1 (02/28/2023).

3.3.2. Error Analysis

The uncertainty of experimentally determined nitrogen oxide emission indices is assessed in a statistical manner by applying Gaussian Error Propagation. Equation 3.16 states how the error is obtained by approximating the first order Tailor series expansion. It must be noted that both statistical and systematic errors are combined in the presented method, even if the Gaussian Error Propagation is a purely statistical approach. Still, it is believed to provide a meaningful error assessment, being equivalent to methods applied in previous aircraft emission studies (e.g., Stratmann, 2013; Harlass et al., in preparation). A different approach can be to evaluate statistical and systematic errors individually, however for the sake of comparability the established method is chosen.

$$
\begin{aligned}
Error = s_{EI(\mathrm{NO_x})} = \pm \Bigg[& \left(\frac{\partial EI\,(\mathrm{NO_x})}{\partial \Delta NO_y} s_{NO_{y,final}} \right)^2 + \left(\frac{\partial EI\,(\mathrm{NO_x})}{\partial \Delta NO_y} s_{NO_{y,bgr}} \right)^2 \\
& + \left(\frac{\partial EI\,(\mathrm{NO_x})}{\partial \Delta CO_2} s_{CO_2} \right)^2 + \left(\frac{\partial EI\,(\mathrm{NO_x})}{\partial \Delta CO_2} s_{CO_{2,bgr}} \right)^2 \\
& + \left(\frac{\partial EI\,(\mathrm{NO_x})}{\partial EI(\mathrm{CO_2})} s_{EI(\mathrm{CO_2})} \right)^2 + \left(\frac{\partial EI\,(\mathrm{NO_x})}{\partial M(\mathrm{NO_2})} s_{M(\mathrm{NO_2})} \right)^2 + \left(\frac{\partial EI\,(\mathrm{NO_x})}{\partial M(\mathrm{CO_2})} s_{M(\mathrm{CO_2})} \right)^2 \Bigg]^{\frac{1}{2}}
\end{aligned}
\tag{3.16}
$$

The equation indicates that several contributors are considered, covering all terms of Equation 3.1:

- Concentration accuracy of both NO_y and CO_2: $s_{NO_{y,final}}$ and s_{CO_2}
- Background uncertainty of both NO_y and CO_2: $s_{NO_{y,bgr}}$ and $s_{CO_{2,bgr}}$
- Uncertainty of determined EI(CO_2) values: $s_{EI(CO_2)}$
- Uncertainty of molar masses of both NO_2 and CO_2: $s_{M(NO_2)}$ and $s_{M(CO_2)}$

The accuracy of measured CO_2 concentrations is constant with value of 0.221 ppm. The EI(CO_2) uncertainty is determined based on the uncertainty of hydrogen content measurements. A constant value of 0.1% is determined. The estimated molar mass uncertainties of NO_2 and CO_2 are 0.002% and 0.003%. The NO_y concentration accuracy, as well as the background uncertainties of both NO_y and CO_2 require a more extensive analytical approach. Both methods are outlined in the following.

Nitrogen Oxide Concentration Accuracy

Different to the accuracy of measured CO_2 concentrations, the NO_y accuracy is not constant and scales with the NO_y mixing ratio. Lowest values of about 4.9 ppb are obtained at background concentration levels of 3.5 ppb near the detection limit and highest values of about 450 ppb are derived for highest encountered concentrations of about 4080 ppb. According to Harlass et al. (in preparation), three contributors are distinguished and combined, as specified in Equation 3.17: the uncertainty of the NO mixing ratio within the measurement instrument $s_{NO_{y,measured}}$, the uncertainty resulting from the integrated dilution system $s_{NO_{y,dilution}}$ and an additional conversion efficiency uncertainty $s_{NO_{y,C}}$ relevant for very high concentrations in the near field. Linear error propagation is applied to derive the individual terms, as explained below.

$$s_{NO_{y,final}} = \sqrt{\left(s_{NO_{y,measured}}\right)^2 + \left(s_{NO_{y,dilution}}\right)^2 + \left(s_{NO_{y,C}}\right)^2} \tag{3.17}$$

The NO mixing ratio uncertainty $s_{NO_{y,measured}}$ is quantified considering several contributors:

- Statistical variation of the main chamber count rate: $s_{S_{main}}$
- Statistical variation of the pre-chamber count rate: $s_{S_{pre}}$
- Offset uncertainty: $s_{S_{NO,ZA}}$ (±165 counts)
- Sensitivity uncertainty: s_m (±95 counts ppb^{-1})
- Converter efficiency uncertainty (for moderate concentrations): s_{η_C} (±2.7 %)

As stated in Equation 3.18, linear error propagation is applied (Stratmann, 2013) to obtain a more conservative estimate.

$$\begin{aligned} s_{NO_{y,measured}} = &\frac{\partial NO_{y,measured}}{\partial S_{main}} s_{S_{main}} + \frac{\partial NO_{y,measured}}{\partial S_{pre}} s_{S_{pre}} + \frac{\partial NO_{y,measured}}{\partial S_{NO,ZA}} s_{S_{NO,ZA}} \\ &+ \frac{\partial NO_{y,measured}}{\partial m} s_m + \frac{\partial NO_{y,measured}}{\partial \eta_C} s_{\eta_C} \end{aligned} \tag{3.18}$$

Uncertainties resulting from the applied dilution system are estimated based on the respective mass flow controller accuracy, as stated in Equation 3.19. $s_{Q_{total}}$ is the total volume flow uncertainty within the instrument and $s_{Q_{ZA}}$ is the uncertainty of the dilution volume flow.

Again, the more conservative linear error propagation is applied (Stratmann, 2013).

$$s_{NO_{y,dilution}} = \frac{\partial NO_{y,final}}{\partial NO_{y,measured}} s_{NO_{y,measured}} + \frac{\partial NO_{y,final}}{\partial Q_{ZA}} s_{Q_{ZA}} + \frac{\partial NO_{y,final}}{\partial Q_{total}} s_{Q_{total}} \tag{3.19}$$

For near field measurements an additional uncertainty $s_{NO_{y,C}}$ is introduced due to very high concentrations (Harlass et al., in preparation). It is assumed that NO_2 is responsible for about 15% of measured NO_y and that the converter only converts 70% to NO. Hence, the remaining 30% are not detected and the resulting uncertainty is determined according to Equation 3.20.

$$s_{NO_{y,C}} = \frac{15\% \cdot 30\%}{100\%} = 4.5\% \tag{3.20}$$

Background Uncertainties
Background uncertainties of both NO_y and CO_2 are composed of two terms: the standard deviation of background measurements and the difference between interpolated background and real background. Equation 3.21 and Equation 3.22 specify how the terms are combined (Harlass et al., in preparation).

$$s_{NO_{y,bgr}} = \sqrt{\left(s_{NO_{y,bgr,sdev}}\right)^2 + \left(s_{NO_{y,bgr,mean,diff}}\right)^2} \tag{3.21}$$

$$s_{CO_{2,bgr}} = \sqrt{\left(s_{CO_{2,bgr,sdev}}\right)^2 + \left(s_{CO_{2,bgr,mean,diff}}\right)^2} \tag{3.22}$$

For each plume the standard deviation is determined for a time-wise close background sequence. In Subsection 3.3.1 it is explained that an interpolation of the background concentration is established to obtain background values during plume encounters. For this, several background sequences between certain test points are selected to determine an average concentration over a time of at least 30 s. For each plume encounter the closest of these background sequences is chosen and the standard deviation is determined. This value is then used for the respective plume to calculate the background uncertainty. The same procedure is applied for both NO_y and CO_2 to determine the terms $s_{NO_{y,bgr,sdev}}$ and $s_{CO_{2,bgr,sdev}}$.
As the interpolated background is used to determine the plume enhancement of measured concentrations, the local difference to the real background is considered to determine the background uncertainty of NO_y and CO_2. The mean value of the real background over three seconds is determined directly before the plume encounter and directly after the plume encounter. Both values are compared to the determined background concentration through interpolation for the respective plume and the uncertainty terms $s_{NO_{y,bgr,mean,diff}}$ and $s_{CO_{2,bgr,mean,diff}}$ are established.

3.3.3. Statistical Considerations

Known statistical methods are applied to support the interpretation of obtained data to answer the posed research questions. Two distinguished hypothesis tests are of interest for this research: the two-sided T-test and the Mann-Whitney U rank test.

Two-sided T-test

The T-test according to Welch (1938) is applied to evaluate the statistic significance of experimental observations of this research. It compares the means of two independent sample groups of unequal variance. The according null hypothesis is that these groups have the same mean. An important assumption for its application is that analyzed sample groups are normally distributed. The so-called test statistic t is determined according to Equation 3.23, where $\overline{x}_1$ and $\overline{x}_2$ are the means, s_1 and s_2 the variances, and n_1, as well as n_2 the amount of samples of the two groups. The higher $|t|$, the more likely it is according to the T-test that the null hypothesis is not true, meaning that there is a statistically significant difference between the means of the sample groups. Based on the obtained t-value, a p-value p_T can be derived, describing the probability that observed sample groups would occur for the null hypothesis of equal means. A significance level of $\alpha = 0.05$ is selected. Thus, the null hypothesis is rejected for $p_T < \alpha$. For $p_T > \alpha$ however, the particular sample provides insufficient evidence for rejection. It is important to note that this result does not prove the null hypothesis.

$$t = \frac{(\overline{x}_1 - \overline{x}_2)}{\sqrt{\frac{s_1^2}{n_1} + \frac{s_2^2}{n_2}}} \tag{3.23}$$

Mann-Whitney U Rank Test

The Mann-Whitney U Rank test is another approach to check whether there is a significant difference between two independent sample groups. Different than the T-test, it is a non-parametric method, applied in this research to account for the low number of samples. It goes back to the work of Wilcoxon (1992) and Mann and Whitney (1947). The null hypothesis states that there is no difference in the tendency of the two sample groups. Hence, it slightly deviates from the null hypothesis formulated for the T-test comparing the respective means.
The Mann-Whitney U Rank test establishes a ranking, resulting in the test statistic U. Samples of both groups are combined and sorted according to their value. Equation 3.24 and Equation 3.25 describe how often samples of one group are exceeded by samples of the other group, where T_1 and T_2 are the sums of the positions in the ranking of the respective group. Equation 3.26 describes the null hypothesis that there is no difference between the sample groups, as ranks of both groups are exceeded equally often. Based on the lower U value, a p-value p_{MW} is established. This value is again compared to the selected significance level of $\alpha = 0.05$ and conclusions are drawn in the same manner as explained for the T-test.

$$U_1 = n_1 \cdot n_2 + \frac{n_1 \cdot (n_1 + 1)}{2} - T_1 \tag{3.24}$$

$$U_2 = n_1 \cdot n_2 + \frac{n_2 \cdot (n_2 + 1)}{2} - T_2 \tag{3.25}$$

$$U_1 = U_2 \tag{3.26}$$

3.4. Far Field Measurements VOLCAN and ECO-Demonstrator

Near field results are compared to far field measurements. It is explained in Section 1.2 that due to a lack of experience with near field measurements, well-established far field measurements are conducted for evaluation. This section outlines the applied methods during two distinguished campaigns to obtain relevant data.
Some differences exist between near and far field tests. Emissions in the far field are measured several kilometers behind the source aircraft, while near field emissions during VOLCAN are investigated at a mean distance of about 98m. Due to the higher distance during far field measurements, the plumes of the source aircraft's engines are not clearly separated anymore. Thus, both engines are investigated simultaneously, operating at the same engine setting. Further, the Mach number during far field measurements is higher, since near field measurements require a slightly reduced cruise speed due to performance limitations of the Falcon.
Far field data is obtained during two distinguished emission measurement campaigns. As for near field data, far field data is collected during the VOLCAN campaign, enabling a comparison with the same source aircraft equipped with identical engines. In addition, a chase flight with NASA's measurement platform DC-8 is performed in the far field of a Boeing 737-10 as a part of the ECO-Demonstrator campaign. Cooperation partners include DLR, NASA, Boeing and GE Aerospace. Both involved aircraft are shown in Figure 3.12. The Boeing 737-10 is powered by two LEAP-1B engines, incorporating the same combustion technology as the LEAP-1A engine, investigated during VOLCAN. On board of the DC-8 the same measurement techniques are applied to sample nitrogen oxide and carbon dioxide concentrations. Hence, results obtained for VOLCAN can be set in contrast with measurements obtained independently during a different campaign. In the following, experimental setup and sampling strategy of both campaigns are presented.

(a) **(b)**

Figure 3.12: (a) Measurement platform DC-8 (Registration: N817NA) and (b) source aircraft Boeing 737-10 (Registration: N27601), equipped with two CFM LEAP-1B engines - own illustration.

VOLCAN

As a part of VOLCAN, one far field flight is performed to evaluate near field data. Airspace above the northern Bay of Biscay is used. The route is illustrated in Figure 3.13. As Table 3.11 specifies, Jet A-1 and HEFA SPK are both tested in forced pilot-only, as well as in pilot+main combustion mode. The chosen cruise combustor inlet temperature setting of both engines is comparable with mid T3 setting of the near field flights, deviating by about 3 K. The purpose of the measurements is to identify whether absolute emission indices of near and far field agree and to analyze if uncertainties are reduced in the near field. During VOLCAN, the far field

measurement distance ranges from 8.0 to 14.2 km, with a mean of 9.8 km.

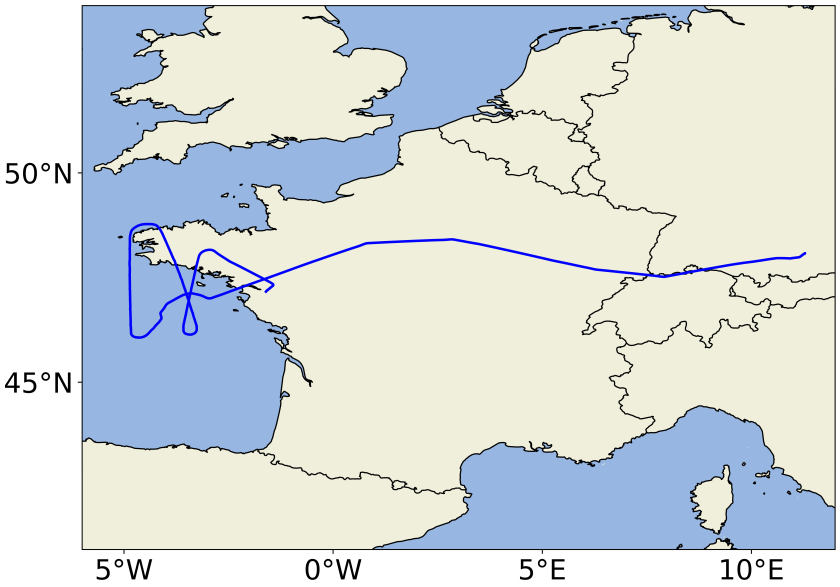

Figure 3.13: Route of the Falcon during VOLCAN far field emission test flight (03/22/2023).

Table 3.11: Flight conditions in terms of Mach number M, flight level FL and total air temperature TAT, as well as test points in terms of tested engine, tested fuel, combustion mode, T3 setting, mean normalized combustor inlet temperature $\Delta T3$, mean normalized fuel flow ΔFF and number of samples n during VOLCAN far field test flight (03/22/2023).

Flight	Flight Conditions	Tested Engine	Tested Fuel	Combustion Mode	T3 Setting	Δ T3 / K	Δ FF / kg h^{-1}	n / -
Far Field VOLCAN	M=0.76±0.007 FL=330±2 ft TAT=244±1 K	Both	Jet A-1	Pilot only	Cruise	3.2±0	49.9±16	18
				Pilot+Main	Cruise	3.2±0	57.4±10	11
			HEFA SPK	Pilot only	Cruise	3.2±1	35.4±9	16
				Pilot+Main	Cruise	3.2±0	33.2±11	9

ECO-Demonstrator

During the ECO-Demonstrator campaign one dedicated flight is chosen for comparison with VOLCAN results. The flight route extends along the Pacific coast of Oregon, United States of America, as it can be inferred from Figure 3.14. As for the VOLCAN farifield flight, two fuels are investigated: Jet A-1 and HEFA SPK. Finalized fuel sample analyses are not available prior publication of this research. Thus, values for $EI(CO_2)$ determined for VOLCAN are applied. Emission indices are determined at cruise condition, as provided in Table 3.12. However, it must be noted that engine specific data including combustor inlet temperature and fuel flow are not available at this point, as the campaign took place in October 2023. Thus, presented ECO-Demonstrator data is preliminary. Nevertheless, initial data analysis indicates stabilized engine operating conditions during sampling. The purpose of the measurements is to investigate if dependencies between engine operation and nitrogen oxides derived from VOLCAN near field measurements can be confirmed.

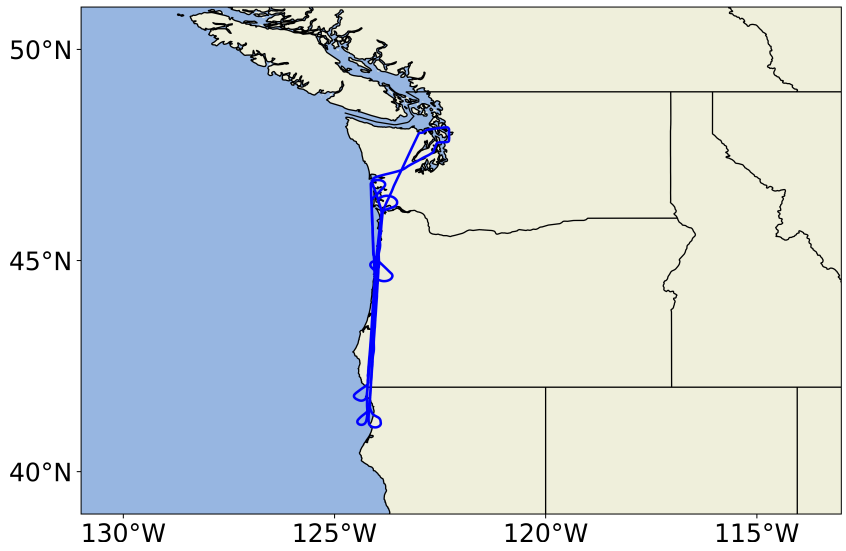

Figure 3.14: Route of the DC8 during ECO-Demonstrator far field emission test flight (10/26/2023).

Table 3.12: Flight conditions in terms of Mach number M, flight level FL and total air temperature TAT, as well as test points in terms of tested engine, tested fuel, combustion mode and number of samples n during ECO-Demonstrator far field test flight (10/26/2023).

Flight	Flight Conditions	Tested Engine	Tested Fuel	Combustion Mode	n
Far Field ECO-Demonstrator	M≈0.76 FL≈330 TAT≈218 K	Both	Jet A-1	Pilot+Main	15
			HEFA SPK	Pilot+Main	8

4
Results and Discussion

This chapter presents and discusses results of the conducted research. While Section 4.1 addresses the first research question with its four subquestions focused on dependencies between engine parameters and nitrogen oxides, Section 4.2 compares obtained near field emission indices with far field measurements to answer the second research question.

Disclaimer: Normalized values are used to describe this research's outcome. As outlined in Section 3.1, the combustor inlet temperature is proprietary and therefore, values relative to mid T3 setting are provided. Fuel flow FF and nitrogen oxide emission indices $EI(\mathrm{NO_x})$ are described relative to representative values at mid T3 setting. For the latter, the chosen reference value $EI(\mathrm{NO_x})_{ref}$ is given below. It is not disclosed in the public version of this thesis.

Continuous color- and shape coding is applied for presented figures. Colors specify the fuel type burned during the plume sequence of the respective emission index. The circular shape indicates measurements in forced pilot-only mode, while triangles mark pilot+main combustion.

4.1. Observed Dependencies between Nitrogen Oxides and Engine Parameters

This section aims to answer the first research question:

> **1. Do in situ near field measurements confirm expected dependencies between engine parameters and $\mathrm{NO_x}$ emissions?**

Four subquestions are defined to investigate the problem, focusing on fuel type, T3 setting, combustion mode and engine degradation. Each subsection from Subsection 4.1.1 to Subsection 4.1.4 is dedicated to one of these aspects.

4.1.1. Fuel Type

This subsection focuses on the first subquestion:

> **1.1 Does a change from Jet A-1 to Sustainable Aviation Fuel affect $\mathrm{NO_x}$ emissions?**

As outlined in Section 3.1, three different SAF blends are compared to Jet A-1 as a part of this research: 100% HEFA SPK, HEFA SPK+LA and HEFA SPK+HA. Their properties are specified in Table 3.1. Emissions are measured for different T3 settings, as well as combustion modes, defined in Table 3.3 and Table 3.4. In the following, normalized emission indices of each alternative fuel are compared to Jet A-1 individually. A summary discussing the results with relevant literature is provided.

HEFA SPK

Nitrogen oxide emissions obtained burning Jet A-1 and HEFA SPK are compared during Flight 4 (03/27/2023). The fuels are tested at mid T3 setting in forced pilot-only and pilot+main combustion mode. The test matrix with flight conditions is provided in Table 3.9.

At mid T3 setting in forced pilot-only combustion mode, agreement is found between the normalized emission indices obtained for Jet A-1 and HEFA SPK. The six Jet A-1 plume encounters shown in Figure 4.1 lead to a mean $\Delta EI(NO_x)$ of 2.99 g NO_2 kg^{-1}. Four measurements with HEFA SPK result in a mean of 1.76 g NO_2 kg^{-1}. As specified in Table 4.1, a deviation Δ of 1.23 g NO_2 kg^{-1} is identified. Considering that typical absolute values of nitrogen oxide emission indices lay in the range from 12 to 17 g NO_2 kg^{-1} (Lee et al., 2010), it can be concluded that the difference is in the order of 7-10%. However, it is shown that combined standard deviations s and combined mean errors $\overline{Error}$ exceed observed discrepancies between the two sample groups. Hence, no distinct differences can be inferred from presented data.

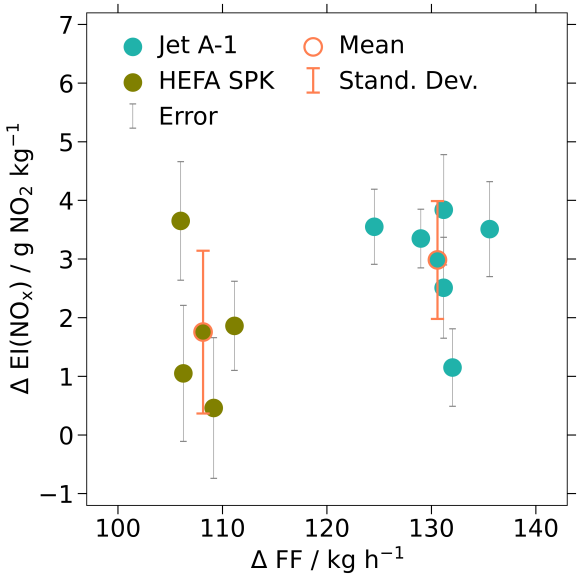

Figure 4.1: Normalized nitrogen oxide emission indices $\Delta EI(NO_x)$ for Jet A-1 and HEFA SPK at mid T3 setting in forced pilot-only combustion mode during Flight 4 (03/27/2023), including individual measurement errors $Error$, as well as the mean emission index $\overline{\Delta EI(NO_x)}$ and the standard deviation s for each fuel.

Table 4.1: Comparison between Jet A-1 and HEFA SPK at mid T3 setting in forced pilot-only combustion mode during Flight 4 (03/27/2023), including the number of samples n, normalized mean emission indices $\overline{\Delta EI(NO_x)}$, absolute mean emission index errors $\overline{Error}$, absolute standard deviations of the sample groups s, the absolute difference between normalized mean emission indices of the sample groups Δ, the p-value resulting from the T-test p_t and the p-value resulting from the Mann-Whitney U rank test p_{MW}.

Fuel	n / -	$\overline{\Delta EI(NO_x)}$ / g NO_2 kg^{-1}	$\overline{Error}$ / g NO_2 kg^{-1}	s / g NO_2 kg^{-1}	Δ / g NO_2 kg^{-1}	p_T / -	p_{MW} / -
Jet A-1	6	2.99	0.74	1.01	1.23	0.187	0.257
HEFA SPK	4	1.76	1.03	1.39			

Statistical analyses support the described observations. As described in Subsection 3.3.3, a T-test and a Mann-Whitney U rank test are performed to obtain an additional indication whether investigated sample groups agree. Table 4.1 shows that a p-value p_T of 0.187 is

obtained for the T-test. This value is higher than the chosen significance level of 0.05. Therefore, the null-hypothesis stating that there is no statistically significant difference between the means of the two sample groups cannot be rejected. The same conclusion is drawn regarding the Mann-Whitney U rank test, resulting in a p-value p_{MW} of 0.114 and hence, not suggesting that the groups belong to different populations.

Statistically significant differences between emissions of Jet A-1 and HEFA SPK are observed at mid T3 setting in pilot+main combustion mode. As illustrated in Figure 4.2, both sample groups show similar $\Delta EI(NO_x)$ scattering and two distinctive accumulations of emission indices are visible. The mean index determined for HEFA SPK is by 1.38 g NO_2 kg^{-1} lower compared to the Jet A-1 value, as specified in Table 4.2. Engine data does not indicate significant differences during the respective measurement sequences and both statistical tests suggest to reject the null hypothesis of equal means, resulting in p-values of 0.006 and 0.014. Thus, even if determined mean nitrogen oxide emission indices agree within combined standard deviations and quantified mean measurement errors add up to the observed difference, discrepancies between the sample groups are significant at the investigated engine setting.

Table 4.2: Comparison between Jet A-1 and HEFA SPK at mid T3 setting in pilot+main combustion mode during Flight 4 (03/27/2023), including the number of samples n, normalized mean emission indices $\overline{\Delta EI(NO_x)}$, absolute mean emission index errors $\overline{Error}$, absolute standard deviations of the sample groups s, the absolute difference between normalized mean emission indices of the sample groups Δ, the p-value resulting from the T-test p_t and the p-value resulting from the Mann-Whitney U rank test p_{MW}.

Fuel	n / -	$\overline{\Delta EI(NO_x)}$ / g NO_2 kg^{-1}	$\overline{Error}$ / g NO_2 kg^{-1}	s / g NO_2 kg^{-1}	Δ / g NO_2 kg^{-1}	p_T / -	p_{MW} / -
Jet A-1	7	3.29	1.18	0.69	1.38	0.006	0.014
HEFA SPK	6	1.92	0.79	0.76			

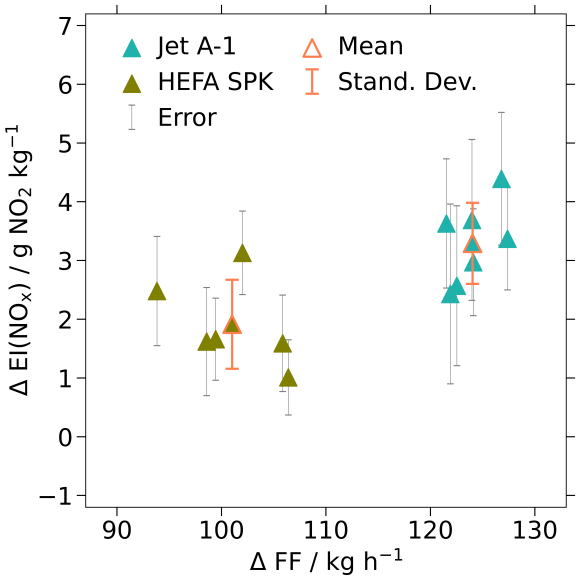

Figure 4.2: Normalized nitrogen oxide emission indices $\Delta EI(NO_x)$ for Jet A-1 and HEFA SPK at mid T3 setting in pilot+main combustion mode during Flight 4 (03/27/2023), including individual measurement errors $Error$, as well as the mean emission index $\overline{\Delta EI(NO_x)}$ and the standard deviation s for each fuel.

In summary, Jet A-1 and HEFA SPK are investigated in two different combustion modes

at the same combustion inlet temperature setting. For both conditions, determined nitrogen oxide emission indices of the respective fuels agree within the standard deviation of the sample groups. Considering estimated measurement uncertainties, no distinct discrepancies can be inferred from the reported results. This interpretation is endorsed by measurements with two different blends of Jet A-1 and HEFA SPK during Flight 1 (02/28/2023), provided in Appendix A. However, in one of the two here presented cases, statistically significant differences are indicated by statistical tests. Thus, minor deviations in nitrogen oxide emissions between the fuels cannot be excluded. It is observed that normalized mean emission indices for HEFA SPK are always lower than for Jet A-1.

HEFA SPK+LA

Jet A-1 and HEFA SPK+LA emissions are analyzed at three different T3 settings and in two different combustion modes. In forced pilot+only combustion mode nitrogen oxides are quantified at mid, low and high power setting. For pilot+main combustion only mid power setting is tested. Conditions and test points during the with HEFA SPK+LA measurements associated Flight 2 (03/11/2023) are provided in Table 3.7.

Very good agreement is found between emissions indices for Jet A-1 and HEFA SPK+LA when testing the fuels at mid power setting in pilot-only combustion mode. The results illustrated in Figure 4.3 indicate that the obtained mean values of both sample groups are almost identical with a difference of 0.04 g NO_2 kg^{-1} as specified in Table 4.3, recalling typical absolute values for nitrogen oxide emission indices mentioned above. This observation is underlined by the statistical tests, resulting in very distinctive p-values of 0.960 and 1.000 for the T and Mann-Whitney U rank test. Shown standard deviations of the sample groups and measurement errors of the individual indices support that based on the presented data no significant difference between the emissions of the two fuels can be inferred at the analyzed setting.

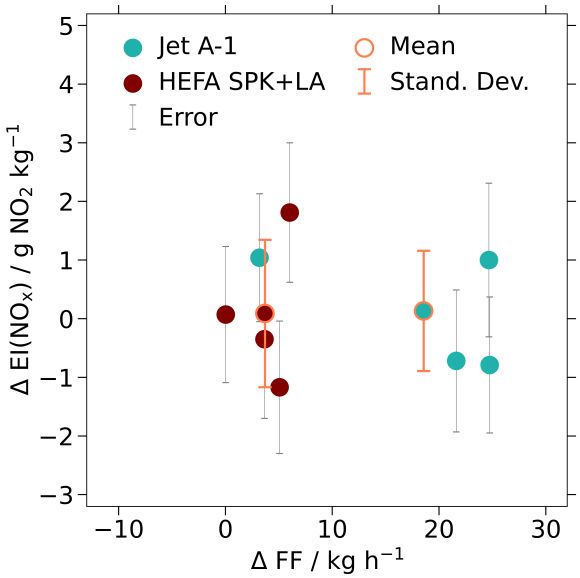

Figure 4.3: Normalized nitrogen oxide emission indices $\Delta EI(NO_x)$ for Jet A-1 and HEFA SPK+LA at mid T3 setting in forced pilot-only combustion mode during Flight 2 (03/11/2023), including individual measurement errors $Error$, as well as the mean emission index $\overline{\Delta EI(NO_x)}$ and the standard deviation s for each fuel.

Table 4.3: Comparison between Jet A-1 and HEFA SPK+LA at mid T3 setting in forced pilot-only combustion mode during Flight 2 (03/11/2023), including the number of samples n, normalized mean emission indices $\overline{\Delta EI(NO_x)}$, absolute mean emission index errors $\overline{Error}$, absolute standard deviations of the sample groups s, the absolute difference between normalized mean emission indices of the sample groups Δ, the p-value resulting from the T-test p_t and the p-value resulting from the Mann-Whitney U rank test p_{MW}.

Fuel	n / -	$\overline{\Delta EI(NO_x)}$ / g NO_2 kg^{-1}	$\overline{Error}$ / g NO_2 kg^{-1}	s / g NO_2 kg^{-1}	Δ / g NO_2 kg^{-1}	p_T / -	p_{MW} / -
Jet A-1	4	0.13	1.19	1.03	0.04	0.960	1.000
HEFA SPK+LA	4	0.09	1.21	1.26			

Measurements at low and high combustor inlet temperature in forced pilot-only mode are in good agreement with here presented results for mid T3 setting. In both cases the deviation between the means is lower than 1 g NO_2 kg^{-1} and exceeded by combined standard deviations of the sample groups, as well as by combined errors of the individual indices. Statistical tests suggest that there is no statistically significant difference between the compared sample groups. Detailed results are provided in Appendix A.

As for the HEFA SPK measurements, highest differences between the fuels are obtained in pilot+main combustion mode. The results provided in Figure 4.4 indicate that emissions determined for HEFA SPK+LA are by 1.44 g NO_2 kg^{-1} higher than the values for Jet A-1. Both T and Mann-Whintey U rank test agree in their outcome that there is a statistically significant difference between the two sample groups, as the p-values reported in Table 4.4 are below the chosen significance level of 0.05. As for the comparison between Jet A-1 and HEFA SPK, this is the case even if the mean values of both groups agree within combined standard deviations and combined mean measurement errors exceed the observed deviation. Hence, as concluded for measurements with HEFA SPK at the here investigated engine setting, data suggests a statistically significant difference between the emissions of the tested fuels. A reason for higher $\Delta EI(NO_x)$ scattering while burning HEFA SPK+LA compared to Jet A-1 is not found in available data.

Table 4.4: Comparison between Jet A-1 and HEFA SPK+LA at mid T3 setting in pilot+main combustion mode during Flight 2 (03/11/2023), including the number of samples n, normalized mean emission indices $\overline{\Delta EI(NO_x)}$, absolute mean emission index errors $\overline{Error}$, absolute standard deviations of the sample groups s, the absolute difference between normalized mean emission indices of the sample groups Δ, the p-value resulting from the T-test p_t and the p-value resulting from the Mann-Whitney U rank test p_{MW}.

Fuel	n / -	$\overline{\Delta EI(NO_x)}$ / g NO_2 kg^{-1}	$\overline{Error}$ / g NO_2 kg^{-1}	s / g NO_2 kg^{-1}	Δ / g NO_2 kg^{-1}	p_T / -	p_{MW} / -
Jet A-1	6	0.38	1.28	0.68	1.44	0.023	0.026
HEFA SPK+LA	6	1.82	1.57	1.07			

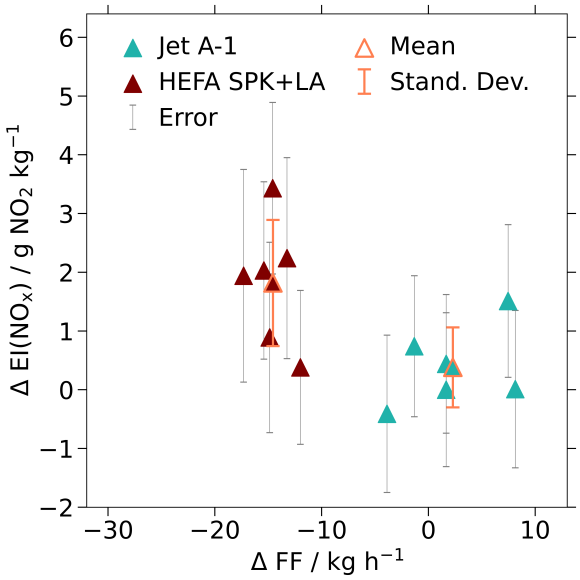

Figure 4.4: Normalized nitrogen oxide emission indices $\Delta EI(\mathrm{NO_x})$ for Jet A-1 and HEFA SPK+LA at mid T3 setting in pilot+main combustion mode during Flight 2 (03/11/2023), including individual measurement errors $Error$, as well as the mean emission index $\overline{\Delta EI(\mathrm{NO_x})}$ and the standard deviation s for each fuel.

For all four analyzed engine settings determined nitrogen oxide emission indices of Jet A-1 and HEFA SPK+LA agree within combined standard deviations and combined errors. The performed statistical tests do not indicate statistically significant differences between the fuels, except for measurements at pilot+main mode. Thus, based on the data acquired during the presented research no difference in nitrogen oxide emissions can be inferred for the two fuels at in-flight conditions. Nevertheless, minor differences below accuracy and scattering of presented measurements are possible. These findings agree with the presented outcome for HEFA SPK measurements. A difference is that here presented means are always higher for the alternative fuel, while means for HEFA SPK are always lower than for Jet A-1.

HEFA SPK+HA

As for HEFA SPK+LA, HEFA SPK+HA is compared with Jet A-1 in two different combustion modes at three different T3 settings. Again, mid, low and high power setting are investigated in forced pilot-only mode and only mid power setting is tested for pilot+main combustion. Measurements are performed during Flight 3 (03/16/2023). Conditions and test points are provided in Table 3.8.

At mid power setting in forced pilot-only combustion mode, measurements with Jet A-1 and HEFA SPK+HA do not result in significant differences. Figure 4.5 indicates that emissions measured while burning HEFA SPK+HA are slightly higher than for Jet A-1. However, the difference of 1.11 g NO_2 kg^{-1} as specified in Table 4.5 lays within combined standard deviations of the sample groups. The mean values also agree within the average measurement errors of the individual indices. Hence, no difference can be inferred from the presented data. This interpretation is in line with performed statistical tests. P-values of 0.185 and 0.111 are reported for the T-test and the Mann-Whitney U rank test, being both higher than the selected significance level.

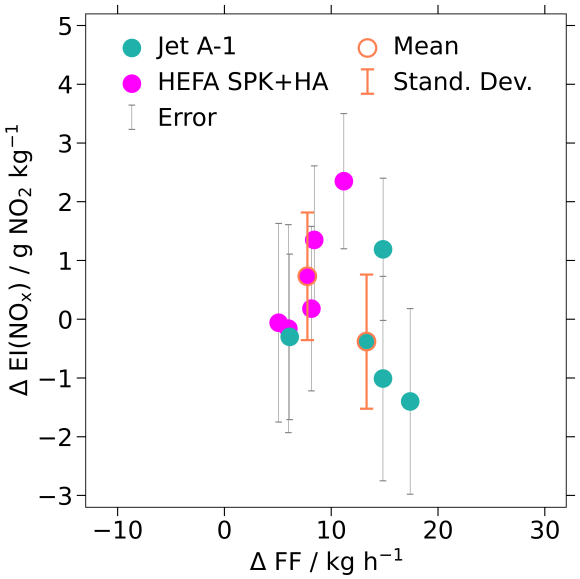

Figure 4.5: Normalized nitrogen oxide emission indices $\Delta EI(\mathrm{NO_x})$ for Jet A-1 and HEFA SPK+HA at mid T3 setting in forced pilot-only combustion mode during Flight 3 (03/16/2023), including individual measurement errors $Error$, as well as the mean emission index $\overline{\Delta EI(\mathrm{NO_x})}$ and the standard deviation s for each fuel.

Table 4.5: Comparison between Jet A-1 and HEFA SPK+HA at mid T3 setting in forced pilot-only combustion mode during Flight 3 (03/16/2023), including the number of samples n, normalized mean emission indices $\overline{\Delta EI(\mathrm{NO_x})}$, absolute mean emission index errors $\overline{Error}$, absolute standard deviations of the sample groups s, the absolute difference between normalized mean emission indices of the sample groups Δ, the p-value resulting from the T-test p_t and the p-value resulting from the Mann-Whitney U rank test p_{MW}.

Fuel	n / -	$\overline{\Delta EI(NO_x)}$ / g NO_2 kg^{-1}	$\overline{Error}$ / g NO_2 kg^{-1}	s / g NO_2 kg^{-1}	Δ / g NO_2 kg^{-1}	p_T / -	p_{MW} / -
Jet A-1	4	-0.38	1.48	1.14	1.11	0.185	0.111
HEFA SPK+HA	5	0.73	1.45	1.09			

Similar observations are obtained for T3 settings low and high. Statistical tests do not suggest significant differences between nitrogen oxide emissions of the fuels and observed differences are lower than combined standard deviations and errors. It must be noted that for high T3 setting this difference is relatively high with a value of 2.81 g NO_2 kg^{-1}, however it can be attributed to a single measurement point with higher engine instability during the respective plume encounter.

Different than for previously discussed fuels, comparing nitrogen oxide measurements with HEFA SPK+HA and Jet A-1 in pilot+main combustion mode indicates clear agreement. With a difference in reported means of 0.22 g NO_2 kg^{-1} as presented in Table 4.6, the smallest deviation is obtained compared to the other investigated engine settings with these fuels. For HEFA SPK and HEFA SPK+LA, discussed above, the difference to Jet A-1 is highest for the here analyzed combustion mode. As shown in Figure 4.6, the means agree within individual standard deviations and individual mean errors are higher than the observed discrepancy. In this case also the statistical tests suggest to not reject the null hypothesis of no significant difference between the fuels. The opposite is the case when comparing the other two alternative fuels with Jet A-1 in pilot+main combustion mode.

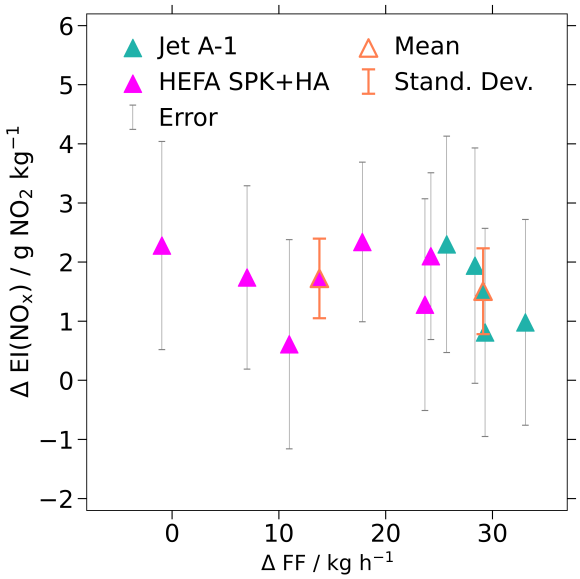

Figure 4.6: Normalized nitrogen oxide emission indices $\Delta EI(\mathrm{NO_x})$ for Jet A-1 and HEFA SPK+HA at mid T3 setting in pilot+main combustion mode during Flight 3 (03/16/2023), including individual measurement errors $Error$, as well as the mean emission index $\overline{\Delta EI(\mathrm{NO_x})}$ and the standard deviation s for each fuel.

Table 4.6: Comparison between Jet A-1 and HEFA SPK+HA at mid T3 setting in pilot+main combustion mode during Flight 3 (03/16/2023), including the number of samples n, normalized mean emission indices $\overline{\Delta EI(\mathrm{NO_x})}$, absolute mean emission index errors $\overline{Error}$, absolute standard deviations of the sample groups s, the absolute difference between normalized mean emission indices of the sample groups Δ, the p-value resulting from the T-test p_t and the p-value resulting from the Mann-Whitney U rank test p_{MW}.

Fuel	n / -	$\overline{\Delta\mathrm{EI(NO_x)}}$ / g NO_2 kg^{-1}	$\overline{\mathrm{Error}}$ / g NO_2 kg^{-1}	s / g NO_2 kg^{-1}	Δ / g NO_2 kg^{-1}	p_T / -	p_{MW} / -
Jet A-1	4	1.51	1.83	0.73	0.22	0.649	0.762
HEFA SPK+HA	6	1.73	1.61	0.67			

As for HEFA SPK+LA, four different cases are investigated to determine whether nitrogen oxide emissions differ between burning Jet A-1 and HEFA SPK+HA. All analyzed engine settings do not result in distinct differences between the two fuels. This is consistently in agreement with performed T- and Mann-Whitney U rank tests. Thus, burning Jet A-1 or HEFA SPK+HA does not affect the formation of nitrogen oxides according to the performed experimental work. As concluded for the other fuels, minor differences below accuracy and scattering of presented data cannot be excluded. HEFA SPK+HA nitrogen oxide mean indices are higher than for Jet A-1 in all investigated cases. This behavior is also observed for HEFA SPK+LA.

Summary Fuel Type versus Nitrogen Oxide Emissions

Three different fuels are compared with Jet A-1: HEFA SPK, HEFA SPK+LA and HEFA SPK+HA. Measurements are performed at different engine settings in terms of combustor inlet temperature and combustion mode. All results show that the respective sample groups agree within the combined standard deviation with differences between the means ranging from 0.04 to 2.8 g NO_2 kg^{-1}. Considering that absolute mean measurement errors between 0.6 and 1.8 g NO_2 kg^{-1} are observed, supports this perspective. In addition, statistical tests are performed,

not suggesting significant differences in nitrogen oxide emissions between the compared fuels in eight of ten cases. Hence, based on data collected during this research no major differences in nitrogen oxide emissions due to the combustion of different fuels can be derived. It is noted that HEFA SPK mean emission indices are lower than Jet A-1 in all analyzed settings, while the two HEFA SPK blends consistently lead to mean emissions higher than for Jet A-1.
The observation of no distinct differences in nitrogen oxide emissions for the tested fuels is in line with ground-based experimental studies. Khandelwal et al. (2019) do not find significant discrepancies testing Jet A-1, SPK and different blends of the two. Similar results are reported by Fujiwara et al. (2020), not identifying effects on nitrogen oxide emissions burning HEFA SPK and JET A-1 in different combustor types. Nevertheless, other publications identify slight reductions in emitted nitrogen oxides comparing SPK fuels with Jet A-1. Lobo et al. (2012) state by about 5% lower emissions for a coal-to-liquid SPK fuel. However, differences in the order of 5% are not detectable with the applied methodology, given that mean errors lay in the range from 3.5 to 15% when comparing the range of absolute error values specified above with typical absolute emission indices between 12 and 17 g NO_2 kg^{-1} (Lee et al., 2010). Thus, more accurate nitrogen oxide or carbon dioxide emission measurement principles are necessary to detect discrepancies in this order of magnitude by reducing systematic errors. Enhanced chasing procedures with more distinct plume encounters can lead to better statistics.
Differences between the mean nitrogen oxide indices do most likely not result from fuel bound nitrogen. The two exceptional cases with statistical tests indicating significant deviation between the sample groups occur in pilot+main combustion mode (lean). At this mode differences due to fuel bound nitrogen resulting from possibly lower nitrogen content in SPK fuels are most likely according to theory presented in Subsection 2.2.2. Nevertheless, measurements in pilot+main mode with Jet A-1 and HEFA SPK+HA disagree with this observation. Minor differences in fuel bound nitrogen might exist as a result of the respective production procedures of Jet A-1 and HEFA SPK: while raw crude oil used for fossil fuels contains small amounts of nitrogen, this can be avoided when converting feedstocks from biomass as for synthetic HEFA SPK (Blakey, Rye and Wilson, 2011; Undavalli et al., 2023). However, Gleason and Martone (1980) and Blakey, Rye and Wilson, 2011 argue that also for Jet A-1 fuel bound nitrogen is negligible. Fuel sample analyses with regard to fuel bound nitrogen are not available for the presented research, but can support the discussion in future experimental work.
Constant over- or undershooting of Jet A-1 mean nitrogen oxide emissions by the respective alternative fuels in all analyzed settings is not explained by the fuels' hydrogen content. Experimental measurements by (Gleason and Martone, 1980) indicate a correlation between fuels' hydrogen to carbon ratio and emitted nitrogen oxides. The effect is assigned to the ratio's effect on flame temperature, influencing the dominant thermal NO formation path (see Section 2.2). This path is sensitive to the activation energy required to break the strong bond of nitrogen molecules (Warnatz, 2001). According to the hydrogen content of the here investigated fuels, specified in Table 3.1, all alternative fuels should result in lower nitrogen oxide emissions than Jet A-1 if there would be a significant effect. However, only measurements with 100% HEFA SPK undershoot Jet A-1 mean indices. Hence, no distinct correlation between nitrogen oxide emissions and hydrogen to carbon ratio can be established from the presented data.

The following answer to the first subquestion is formulated:

In situ measurements do not detect distinct differences in nitrogen oxide emissions for the tested fuels. Minor differences below the measurement accuracy cannot be excluded.

4.1.2. Combustor Inlet Temperature

This subsection addresses the second subquestion:

> **1.2 Do measured NO_x emissions increase exponentially with combustor inlet temperature?**

In this research normalized nitrogen oxide emission indices are determined for four different T3 settings, specified in Table 3.3: very low, low, mid and high. While the mid setting is investigated during all emission test flights, the remaining settings are tested during selected flights only. Since Subsection 4.1.1 indicates no significant impact of fuel type on nitrogen oxide emissions, determined means for the respective T3 settings do not distinguish between the tested fuels. Presented measurements are performed in forced pilot-only combustion mode. This subsection first presents observed dependencies between nitrogen oxide emissions and T3 for each of the four conducted near field emission test flights individually. In the end, a correlation is established covering all measurements.

Combustor Inlet Temperature Analysis Flight 1 (02/28/2023)

Measurements during Flight 1 (02/28/2023) confirm that a reduction in combustor inlet temperature results in decreased formation of nitrogen oxides. The mean emission index determined for seven plume encounters at mid power setting, illustrated in Figure 4.7, is by 3.77 g NO_2 kg^{-1} higher than the mean of -4.24 g NO_2 kg^{-1} obtained for six plume encounters at low power setting, as it can be inferred from data reported in Table 4.7. The difference in combustor inlet temperature is 28 K. Theory presented in Subsection 2.2.2 agrees with the outcome as a reduction in combustor inlet temperature goes along with reduced flame temperature. Thus, less nitrogen molecules of ambient air directed into the combustor are split up and available for oxidation. The formation rate of thermal NO is lowered. Other NO formation paths are affected by a change in flame temperature as well, however the effect on the thermal mechanism is believed to be dominant (Warnatz, 2001). Therefore, measurements during Flight 1 confirm that a reduction in combustor inlet temperature results in decreased formation of nitrogen oxides.

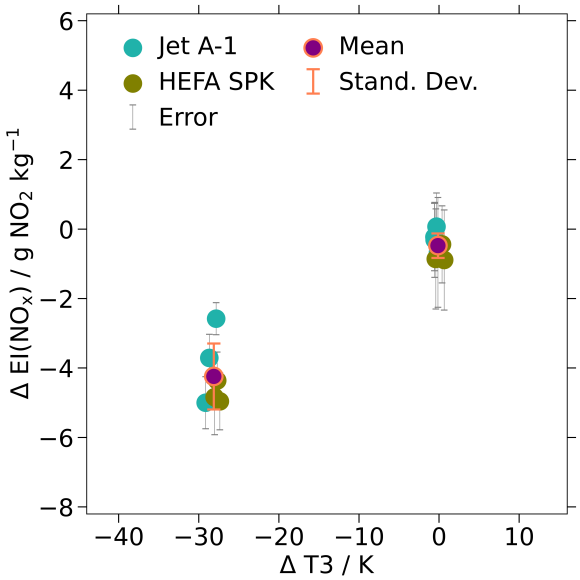

Figure 4.7: Normalized nitrogen oxide emission indices $\Delta EI(NO_x)$ at low and mid T3 setting in forced pilot-only combustion mode during Flight 1 (02/28/2023), including individual measurement errors $Error$, as well as the mean emission index $\overline{\Delta EI(NO_x)}$ and the standard deviation s for each T3 setting.

Table 4.7: Comparison between low and mid T3 setting in forced pilot-only combustion mode during Flight 1 (02/28/2023), including the number of samples n, normalized mean emission indices $\overline{\Delta EI(NO_x)}$, absolute mean emission index errors $\overline{Error}$ and absolute standard deviations of the sample groups s.

T3 Setting	n / -	$\overline{\Delta EI(NO_x)}$ / g NO_2 kg^{-1}	$\overline{Error}$ / g NO_2 kg^{-1}	s / g NO_2 kg^{-1}
Very Low	-	-	-	-
Low	6	-4.24	0.77	0.95
Mid	7	-0.48	1.23	0.35
High	-	-	-	-

Combustor Inlet Temperature Analysis Flight 2 (03/11/2023) and Flight 3 (03/16/2023)
Results obtained for Flight 2 (03/11/2023) and Flight 3 (03/16/2023) agree with the outcome of Flight 1. The flights are analyzed together, since the same combustor inlet temperature settings are tested. As Figure 4.8 illustrates, a clear increase in nitrogen oxide emissions with T3 is obtained for both emission test flights. It can be inferred from Table 4.8 that for Flight 2 emissions increase by 5.20 g NO_2 kg^{-1} from a $\Delta EI(NO_x)$ value of -5.09 g NO_2 kg^{-1} at low T3 setting to 0.238 g NO_2 kg^{-1} at mid T3 setting. From mid to high T3 an increase of 9.53 g NO_2 kg^{-1} is quantified. For Flight 3 increments of 4.20 and 10.74 g NO_2 kg^{-1} are determined, respectively, as Table 4.9 shows. Differences in emission rise between the T3 settings observed during the respective flights lay within standard deviations and errors. Thus, measurements of both flights agree to a great extend. Further, the data reveals that the nitrogen oxide emission gradient increases with rising T3, since for the same step size of 28 K, emission indices increase more from mid T3 to high T3 than from low T3 to mid T3. This behavior is in line with literature, as an exponential relation between the dominant thermal NO formation path and flame temperature is suggested by Lefebvre and Ballal (2010).
It can be inferred from presented data that $\Delta EI(NO_x)$ scattering increases with power setting. For Flight 2 specified standard deviations increase from 0.70 g NO_2 kg^{-1} at low power setting to 3.37 g NO_2 kg^{-1} at high power setting. A similar behavior is observed during Flight 3. Engine stability data does not indicate significant differences between the analyzed settings. The reason can lay in the applied nitrogen oxide measurement technique, as absolute errors increase with rising concentration. Further, higher vibrations and a slightly more dynamic chase procedure with increasing T3 setting can contribute to the noted differences. Another explanation can be a change in turbulent plume mixing with increasing combustor inlet temperature.

Table 4.8: Comparison between low, mid and high T3 setting in forced pilot-only combustion mode during Flight 2 (03/11/2023), including the number of samples n, normalized mean emission indices $\overline{\Delta EI(NO_x)}$, absolute mean emission index errors $\overline{Error}$ and absolute standard deviations of the sample groups s.

T3 Setting	n / -	$\overline{\Delta EI(NO_x)}$ / g NO_2 kg^{-1}	$\overline{Error}$ / g NO_2 kg^{-1}	s / g NO_2 kg^{-1}
Very Low	-	-	-	-
Low	8	-5.09	1.02	0.70
Mid	8	0.11	1.20	1.06
High	8	9.64	1.71	3.37

Table 4.9: Comparison between low, mid and high T3 setting in forced pilot-only combustion mode during Flight 3 (03/16/2023), including the number of samples n, normalized mean emission indices $\overline{\Delta EI(NO_x)}$, absolute mean emission index errors $\overline{Error}$ and absolute standard deviations of the sample groups s.

T3 Setting	n / -	$\overline{\Delta EI(NO_x)}$ / g NO_2 kg^{-1}	$\overline{Error}$ / g NO_2 kg^{-1}	s / g NO_2 kg^{-1}
Very Low	-	-	-	-
Low	10	-3.96	1.01	1.13
Mid	9	0.24	1.47	1.19
High	7	10.98	1.67	3.30

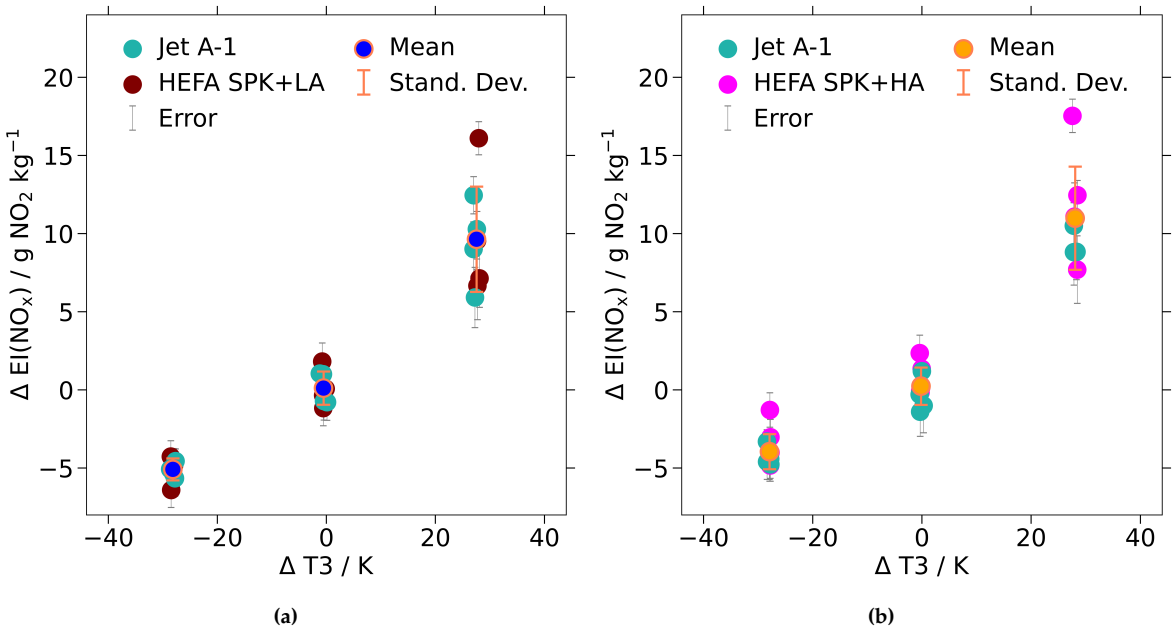

Figure 4.8: Normalized nitrogen oxide emission indices $\Delta EI(NO_x)$ at low, mid and high T3 setting in forced pilot-only combustion mode during (a) Flight 2 (03/11/2023) and (b) Flight 3 (03/16/2023), including individual measurement errors $Error$, as well as the mean emission index $\overline{\Delta EI(NO_x)}$ and the standard deviation s for each T3 setting.

Combustor Inlet Temperature Analysis Flight 4 (03/27/2023)

Nitrogen oxide emission indices for the very low T3 setting determined during Flight 4 (03/27/2023) are not fully in line with the expected correlation between emissions and combustor inlet temperature. As Table 4.10 specifies, values of -6.75 g NO_2 kg^{-1} and 2.49 g NO_2 kg^{-1} are reported for the T3 settings very low and mid - an increment of 9.24 g NO_2 kg^{-1} for a step of 52 K. If previously reported increments in nitrogen oxide emission indices between the settings low and mid, a change of 28 K, are compared to these values, it can be inferred that the measurements of Flight 4, illustrated in Figure 4.9, do not support the expected increase in nitrogen oxide emission slope with T3. However, it must be considered that as provided in Table 4.10, the statistical basis for measurements at the lowest investigated power setting is limited due to a lack of plume encounters.

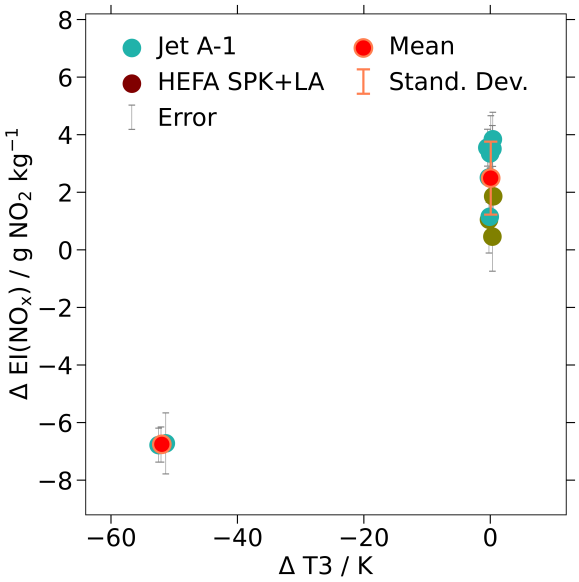

Figure 4.9: Normalized nitrogen oxide emission indices $\Delta EI(\mathrm{NO_x})$ at very low and mid T3 setting in forced pilot-only combustion mode during Flight 4 (03/27/2023), including individual measurement errors $Error$, as well as the mean emission index $\overline{\Delta EI(\mathrm{NO_x})}$ and the standard deviation s for each T3 setting.

Table 4.10: Comparison between very low and mid T3 setting in forced pilot-only combustion mode during Flight 4 (03/27/2023), including the number of samples n, normalized mean emission indices $\overline{\Delta EI(\mathrm{NO_x})}$, absolute mean emission index errors $\overline{Error}$ and absolute standard deviations of the sample groups s.

T3 Setting	n / -	$\overline{\Delta\mathrm{EI(NO_x)}}$ / g NO_2 kg^{-1}	$\overline{\mathrm{Error}}$ / g NO_2 kg^{-1}	s / g NO_2 kg^{-1}
Very Low	3	-6.75	0.75	0.03
Low	-	-	-	-
Mid	10	2.49	0.85	1.27
High	-	-	-	-

Correlation

An exponential correlation between nitrogen oxide emission indices and combustor inlet temperature can be established based on data acquired during the presented research. As not all power settings are investigated during all flights and as a more extensive data basis is preferred, weighted means covering pilot-only measurements of all flights at the respective power setting are included to determine the relationship between emissions and T3. Very similar flight conditions during the flights, specified in Table 3.6 to Table 3.9, support this approach: maximum deviations in terms of total air temperature, pressure altitude and Mach number are ≈ 4 K, 3000 ft and 0.04. It is expected that accuracy and precision of the measurements exceed resulting discrepancies in emissions (Aygun and Turan, 2023). Figure 4.10 illustrates the logarithm of the obtained weighted mean emission indices in an arbitrary unit due to confidentiality. A linear regression is established by applying the method of Least Squares. Since all points lay very close to the regression curve, a linear relation between combustor inlet temperature and the logarithm of determined emissions can be inferred. The interpretation is supported by the quantified coefficient of determination R^2 with a value of 0.98. Thus, experimentally determined emission indices increase exponentially with combustor inlet temperature. The obtained correlation is provided in Equation 4.1, not being disclosed in

the public version of this thesis.

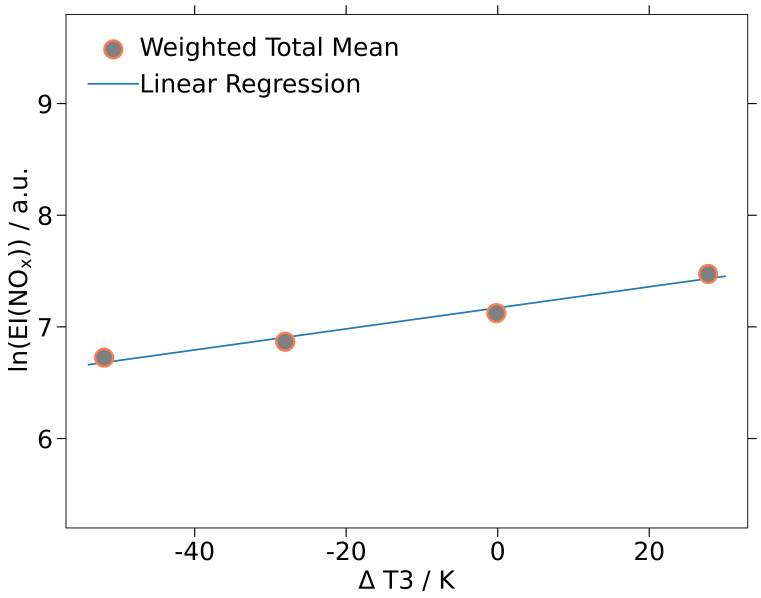

Figure 4.10: Established linear regression ($R^2 = 0.98$) for the logarithm of weighted total mean emission indices in an arbitrary unit at different T3 settings in pilot-only combustion mode covering all near field flights.

(4.1)

The established regression and measurements agree. Figure 4.11 shows each flight's mean emission indices relative to the reference value $EI(\mathrm{NO_x})_{ref}$ and weighted means covering all measurements at the respective power setting. The curve resulting from the linear regression matches the data. It overestimates two mean values, while underestimating the remaining two slightly. For all points the curve lays within the standard deviation, except for the lowest power setting with limited data basis. Thus, it is concluded that the collected data follows an exponential relationship.

Findings agree with literature. Ground-based experimental studies find exponential correlations between combustor inlet temperature and nitrogen oxide emissions. He, Chang and Follen (2015) investigate a lean direct injection combustor. An exponential relationship between combustor inlet temperature is reported and linear regression slopes are in the same order of magnitude as the value presented in Equation 4.1. A summary of ground based experimental measurements for different turbofan engines presented in Lipfert (1972) also indicates a strong dependency between combustor inlet temperature and nitrogen oxide emissions and an exponential relationship can be inferred from the presented correlation.

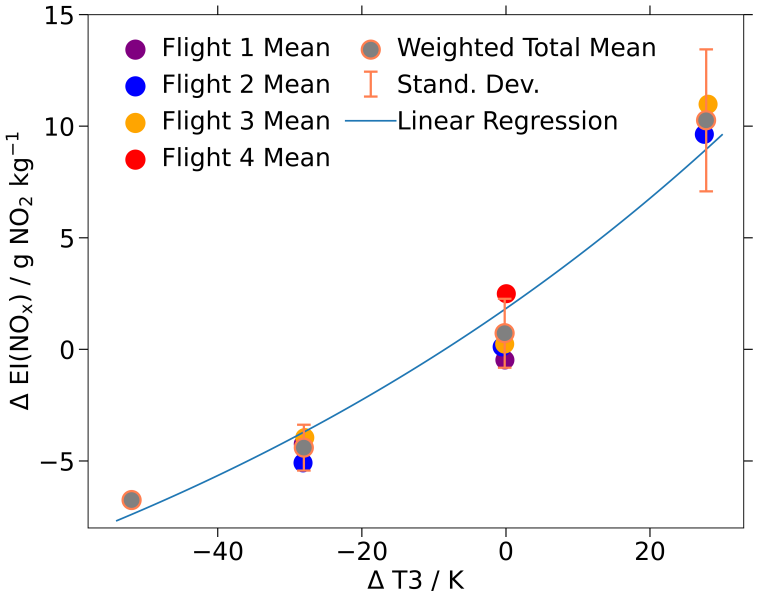

Figure 4.11: Obtained exponential relationship between normalized nitrogen oxide emission indices and T3 setting in pilot-only combustion mode covering all near field flights.

The following answer to the second subquestion is formulated:

> **Near field data collected during this work shows that measured nitrogen oxide emissions increase exponentially with combustor inlet temperature when operating in forced pilot-only combustion mode.**

4.1.3. Combustion Mode

This subsection investigates the third subquestion:

> **1.3 Does lean combustion reduce NO_x emissions?**

Normalized emission indices for two different combustion modes are compared at mid T3 setting. The first investigated combustion mode is forced pilot-only. The combustor runs at 100% pilot injection, hence burning rich. As introduced in Section 3.1, the mode is normally not active at the selected T3 setting. Hence, this operating condition is not reached along the engine's conventional operation envelope. The second tested combustion mode is pilot+main, representing the normal operating condition of the combustor at the selected T3 setting. Pilot and main injectors are active and combustion is primarily lean. In the following, the results obtained during all four near field emission test flights are presented and discussed together. As in Subsection 4.1.2, it is assumed that there is no significant difference between the fuels when determining mean emission indices.

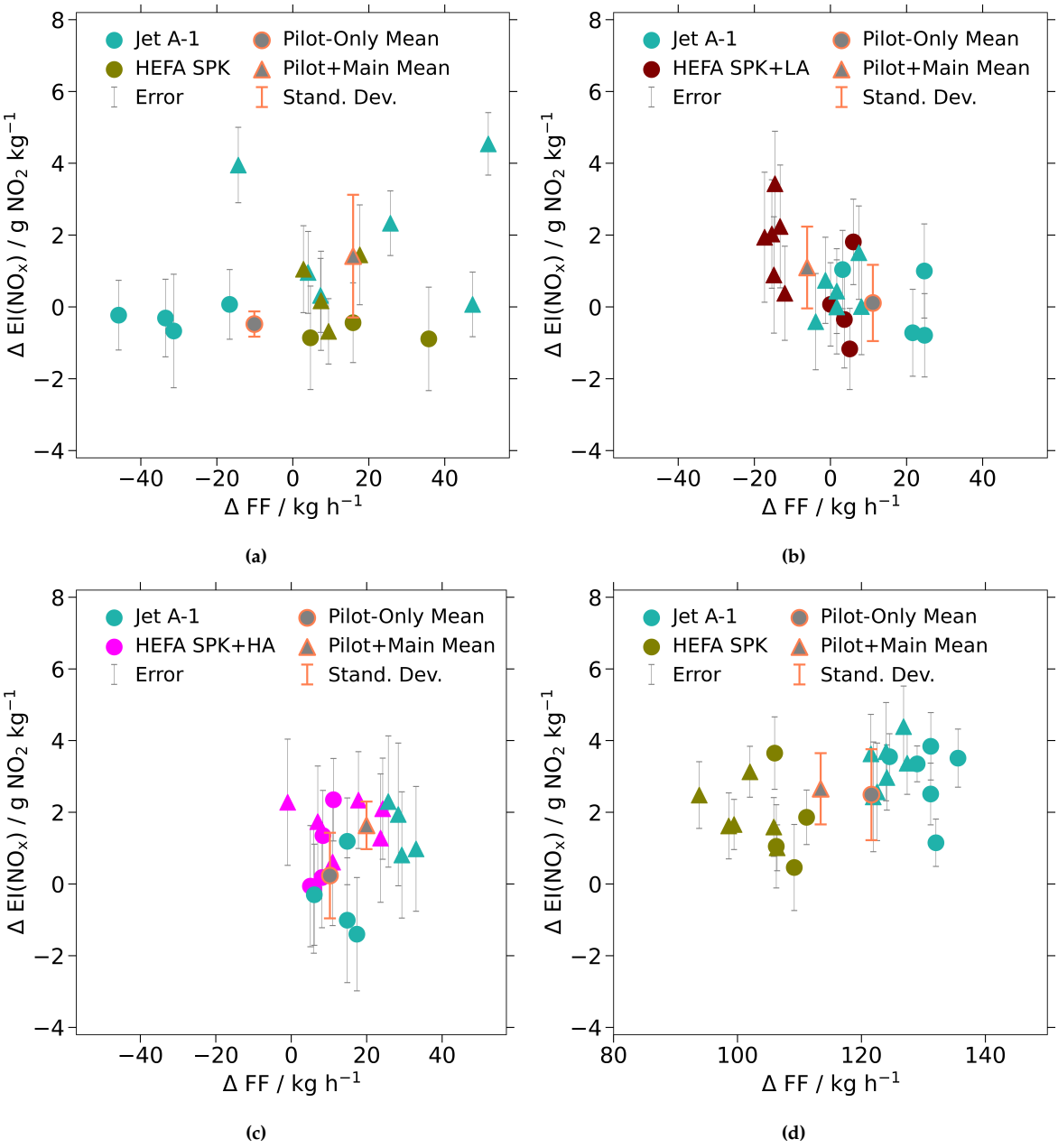

Figure 4.12: Normalized nitrogen oxide emission indices $\Delta EI(NO_x)$ for forced pilot-only and pilot+main combustion mode at mid T3 setting during (a) Flight 1 (02/28/2023), (b) Flight 2 (03/11/2023), (c) Flight 3 (03/16/2023) and (d) Flight 4 (03/27/2023), including individual measurement errors $Error$, as well as the mean emission index $\overline{\Delta EI(NO_x)}$ and the standard deviation s for each combustion mode. Note different fuel flow axis interval for Flight 4.

Mean emission indices indicate no distinct differences in nitrogen oxides between the two combustion modes. Figure 4.12 compares normalized nitrogen oxide emissions obtained for forced pilot-only and pilot+main combustion mode for all four conducted emission test flights. Starting with Figure 4.12 (a), it is observed that during Flight 1 (02/28/2023) emissions for the two combustion modes deviate by 1.89 g NO_2 kg^{-1}, with a mean $\Delta EI(NO_x)$ value of -0.48 g NO_2 kg^{-1} for forced pilot-only and a mean $\Delta EI(NO_x)$ value of 1.42 g NO_2 kg^{-1} for pilot+main mode. The results of statistical tests, reported in Table 4.11, suggest that the indices obtained for the two modes are not from the same population, since reported p-values

are below the selected level of significance. Further, the means only agree slightly within the standard deviation. However, taking a closer look at the distribution of the determined emission indices in Figure 4.12 (a) shows very high $EI(NO_x)$ scattering in the pilot+main measurements compared to the forced pilot-only sample group. This can possibly be explained by the two highest pilot+main indices obtained while burning Jet A-1, as comparably high engine instability values in terms of combustor inlet temperature are determined. Hence, it can be argued that emissions of both combustion modes might agree at continuous stable conditions. Combined mean errors exceed the reported difference in mean $\Delta EI(NO_x)$ between the sample groups.

Table 4.11: Comparison between forced pilot-only and pilot+main combustion mode at mid T3 setting during Flight 1 (02/28/2023), including the number of samples n, normalized mean emission indices $\overline{\Delta EI(NO_x)}$, absolute mean emission index errors $\overline{Error}$, absolute standard deviations of the sample groups s, the absolute difference between normalized mean emission indices of the sample groups Δ, the p-value resulting from the T-test p_t and the p-value resulting from the Mann-Whitney U rank test p_{MW}.

Comb. Mode	n / -	$\overline{\Delta EI(NO_x)}$ / g NO_2 kg^{-1}	$\overline{Error}$ / g NO_2 kg^{-1}	s / g NO_2 kg^{-1}	Δ / g NO_2 kg^{-1}	p_T / -	p_{MW} / -
Pilot-Only	7	-0.48	1.23	0.35	1.89	0.007	0.005
Pilot+Main	10	1.42	1.08	1.71			

Measurements of the remaining three flights are in line with observations from Flight 1. Results of Flight 3 (03/16/2023) indicate a similar difference between the mean emission indices of the combustion modes. Table 4.13 shows by 1.4 g NO_2 kg^{-1} higher emissions for pilot+main combustion mode. As for Flight 1, statistical tests suggest no agreement even if the discrepancy lays within combined standard deviations and each of the two mean errors exceeds the observed difference. In this case however, engine stability data does not provide any explanation. Nevertheless, measurements during Flight 2 (03/11/2023) and Flight 4 (03/27/2023) show lower differences in nitrogen oxide emissions between the combustion modes, as specified in Table 4.12 and Table 4.14, while for both flights the two statistical tests fail to reject the null hypothesis. Thus, it is concluded that all together, no significant difference in nitrogen oxide emissions between forced pilot-only and pilot+main combustion mode can be inferred from measurements conducted during the four emission test flights.

Table 4.12: Comparison between forced pilot-only and pilot+main combustion mode at mid T3 setting during Flight 2 (03/11/2023), including the number of samples n, normalized mean emission indices $\overline{\Delta EI(NO_x)}$, absolute mean emission index errors $\overline{Error}$, absolute standard deviations of the sample groups s, the absolute difference between normalized mean emission indices of the sample groups Δ, the p-value resulting from the T-test p_t and the p-value resulting from the Mann-Whitney U rank test p_{MW}.

Comb. Mode	n / -	$\overline{\Delta EI(NO_x)}$ / g NO_2 kg^{-1}	$\overline{Error}$ / g NO_2 kg^{-1}	s / g NO_2 kg^{-1}	Δ / g NO_2 kg^{-1}	p_T / -	p_{MW} / -
Pilot-Only	8	0.11	1.20	1.06	0.99	0.0652	0.0979
Pilot+Main	12	1.10	1.42	1.14			

Table 4.13: Comparison between forced pilot-only and pilot+main combustion mode at mid T3 setting during Flight 3 (03/16/2023), including the number of samples n, normalized mean emission indices $\overline{\Delta EI(NO_x)}$, absolute mean emission index errors $\overline{Error}$, absolute standard deviations of the sample groups s, the absolute difference between normalized mean emission indices of the sample groups Δ, the p-value resulting from the T-test p_t and the p-value resulting from the Mann-Whitney U rank test p_{MW}.

Comb. Mode	n / -	$\overline{\Delta EI(NO_x)}$ / g NO_2 kg^{-1}	$\overline{Error}$ / g NO_2 kg^{-1}	s / g NO_2 kg^{-1}	Δ / g NO_2 kg^{-1}	p_T / -	p_{MW} / -
Pilot-Only	9	0.24	1.47	1.19	1.40	0.009	0.025
Pilot+Main	10	1.64	1.70	0.66			

Table 4.14: Comparison between forced pilot-only and pilot+main combustion mode at mid T3 setting during Flight 4 (03/27/2023), including the number of samples n, normalized mean emission indices $\overline{\Delta EI(NO_x)}$, absolute mean emission index errors $\overline{Error}$, absolute standard deviations of the sample groups s, the absolute difference between normalized mean emission indices of the sample groups Δ, the p-value resulting from the T-test p_t and the p-value resulting from the Mann-Whitney U rank test p_{MW}.

Comb. Mode	n / -	$\overline{\Delta EI(NO_x)}$ / g NO_2 kg^{-1}	$\overline{Error}$ / g NO_2 kg^{-1}	s / g NO_2 kg^{-1}	Δ / g NO_2 kg^{-1}	p_T / -	p_{MW} / -
Pilot-Only	10	2.49	0.85	1.27	0.16	0.740	0.975
Pilot+Main	13	2.66	1.00	0.99			

Results do not agree with expectations from literature. From information provided in Section 2.2 it can be inferred that the staging from rich combustion mode, with fuel injection only through the pilot, to lean combustion, with fuel injection through both main and pilot, results in a sharp drop in nitrogen oxide emissions (Foust et al., 2012). This behavior is confirmed by ground based emission measurements for different settings of a LEAP-1B engine (Moore, in preparation; Boeing ecoDemonstrator Science and Engineering Team, in preparation). Thus, it is expected that lower emissions would be obtained for pilot+main combustion while operating at the same combustor inlet temperature. This cannot be inferred from the presented data, showing no distinct differences in emissions between a forced pilot-only and the conventional pilot+main combustion mode. Hence, two hypotheses can be derived: either there is no staging effect at flight conditions encountered during the measurements or the forced pilot-only mode also results in reduced emissions at the selected T3 setting.

It is unlikely that the first hypothesis is true. There is no publication discussing the sensitivity of reduced nitrogen oxide emissions through staging to certain flight conditions. Thus, it is assumed that the principles described by Foust et al. (2012) and Stickles and Barrett (2013) are valid for all ambient conditions and Mach numbers. It is possible that at constant combustor inlet temperature, effects of pressure due to different flight levels or air speeds influence the equivalence ratio distribution within the combustion chamber, but it is unlikely that the staging effect in canceled completely due to the flight conditions during the measurements. As the pilot+main mode is not forced, but normally active at the investigated engine setting, it is more likely that similar emissions are obtained due to the forced nature of the investigated pilot-only mode.

More insights are required to fully understand why no difference in emissions is observed between the modes. It is possible that a reduction in nitrogen oxide emissions is also obtained for forced pilot-only combustion. It is worth considering that also for rich combustion NO formation rates are reduced due to a decrease in flame temperature, compared to stoichiometric combustion (Lefebvre and Ballal, 2010). However, it is difficult to identify, how the equivalence ratio is distributed within the combustion chamber, since all excess air is directed into the

combustor in the primary zone and no continuous mixing with excess air along the combustion chamber is present, as it would be the case for a Rich-Quench-Lean engine. Further, interaction effects within the combustor at an operating condition outside the operation envelope cannot be excluded. Hence, to completely understand the results, a simulation of both the forced pilot-only and the conventional pilot+main mode might be helpful to establish a valid comparison between measurements and theory. A Computational Fluid Dynamics (CFD) analysis can deliver useful insights.
To conclude, due to the setup of this study with a forced pilot-only mode for particular matter emission quantification, it is not possible to confirm that the lean combustion mode of a lean burn engine results in the desired reduction in nitrogen oxide emissions. Additional measurements at operating points within the operation envelope just before and just after staging are necessary to determine whether in situ measurements can confirm a drop in nitrogen oxide emissions when switching from rich to lean.

The following answer to the third subquestion is derived:

Due to the measurement strategy, sampling emissions with engine settings outside the operation envelope of the CFM LEAP-1A installed on an Airbus A321neo, the results cannot confirm that pilot+main combustion reduces nitrogen oxide emissions.

4.1.4. Engine Degradation

This subsection analyzes the fourth subquestion:

1.4 Does engine degradation affect NO_x emissions?

As a part of this research emissions from two different, but technically identical engines are investigated. While ENG 2 is the default engine used for measurements to discuss subquestions 1-3, ENG 1 measurements are only used to analyze the variability of emissions for two different engines of the same type, but a different degree of degradation. The deviation in EGTM is specified in Table 3.5. ENG 1 is exclusively tested burning Jet A-1. The data of ENG 2 includes measurements of both Jet A-1 and HEFA SPK. As motivated before, plume encounters with both fuels are assigned to the same sample group to increase statistics, since no distinct differences in NO_x emissions are identified in the presented study. In the following, both engines are compared in forced pilot-only and in pilot+main combustion mode.

Comparing nitrogen oxide emission indices of ENG 2 and ENG 1 at mid power setting in pilot-only combustion mode results in notable differences. The measurements are presented in Figure 4.13 (a). It is shown that the mean index quantified for ENG 2 exceeds the representative value by 2.49 g NO_2 kg^{-1}, while a value of 6.46 g NO_2 kg^{-1} is determined for ENG 1. The difference of 3.96 g NO_2 kg^{-1} does not lay within the combined standard deviation of both sample groups and the results of performed statistical tests, specified in Table 4.15, indicate that the measurement points do not belong to the same sample group, both undercutting the significance level of 0.05. Also the combined mean errors do not add up to the observed deviation in emissions. Thus, ENG 1 with a 15 K lower EGTM emits more nitrogen oxides than ENG 2, according to reported data. Nevertheless, it must be considered that with only four plume encounters the statistical basis for emissions of ENG 1 is relatively small together with a significant $EI(NO_x)$ scattering. This scattering possibly occurs due to higher engine instability for the measurement sequence with the highest reported emission index of 8.78 g NO_2 kg^{-1}. For this specific plume encounter standard deviations of fuel flow and combustor inlet temperature are about three times higher than for the remaining samples of the group.

Table 4.15: Comparison between ENG 2 and ENG 1 at mid T3 setting in forced pilot-only combustion mode during Flight 4 (03/27/2023), including the number of samples n, normalized mean emission indices $\overline{\Delta EI(NO_x)}$, absolute mean emission index errors $\overline{Error}$, absolute standard deviations of the sample groups s, the absolute difference between normalized mean emission indices of the sample groups Δ, the p-value resulting from the T-test p_t and the p-value resulting from the Mann-Whitney U rank test p_{MW}.

Engine	n / -	$\overline{\Delta EI(NO_x)}$ / g NO_2 kg^{-1}	$\overline{Error}$ / g NO_2 kg^{-1}	s / g NO_2 kg^{-1}	Δ / g NO_2 kg^{-1}	p_T / -	p_{MW} / -
ENG 2	10	2.49	0.85	1.27	3.96	0.013	0.002
ENG 1	4	6.46	1.30	1.77			

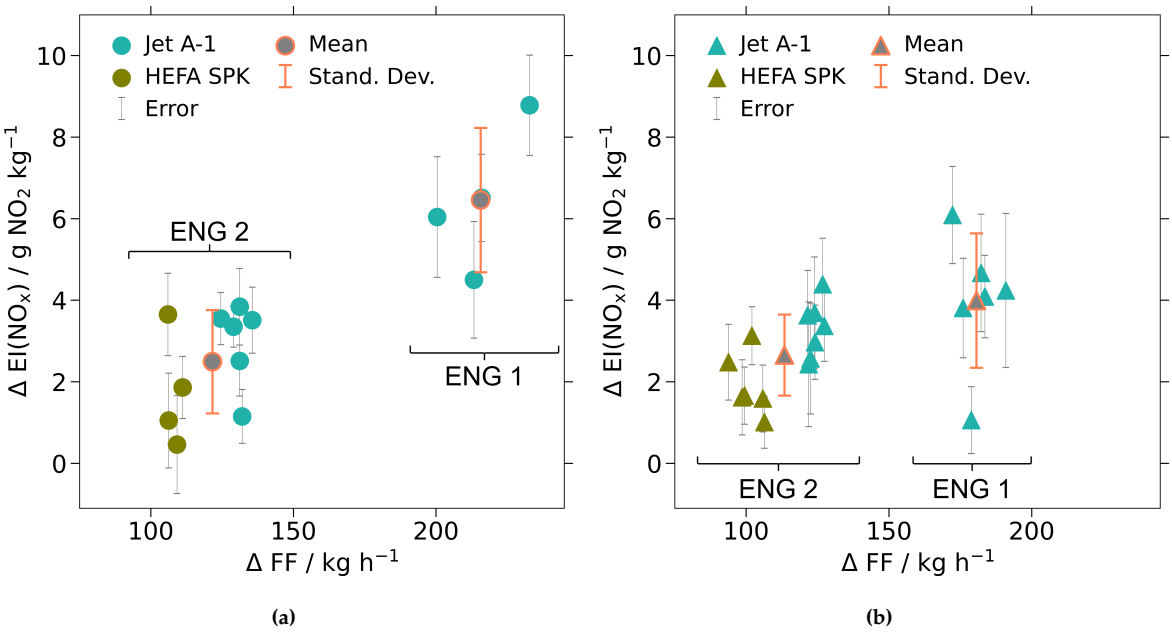

Figure 4.13: Normalized nitrogen oxide emission indices $\Delta EI(NO_x)$ for ENG 2 and ENG 1 obtained from measurements at mid T3 setting during Flight 4 (03/27/2023) in (a) forced pilot-only and (b) pilot+main combustion mode, including individual measurement errors $Error$, as well as the mean emission index $\overline{\Delta EI(NO_x)}$ and the standard deviation s for each engine.

In pilot+main combustion mode smaller differences in nitrogen oxide emissions are observed between the two engines. The mean obtained for ENG 1 measurements exceeds the mean of ENG 2 by only 1.336 g NO_2 kg^{-1}, compared to 3.964 g NO_2 kg^{-1} in forced pilot-only combustion mode, as it can be inferred from Figure 4.13 (b) and Table 4.16. Agreement is found within combined standard deviations and measurement errors. This interpretation is underlined by the p-value of 0.110, reported by the T-test. However, the Mann Whitney U rank test suggests that the measurements belong to two different populations, resulting in a p-value below the chosen significance level. As it is found for the engine comparison in forced pilot-only combustion mode, the measurements for ENG 1 show higher $EI(NO_x)$ scattering. In this case no distinct reason arises from engine stability data. Considering that the observed difference in $EI(NO_x)$ is smaller than in forced pilot-only mode and the disagreement of the statistical tests, pilot+main data does not provide an explicit indication whether there is a difference in nitrogen oxide emissions between the two engines.

Table 4.16: Comparison between ENG 2 and ENG 1 at mid T3 setting in pilot+main combustion mode during Flight 4 (03/27/2023), including the number of samples n, normalized mean emission indices $\overline{\Delta EI(NO_x)}$, absolute mean emission index errors $\overline{Error}$, absolute standard deviations of the sample groups s, the absolute difference between normalized mean emission indices of the sample groups Δ, the p-value resulting from the T-test p_t and the p-value resulting from the Mann-Whitney U rank test p_{MW}.

Engine	n / -	$\overline{\Delta EI(NO_x)}$ / g NO_2 kg^{-1}	$\overline{Error}$ / g NO_2 kg^{-1}	s / g NO_2 kg^{-1}	Δ / g NO_2 kg^{-1}	p_T / -	p_{MW} / -
ENG 2	13	2.66	1.00	0.99	1.34	0.110	0.036
ENG 1	6	3.99	1.26	1.65			

Results agree with expectations from literature. Apostolidis and Stamoulis (2021) describe that exhaust gas temperature margin is an indicator for the thermal efficiency of an engine. Since thermal efficiency is affected by contamination inside the engine and mechanical deterioration, the amount of emitted nitrogen oxides can increase with a decreasing exhaust gas temperature margin value: Lukachko and Waitz (1997) model nitrogen oxide emissions of turbofan engines and simulate deterioration effects through adapted engine component efficiencies. It is found that fan, LPC, HPC and LPT degradation can lead to an increase in emitted nitrogen oxides, while aging of the HPT can result in a reduction. Further, nitrogen oxide increments are related to increased fuel flow at reduced cycle efficiency. The here reported data for forced pilot-only mode is in line with this understanding: significantly higher emissions are obtained for ENG 1, having a lower exhaust gas temperature margin. Thus, it is likely that degradation is the reason for the observations. Higher fuel flow values for ENG 1 support this interpretation, indicating higher efficiency for ENG 2. Operating at the same combustor inlet temperature, more energy is needed by ENG 1, resulting in a higher flame temperature at the same T3 setting. Hence, the thermal NO production rate increases and higher nitrogen oxide emission indices are obtained. The presented results for pilot+main mode indicate the same tendency. However, according to quantified standard deviations and the performed T-test, the outcome is not significant. More certainty can be achieved through detailed analysis of engine components and individual engine history, providing more specific insights than exhaust gas temperature margin only. Investigating literature shows that there is need for further research on this topic. No publication comparing experimentally determined nitrogen oxide emissions of engines with a different degree of degradation is found. Nevertheless, it is essential to quantify in how far emissions among technically identical engines can vary due to aging to determine more accurate emission inventories. Thus, more experimental work dedicated to the described effects is suggested to increase availability of empirical data.

The following answer to the fourth subquestion is formulated:

> **Based on performed measurements it is likely that engine degradation affects nitrogen oxide emissions, noting that available engine status information is limited.**

4.2. Comparison with Far Field Measurements

Previously, only near field measurements at a mean distance of 98m between chase and source aircraft are analyzed. This section compares obtained results with well-established far field chase flights at distances of several kilometers, to answer the second research question:

> **2. Do near field measurements agree with observations in the far field?**

Far field measurements are conducted as a part of two different campaigns: VOLCAN and ECO-Demonstartor. During VOLCAN, far field data is acquired for the exact same engines investigated in the near field. It is analyzed whether the absolute emission indices obtained in the two setups agree. Additional measurements are performed as a part of the ECO-Demonstrator campaign in October 2023. It is checked whether dependencies between nitrogen oxides and engine operation obtained during VOLCAN can be confirmed by another, independent emission test campaign.

4.2.1. VOLCAN Far Field Results

This subsection covers the first subquestion of the second research question, focusing on VOLCAN far field measurements:

2.1 Do emission indices derived from near and far field measurements during the VOLCAN campaign agree?

An extensive set of near field measurements is performed as a part of the VOLCAN campaign. During the same campaign, one dedicated far field flight is performed for comparison. Differences between the methods are outlined in Section 3.4. Jet A-1 and HEFA SPK are investigated and results obtained for both methods are set in contrast for forced pilot-only mode and for pilot+main combustion. Error contributors are analyzed. Near field Flight 1 (02/28/2023) is chosen for comparison, as ambient conditions are most similar to the conducted far field flight.

Forced Pilot-Only Mode - Near Field versus Far Field

Near field results of Flight 1 agree with measurements in the far field. Figure 4.14 presents emission indices obtained in forced pilot-only mode while burning Jet A-1 and HEFA SPK. Near field results are illustrated in Figure 4.14 (a), while the outcome of the dedicated far field flight is provided in Figure 4.14 (b). As specified in Table 4.17, obtained mean values only deviate slightly by 0.562. Considering very high errors along with very high standard deviations for reported far field measurements, exceeding the respective values of the near field by factors of ≈4.6 and ≈13.0, results are in very good agreement. This can also be inferred from presented p-values of the performed T- and Mann Whitney U rank test, being higher than the selected significance level of 0.05. A more detailed analysis of estimated errors is provided below.

Table 4.17: Comparison between VOLCAN near field measurements during Flight 1 (02/28/2023) at mid T3 setting in forced pilot-only combustion mode and VOLCAN far field measurements (03/22/2023) at cruise T3 setting in forced pilot-only combustion mode, including the number of samples n, normalized mean emission indices $\overline{\Delta EI(\mathrm{NO_x})}$, absolute mean emission index errors $\overline{Error}$, absolute standard deviations of the sample groups s, the absolute difference between normalized mean emission indices of the sample groups Δ, the p-value resulting from the T-test p_t and the p-value resulting from the Mann-Whitney U rank test p_{MW}.

Setup	n / -	$\overline{\Delta \mathrm{EI}(\mathrm{NO_x})}$ / g NO_2 kg^{-1}	$\overline{\mathrm{Error}}$ / g NO_2 kg^{-1}	s / g NO_2 kg^{-1}	Δ / g NO_2 kg^{-1}	p_T / -	p_{MW} / -
Near Field	7	-0.48	1.23	0.35	0.56	0.459	0.544
Far Field	34	-1.04	5.59	4.31			

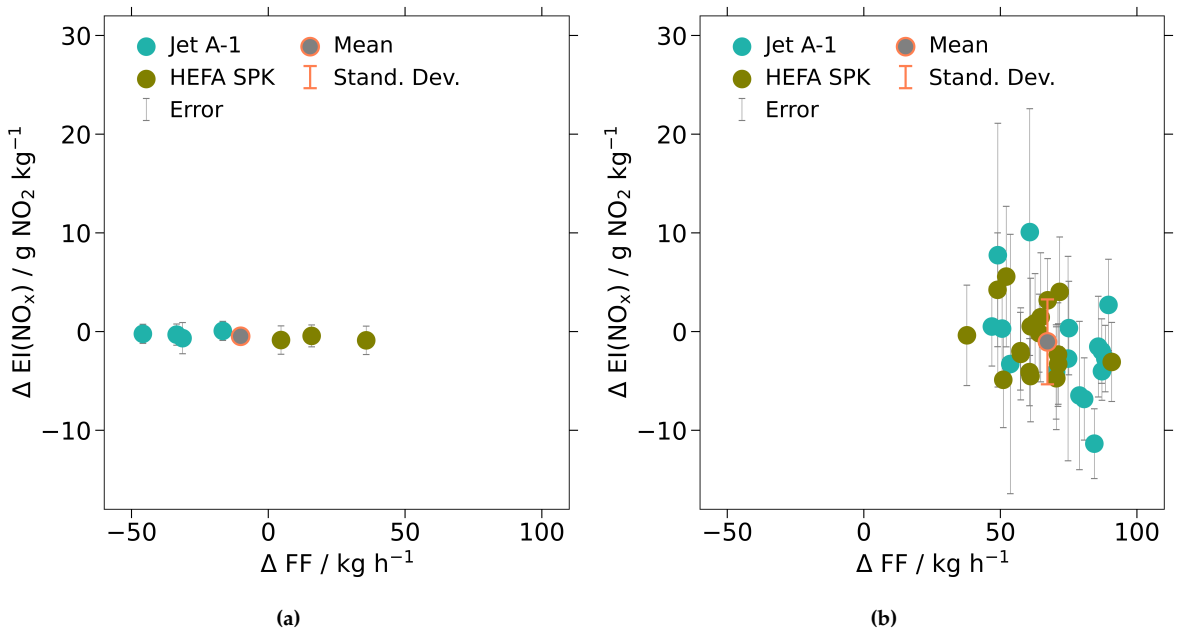

Figure 4.14: Normalized nitrogen oxide emission indices $\Delta EI(NO_x)$ for (a) VOLCAN near field measurements during Flight 1 (02/28/2023) at mid T3 setting in forced pilot-only combustion mode and (b) VOLCAN far field measurements (03/22/2023) at cruise T3 setting in forced pilot-only combustion mode, including individual measurement errors $Error$, as well as the mean emission index $\overline{\Delta EI(NO_x)}$ and the standard deviation s for each experimental setup.

Presented results are in line with expectations. It can be inferred from Table 3.6 and Table 3.11 that conditions during the flights in terms of pressure altitude, total air temperature and Mach number deviate by 1000ft, 0.5K, and 0.16. Since the power setting is selected in terms of combustor inlet temperature, deviating by 3 K between near and far field measurements, no significant changes in emissions are expected due to temperature. However, changes in total pressure at the engine's inlet might affect emissions. Lower static pressure due to the slight increase in cruise altitude for far field measurements reduces nitrogen oxide emissions, while an increase in Mach number by 0.16 increases dynamic pressure at the inlet and hence, emissions. According to findings by Aygun and Turan (2023), applying P3-T3, as well as fuel flow methods, the effect of increasing Mach number is dominant and higher emissions in the order of 1-2 g NO_2 kg^{-1} are likely for far field measurements. Nevertheless, it is not expected to detect distinct discrepancies, considering measurement accuracy and precision, especially of the far field setup.
No differences in measured nitrogen oxide emissions are expected due to deviations in plume age. As presented in Table 4.18, the mean far field plume age is significantly higher than for the near field. This leads to more oxidization of emitted nitrogen oxides due to mixing with ambient air (Schumann, 1997). However, as a converter is implemented in the measurement setup as described in Section 3.2, species resulting from oxidization are still detected. Considering the converter efficiency of 99.1% determined by instrument calibrations, no differences in measured emissions are expected due to plume aging.

Table 4.18: Mean plume age during VOLCAN near and far field measurements.

Setup	Mean Plume Age / s
Near Field	0.5
Far Field	47.9

Pilot+Main Mode - Near Field versus Far Field

A comparison between near- and far field measurements in pilot+main mode provided in Figure 4.15 agrees with the outcome for forced pilot-only mode. Table 4.19 specifies by 1.941 g NO_2 kg^{-1} lower emissions for far field measurements. However, as for forced pilot-only plume encounters, determined errors and standard deviations are relatively high in the far field. Therefore, agreement is found within standard deviations and errors. This perspective is underlined by performed statistical test, both not suggesting statistically significant differences between the two sample groups. As explained above, this outcome is expected and agrees with literature (Aygun and Turan, 2023; Schumann, 1997).

Table 4.19: Comparison between VOLCAN near field measurements during Flight 1 (02/28/2023) at mid T3 setting in pilot+main combustion mode and VOLCAN far field measurements (03/22/2023) at cruise T3 setting in pilot+main combustion mode, including the number of samples n, normalized mean emission indices $\overline{\Delta EI(NO_x)}$, absolute mean emission index errors $\overline{Error}$, absolute standard deviations of the sample groups s, the absolute difference between normalized mean emission indices of the sample groups Δ, the p-value resulting from the T-test p_t and the p-value resulting from the Mann-Whitney U rank test p_{MW}.

Setup	n / -	$\overline{\Delta EI(NO_x)}$ / g NO_2 kg^{-1}	$\overline{Error}$ / g NO_2 kg^{-1}	s / g NO_2 kg^{-1}	Δ / g NO_2 kg^{-1}	p_T / -	p_{MW} / -
Near Field	10	1.42	1.08	1.71	1.94	0.062	0.129
Far Field	20	-0.52	6.19	3.76			

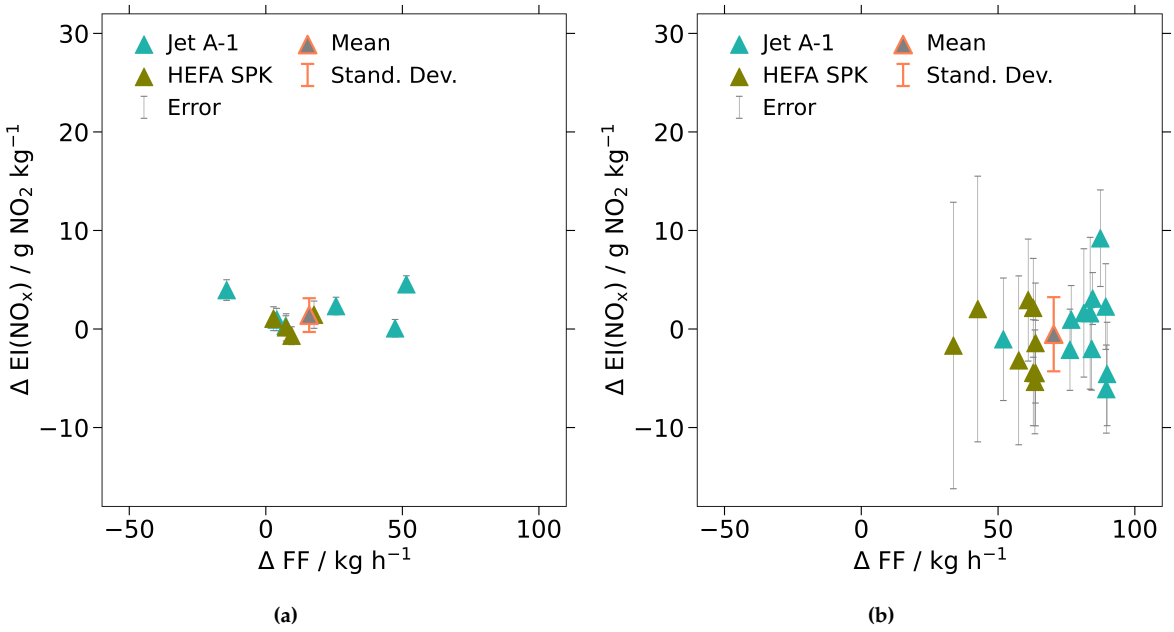

Figure 4.15: Normalized nitrogen oxide emission indices $\Delta EI(NO_x)$ for (a) VOLCAN near field measurements during Flight 1 (02/28/2023) at mid T3 setting in pilot+main combustion mode and (b) VOLCAN far field measurements (03/22/2023) at cruise T3 setting in pilot+main combustion mode, including individual measurement errors $Error$, as well as the mean emission index $\overline{\Delta EI(NO_x)}$ and the standard deviation s for each experimental setup.

Estimated Uncertainties - Near Field versus Far Field

Boundary conditions lead to higher measurement errors in the far field setup. The presented comparative analysis between near- and far field emission indices shows that significantly higher scattering and measurement errors are obtained for the latter. Figure 4.16 quantifies the

relative error contribution of measurement accuracy and background uncertainty for both NO_y and CO_2 concentrations. Their quantification is outlined in Section 3.3. Errors due to estimates for molar masses and the assumed carbon dioxide emission index are negligible. It is shown in Figure 4.16 (a) that for near field errors main contributors are the CO_2 background uncertainty and measurement accuracy of both CO_2, as well as NO_y concentrations. However, for far field errors characterized in Figure 4.16 (b), NO_y related uncertainties are insignificant. The reason is that due to a relatively low increase in concentrations above the background in the far field plume and an in general lower relative rise in CO_2 compared to NO_y, local CO_2 background fluctuations are in the same order of magnitude than the plume increase. This leads to very high background uncertainties. Further, the constant error in CO_2 concentration gains weight with reduced emission intensity compared to the concentration-dependent NO_y error. Higher absolute measurement errors in the far field can be attributed to the described effects.

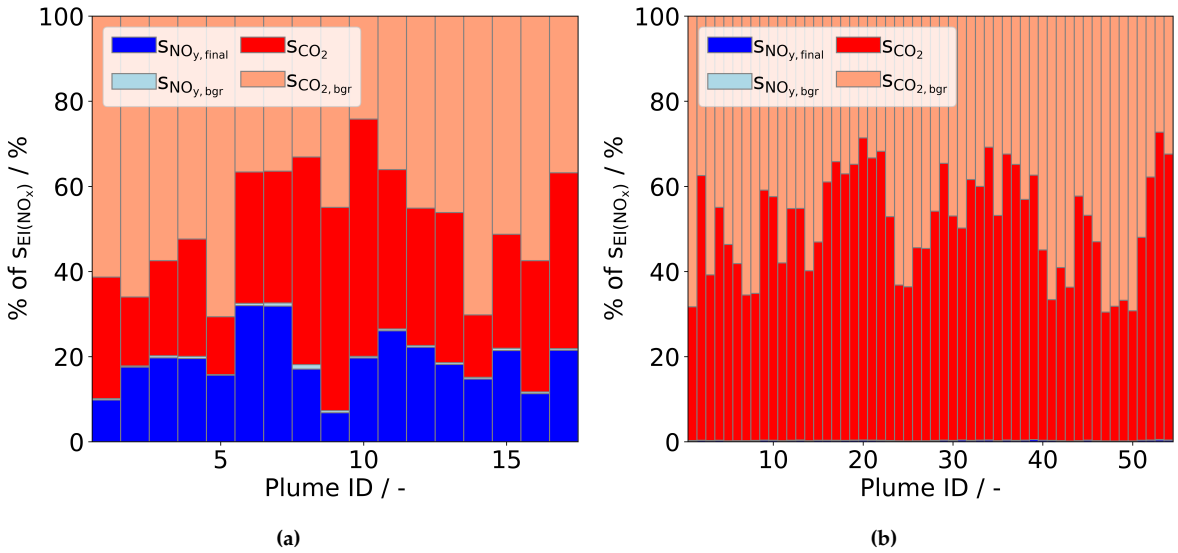

Figure 4.16: Relative contribution of uncertainty terms to total error of individual emission indices during (a) VOLCAN near field Flight 1 (02/27/2023) and (b) VOLCAN far field flight (03/22/2023), including data for both forced pilot-only and pilot+main combustion mode.

Summary Near Field versus Far Field

Emission indices based on measurements in the far field are compared with results obtained for near field Flight 1. For both forced pilot-only mode and pilot+main mode agreement is found. Compared to determined errors and obtained standard deviations in the far field, the difference in mean emission indices is relatively low. Statistical tests do not suggest statistically significant differences between the two measurement setups. The outcome fulfills the expectation that there are no distinct differences in emissions between near and far field, since slight discrepancies in power setting and ambient conditions cannot be identified with the applied methodology. Hence, it is proven that near field measurements are suitable to investigate nitrogen oxide emissions. Further, it is shown that due to higher signals relative to background concentrations, higher accuracy with less scattering is enabled. The following answer is formulated to the first subquestion of the second research question:

Absolute nitrogen oxide emissions of near and far field measurements agree during VOLCAN. The near field setup leads to lower uncertainties.

4.2.2. ECO-Demonstrator Far Field Results

This subsection focuses on the second subquestion:

2.2 Are NO_x dependencies observed during VOLCAN confirmed by far field emission measurements during the ECO-Demonstrator campaign?

Four different factors are investigated regarding their impact on nitrogen oxide formation by conducting near field in situ measurements during the campaign VOLCAN: fuels, T3, combustion mode and engine degradation. This subsection analyzes if far field data acquired for a comparable engine during the ECO-Demonstrator campaign confirms established dependencies. The focus is on fuel type only, since data availability does not allow for an investigation with regard to other parameters at this point. Section 3.4 outlines the setup of the ECO-Demonstrator campaign.

Disclaimer: Provided results are preliminary. To avoid wrong conclusions in comparison with VOLCAN data, a not specified reference value is applied for normalization.

Determined emission indices for Jet A-1 and HEFA SPK do not indicate significant differences in nitrogen oxide emissions. Figure 4.17 illustrates determined preliminary emission indices for both fuels and their respective means. As specified in Table 4.20, the means deviate by 0.61 g NO_2 kg^{-1}. This difference is comparable with values obtained for VOLCAN near field measurements, presented in Subsection 4.1.1. Considering provided standard deviations, it can be inferred that emission indices of both fuels agree. This interpretation of the data is supported by reported p-values for performed statistical tests, clearly exceeding the chosen significance level of 0.05 and hence, not indicating significant differences between the sample groups. Thus, as for discussed near field measurements, it can be concluded that within accuracy and precision of the applied methods, no statistically significant differences between nitrogen oxide emissions of the tested fuels can be inferred.
Absolute nitrogen oxide emission indices based on measurements agree with predictions. An analysis is performed by GE Aerospace, comparing not normalized values of the here presented data with values derived by a not disclosed, internal prediction method. For the investigated flight configuration, experimental and predicted emissions are in line.

Table 4.20: Comparison between Jet A-1 and HEFA SPK in pilot+main combustion mode during a dedicated ECO-Demonstrator far field flight (10/26/2023), including the number of samples n, normalized mean emission indices $\overline{\Delta EI(NO_x)}$, absolute standard deviations of the sample groups s, the absolute difference between normalized mean emission indices of the sample groups Δ, the p-value resulting from the T-test p_t and the p-value resulting from the Mann-Whitney U rank test p_{MW}. Note that a different reference value is applied for emission index normalization than for VOLCAN results.

Fuel	n / -	$\overline{\Delta EI(NO_x)}$ / g NO_2 kg^{-1}	s / g NO_2 kg^{-1}	Δ / g NO_2 kg^{-1}	p_T / -	p_{MW} / -
Jet A-1	15	0.32	1.98	0.61	0.331	0.651
HEFA SPK	8	-0.29	0.94			

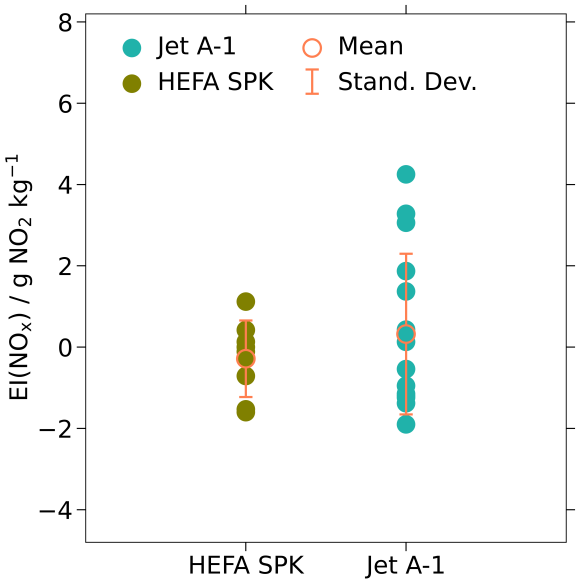

Figure 4.17: Normalized nitrogen oxide emission indices $\Delta EI(NO_x)$ for Jet A-1 and HEFA SPK in pilot+main combustion mode during a dedicated ECO-Demonstrator far field flight (10/26/2023), including the mean emission index $\overline{\Delta EI(NO_x)}$ and the standard deviation s for each fuel. Note that a different reference value is applied for emission index normalization than for VOLCAN results.

Comparing obtained standard deviations of the analyzed VOLCAN and ECO-Demonstrator far field flights indicates differences in scattering. Taking a closer look at determined standard deviations shows that for ECO-Demonstrator measurements less spread in NO_x emission indices is present. The reason is a more stable CO_2 background with more distinguished concentration enhancements during plume encounters. The significance of this parameter during far field flights can be inferred from Figure 4.16 (b), providing its contribution to estimated uncertainties during VOLCAN. For ECO-Demonstrator, uncertainty terms are not quantified at this point. It must be noted that for both campaigns only one selected far field flight is investigated. During other flights this might not be true, as background stability depends on meteorological parameters.

The following answer to the second subquestion is formulated based on the presented results:

> **For investigated dependencies between nitrogen oxide emissions and fuel type, VOLCAN near field measurements agree with ECO-Demonstrator far field results.**

5 Conclusions

In this work, dependencies between engine parameters and nitrogen oxide emissions are investigated to simplify design choices for future, climate-friendly propulsion concepts. For the first time, in situ near field measurements are performed for different settings of a CFM LEAP-1A engine at cruise conditions, using DLR's research aircraft Falcon. Nitrogen oxide emission indices are determined and correlations regarding fuel type, combustor inlet temperature, combustion mode and engine degradation are analyzed. Well-established far field measurements are conducted for comparison.

5.1. Answers to Research Questions

Two research questions are defined with their respective subquestions and the following answers are derived:

1. Do in situ near field measurements confirm expected dependencies between engine parameters and NO_x emissions?

1.1 Does a change from Jet A-1 to Sustainable Aviation Fuel affect NO_x emissions?

→ In situ measurements performed within the framework of this thesis do not reveal distinct differences in nitrogen oxide emissions comparing different SAF blends with Jet A-1. Minor deviations below the measurement accuracy cannot be excluded.

1.2 Do measured NO_x emissions increase exponentially with combustor inlet temperature?

→ Data collected during this work clearly shows that in a forced rich burn mode measured nitrogen oxide emissions increase exponentially with combustor inlet temperature, as expected based on literature.

1.3 Does lean combustion reduce NO_x emissions?

→ This subquestion cannot be fully answered based on available data. Due to the measurement strategy, which involves sampling of emissions with engine settings outside the operation envelope of the LEAP-1A installed on an Airbus A321neo, the results cannot confirm that lean combustion reduces nitrogen oxide emissions.

1.4 Does engine degradation affect NO_x emissions?

→ Based on performed measurements it is likely that engine degradation affects nitrogen oxide emissions, noting that available engine status information is limited.

⇒ In situ measurements confirm expected NO_x emission dependencies regarding fuel type, combustor inlet temperature setting and engine degradation. The results indicate that the sampling strategy must be adapted to study the effect of lean combustion.

2. Do near field measurements agree with observations in the far field?

2.1 Do emission indices derived from near and far field measurements during the VOLCAN campaign agree?

→ The comparison between absolute nitrogen oxide emissions of near and far field measurements during VOLCAN shows very good agreement. The near field setup leads to significantly lower uncertainties.

2.2 Are NO_x dependencies observed during VOLCAN confirmed by far field emission measurements during the ECO-Demonstrator campaign?

→ ECO-Demonstrator far field results confirm that similar to VOLCAN near field measurements, no dependency between nitrogen oxide emissions and fuel type can be inferred.

⇒ This work shows that results from near field measurements agree very well with observations in the far field. The near field setup allows for a significant reduction in measurement uncertainties due to higher concentration enhancements.

Reported results provide relevant insights in nitrogen oxide dependencies. It can be concluded from conducted in-flight measurements that introducing SAFs is not compromised by nitrogen oxide emissions, since no distinct differences are observed compared to Jet A-1. For the first time, the exponential relationship between combustor inlet temperature and the formation of nitrogen oxides is confirmed based on in-flight measurements, underlining the significance of the thermal NO formation mechanism to the design of low emission combustors. An attempt is made to confirm the reduction in nitrogen oxides through fuel staging. Analysis reveals that the applied sampling strategy is not suitable and must be improved. Comparing emissions of two different but technically identical engines indicates that aging processes must be considered to improve inventories. The presented study adds significant data to extremely rare in-flight nitrogen oxide emission measurements and is besides one additional publication in preparation the only work reporting near field nitrogen oxide emission data.
A comparison to well-established far field measurements shows that the applied near field setup is suitable to reduce uncertainties when quantifying nitrogen oxide emissions. Showing very good agreement in terms of absolute values, less scattering and reduced mean uncertainties by more than 78% are observed in the near field. Hence, it is the preferred method to be applied for future nitrogen oxide emission measurements. Preliminary ECO-Demonstrator far field data shows a very similar outcome comparing emissions while burning Jet A-1 and HEFA SPK. Thus, results of two distinguished campaigns agree that based on in situ measurements, no difference in nitrogen oxide emissions can be inferred due to a change in fuel type.

5.2. Recommendations

Several recommendations are derived based on the presented research. Increased accuracy is required to quantify minor differences in nitrogen oxide emissions between certain engine settings. Results show that even if uncertainties are reduced through measuring in the near field, possible differences in emitted nitrogen oxides between the fuels are below measurement accuracy. For future studies, nitrogen oxide and carbon dioxide measurement instruments optimized for high concentrations in near field plumes are suggested. Currently, the same instrumentation is applied for far and near field measurements, requiring coverage of an extensive emission range. In addition, an increase in measurement time and number of

plume encounters would allow for better statistics and hence, facilitate the detection of minor differences.
An improved sampling strategy is suggested to investigate the effect of fuel staging on nitrogen oxide emissions. It is shown that a forced pilot-only mode designed for a different testing purpose is not suitable to assess whether emissions are reduced through lean combustion. It is recommended to perform measurements at power settings along the engine's conventional operation envelope. With test points just before and just beyond staging, it can be quantified if there is a difference between pilot-only and pilot+main injection. Parallel carbon monoxide measurements are of interest, as a possible reduction in their oxidation due to lean premixed combustion can result in increased emissions.
Further experimental work is recommended to increase insight in nitrogen oxide emission variability among technically identical engines. Provided data indicates differences in emissions for engines deviating in their exhaust gas temperature margin. To establish a correlation, the number of investigated engines at different degradation states must be increased. Detailed engine component analysis along with measurements can provide useful insights.
It is important to expand available in-flight emission data. Due to the high complexity of in situ measurements at cruise conditions and required capabilities, there is a lack of statistics. It is suggested to conduct further measurements covering as many engine types as possible. As for a thorough analysis of data collected during the ECO-Demonstrator campaign, it is expected that additional measurements increase certainty in aviation's climate impact.

References

Airlines for America. (2023). Data and statistics: World airlines traffic and capacity. https://www.airlines.org/dataset/world-airlines-traffic-and-capacity/

Apostolidis, A., and Stamoulis, K. P. (2021). A health monitoring modelling case study: Humidity effects on engine deterioration prediction. https://doi.org/10.1051/matecconf/202134903011

Aygun, H., and Turan, O. (2023). Analysis of cruise conditions on energy, exergy and NOx emission parameters of a turbofan engine for middle-range aircraft. *Energy*, *267*, 126468. https://doi.org/10.1016/j.energy.2022.126468

Ballal, D. R., and Zelina, J. (2004). Progress in aeroengine technology (1939–2003). *Journal of Aircraft*, *41*(1), 43–50. https://doi.org/10.2514/1.562

Berntsen, T. K., Fuglestvedt, J. S., Joshi, M. M., Shine, K. P., Stuber, N., Ponater, M., Sausen, R., Hauglustaine, D. A., and Li, L. (2005). Response of climate to regional emissions of ozone precursors: Sensitivities and warming potentials. *Tellus B: Chemical and Physical Meteorology*, *57*(4), 283. https://doi.org/10.3402/tellusb.v57i4.16549

Blakey, S., Rye, L., and Wilson, C. W. (2011). Aviation gas turbine alternative fuels: A review. *Proceedings of the Combustion Institute*, *33*(2), 2863–2885. https://doi.org/10.1016/j.proci.2010.09.011

Boeing ecoDemonstrator Science and Engineering Team. (in preparation). 2021 Boeing ecoDemonstrator Emissions Ground Test Dataset. https://doi.org/https://doi.org/10.57700/1f7s-tn05

Bollinger, M. J., Sievers, R. E., Fahey, D. W., and Fehsenfeld, F. C. (1983). Conversion of nitrogen dioxide, nitric acid, and n-propyl nitrate to nitric oxide by a gold-catalyzed reduction with carbon monoxide. *Analytical Chemistry*, *55*(12), 1980–1986. https://doi.org/10.1021/ac00262a034

Bozzelli, J. W., and Dean, A. M. (1995). O + NNH: A possible new route for NOx formation in flames. *International Journal of Chemical Kinetics*, *27*(11), 1097–1109. https://doi.org/10.1002/kin.550271107

Cartwright, K. (2017). Simpson's rule cumulative integration with ms excel and irregularly-spaced data. *Journal of Mathematical Science and Mathematics Education*, (12).

Çengel, Y. A., and Boles, M. A. (1989). Thermodynamics: An engineering approach [635–676]. McGraw-Hill.

Correa, S. M. (1993). A review of NOx formation under gas-turbine combustion conditions. *Combustion Science and Technology*, *87*(1-6), 329–362. https://doi.org/10.1080/00102209208947221

Correa, S. M. (1998). Power generation and aeropropulsion gas turbines: From combustion science to combustion technology. *Symposium (International) on Combustion*, *27*(2), 1793–1807. https://doi.org/10.1016/S0082-0784(98)80021-0

Dahlmann, K. (2012). *Eine Methode zur effizienten Bewertung von Maßnahmen zur Klimaoptimierung des Luftverkehrs* [Doctoral dissertation, Ludwig Maximilian University of Munich]. https://elib.dlr.de/76433/

Deidewig, F., Doepelheuer, A., and Lecht, M. (1996). Methods to assess aircraft engine emissions in flight. In *20th congress of the int. council of the aeronautical sciences 1996 (icas), 8-13 sept. 1996, sorrent, italien* (pp. 131–141). https://elib.dlr.de/38317/

Drummond, J. W., Volz, A., and Ehhalt, D. H. (1985). An optimized chemiluminescence detector for tropospheric NO measurements. *Journal of Atmospheric Chemistry*, *2*(3), 287–306. https://doi.org/10.1007/BF00051078

Eco Physics. (2000). *Cld 780 tr: Manual* [Not available online]. Technical manual. Eco Physics.

Feigl, C. (1998). *Aufbau und Charakterisierung eines Messsystems für NO, NO2 und NOy: Laboruntersuchungen und Einsatz in der unteren arktischen Stratosphäre* [Doctoral dissertation, Ludwig Maximilian University of Munich]. https://elib.dlr.de/8952/

Feitelberg, A. S., and Correa, S. M. (1999). The role of carbon monoxide in NO2 plume formation. *Volume 2: Coal, Biomass and Alternative Fuels; Combustion and Fuels; Oil and Gas Applications; Cycle Innovations*. https://doi.org/10.1115/99-GT-053

Fenimore, C. P. (1971). Formation of nitric oxide in premixed hydrocarbon flames. *Symposium (International) on Combustion*, *13*(1), 373–380. https://doi.org/10.1016/S0082-0784(71)80040-1

Fishman, J., and Crutzen, P. J. (1978). The origin of ozone in the troposphere. *Nature*, *274*(5674), 855–858. https://doi.org/10.1038/274855a0

Fishman, J., Solomon, S., and Crutzen, P. J. (1979). Observational and theoretical evidence in support of a significant in-situ photochemical source of tropospheric ozone. *Tellus A: Dynamic Meteorology and Oceanography*, *31*(5), 432. https://doi.org/10.3402/tellusa.v31i5.10458

Forster, P., Ramaswamy, V., Artaxo, P., Bernsten, T., Betts, R., Fahey, D., Haywood, J., Lean, J., Lowe, D., Myhre, G., Nganga, R., Prinn, R., Raga, G., Schulz, M., and van Dorland, R. (2007). Changes in atmospheric constituents and in radiative forcing. In Intergovernmental Panel on Climate Change (Ed.), *Climate change 2007*. Cambridge University Press.

Forster, P., Storelvmo, T., Armour, K., Collins, W., Dufresne, J.-L., Frame, D., Lunt, D. J., Mauritsen, T., Palmer, M. D., Watanabe, M., Wild, M., and Zhang, H. (2023). The earth's energy budget, climate feedbacks and climate sensitivity. In Intergovernmental Panel on Climate Change (Ed.), *Climate change 2021 – the physical science basis* (pp. 923–1054). Cambridge University Press. https://doi.org/10.1017/9781009157896.009

Foust, M., Thomsen, D., Stickles, R., Cooper, C., and Dodds, W. (2012). Development of the ge aviation low emissions taps combustor for next generation aircraft engines. *50th AIAA Aerospace Sciences Meeting including the New Horizons Forum and Aerospace Exposition*. https://doi.org/10.2514/6.2012-936

Frömming, C., Ponater, M., Dahlmann, K., Grewe, V., Lee, D. S., and Sausen, R. (2012). Aviation-induced radiative forcing and surface temperature change in dependency of the emission altitude. *Journal of Geophysical Research: Atmospheres*, *117*(D19), n/a–n/a. https://doi.org/10.1029/2012JD018204

Fuglestvedt, J. (1999). Climatic forcing of nitrogen oxides through changes in tropospheric ozone and methane; global 3d model studies. *Atmospheric Environment*, *33*(6), 961–977. https://doi.org/10.1016/S1352-2310(98)00217-9

Fujiwara, H., Nakaya, S., Tsue, M., and Okai, K. (2020). Emissions from hefa fuelled gas turbine combustors. In A. K. Gupta, A. De, S. K. Aggarwal, A. Kushari and A. Runchal (Eds.), *Innovations in sustainable energy and cleaner environment* (pp. 357–385). Springer Singapore. https://doi.org/10.1007/978-981-13-9012-8{\textunderscore}16

Glaude, P.-A., Sirjean, B., Fournet, R., Bounaceur, R., Vierling, M., Montagne, P., and Molière, M. (2014). Combustion and oxidation kinetics of alternative gas turbines fuels. *Volume 3A: Coal, Biomass and Alternative Fuels; Cycle Innovations; Electric Power; Industrial and Cogeneration*. https://doi.org/10.1115/GT2014-25070

Gleason, C. C., and Martone, J. A. (1980). Fuel character effects on j79 and f101 engine combustor emissions. *Journal of Energy*, *4*(5), 223–226. https://doi.org/10.2514/3.62477

Gokulakrishnan, P., and Klassen, M. S. (2013). NOx and CO formation and control. In T. C. Lieuwen and V. Yang (Eds.), *Gas turbine emissions* (pp. 175–208). Cambridge University Press. https://doi.org/10.1017/CBO9781139015462.011

Grewe, V., and Stenke, A. (2008). Airclim: An efficient tool for climate evaluation of aircraft technology. *Atmospheric Chemistry and Physics*, *8*(16), 4621–4639. https://doi.org/10.5194/acp-8-4621-2008

Grewe, V. (2009). Impact of lightning on air chemistry and climate. In H.-D. Betz (Ed.), *Lightning: Principles, instruments and applications* (pp. 537–549). Springer.

Grewe, V., and Dahlmann, K. (2015). How ambiguous are climate metrics? And are we prepared to assess and compare the climate impact of new air traffic technologies? *Atmospheric Environment*, *106*, 373–374. https://doi.org/10.1016/j.atmosenv.2015.02.039

Grewe, V., Dameris, M., Fichter, C., and Lee, D. S. (2002). Impact of aircraft NOx emissions. part 2: Effects of lowering the flight altitude. *Meteorologische Zeitschrift*, *11*(3), 197–205. https://doi.org/10.1127/0941-2948/2002/0011-0197

Grewe, V., Dameris, M., Hein, R., Köhler, I., and Sausen, R. (1999). Impact of future subsonic aircraft NOx emissions on the atmospheric composition. *Geophysical Research Letters*, *26*(1), 47–50. https://doi.org/10.1029/1998GL900249

Grooß, J.-u., Brühl, C., and Peter, T. (1998). Impact of aircraft emissions on tropospheric and stratospheric ozone. part i. *Atmospheric Environment*, *32*(18), 3173–3184. https://doi.org/10.1016/S1352-2310(98)00016-8

Harlass, T., Dischl, R., Kaufmann, S., Märkl, R., Sauer, D., Scheibe, M., Stock, P., Bräuer, T., Dörnbrack, A., Roiger, A., Schlager, H., Schumann, U., Schripp, T., Grein, T., Bondorf, L., Renard, C., Gauthier, M., Johnson, M., Luff, D., … And Voigt, C. (in preparation). In-flight measurements of nitrogen oxide emissions from latest generation jet engines and 100% sustainable aviation fuel.

He, Z. J., Chang, C., and Follen, C. (2015). NOx emissions performance and correlation equations for a multipoint ldi injector. *53rd AIAA Aerospace Sciences Meeting*. https://doi.org/10.2514/6.2015-0098

Holmes, C. D., Tang, Q., and Prather, M. J. (2011). Uncertainties in climate assessment for the case of aviation NO. *Proceedings of the National Academy of Sciences of the United States of America*, *108*(27), 10997–11002. https://doi.org/10.1073/pnas.1101458108

Isaksen, I. S. A., and HOV, Ø. (1987). Calculation of trends in the tropospheric concentration of O3 , OH, CO, CH4 and NOx. *Tellus B: Chemical and Physical Meteorology*, *39B*(3), 271–285. https://doi.org/10.1111/j.1600-0889.1987.tb00099.x

Jurkat, T., Voigt, C., Arnold, F., Schlager, H., Kleffmann, J., Aufmhoff, H., Schäuble, D., Schaefer, M., and Schumann, U. (2011). Measurements of HONO, NO, NOy and SO2 in aircraft exhaust plumes at cruise. *Geophysical Research Letters*, *38*(10), n/a–n/a. https://doi.org/10.1029/2011GL046884

Khandelwal, B., Cronly, J., Ahmed, I. S., Wijesinghe, C. J., and Lewis, C. (2019). The effect of alternative fuels on gaseous and particulate matter (pm) emission performance in an auxiliary power unit (APU). *The Aeronautical Journal*, *123*(1263), 617–634. https://doi.org/10.1017/aer.2019.16

Köhler, I. (1997). *Auswirkungen der Flugzeugemissionen auf den atmosphärischen NOx-Gehalt* [Doctoral dissertation, Ludwig Maximilian University of Munich]. https://elib.dlr.de/32381/

Köhler, M. O., Rädel, G., Shine, K. P., Rogers, H. L., and Pyle, J. A. (2013). Latitudinal variation of the effect of aviation nox emissions on atmospheric ozone and methane and related climate metrics. *Atmospheric Environment*, *64*, 1–9. https://doi.org/10.1016/j.atmosenv.2012.09.013

Lee, D. S., Fahey, D. W., Skowron, A., Allen, M. R., Burkhardt, U., Chen, Q., Doherty, S. J., Freeman, S., Forster, P. M., Fuglestvedt, J., Gettelman, A., de León, R. R., Lim, L. L., Lund, M. T., Millar, R. J., Owen, B., Penner, J. E., Pitari, G., Prather, M. J., ... And Wilcox, L. J. (2021). The contribution of global aviation to anthropogenic climate forcing for 2000 to 2018. *Atmospheric Environment*, *244*, 117834. https://doi.org/10.1016/j.atmosenv.2020.117834

Lee, D. S., Pitari, G., Grewe, V., Gierens, K., Penner, J. E., Petzold, A., Prather, M. J., Schumann, U., Bais, A., Berntsen, T., Iachetti, D., Lim, L. L., and Sausen, R. (2010). Transport impacts on atmosphere and climate: Aviation. *Atmospheric Environment*, *44*(37), 4678–4734. https://doi.org/10.1016/j.atmosenv.2009.06.005

Lee, D. S., Fahey, D. W., Forster, P. M., Newton, P. J., Wit, R. C. N., Lim, L. L., Owen, B., and Sausen, R. (2009). Aviation and global climate change in the 21st century. *Atmospheric Environment*, *43*(22), 3520–3537. https://doi.org/10.1016/j.atmosenv.2009.04.024

Lefebvre, A. H., and Ballal, D. R. (2010). Gas turbine combustion: Alternative fuels and emissions [359–441]. CRC Press.

Leonard, G., and Stegmaier, J. (1994). Development of an aeroderivative gas turbine dry low emissions combustion system. *Journal of Engineering for Gas Turbines and Power*, *116*(3), 542–546. https://doi.org/10.1115/1.2906853

Leonard, G., and Stegmaier, J. (1993). Development of an aeroderivative gas turbine dry low emissions combustion system. *Volume 3B: General*. https://doi.org/10.1115/93-GT-288

LI-COR. (2007). *Li-7000 CO2/H2O analyzer instruction manual* [Not available online]. Technical manual. LI-COR.

Lipfert, F. W. (1972). Correlation of gas turbine emissions data. *ASME 1972 International Gas Turbine and Fluids Engineering Conference and Products Show*. https://doi.org/10.1115/72-GT-60

Liu, Y., Sun, X., Sethi, V., Nalianda, D., Li, Y.-G., and Wang, L. (2017). Review of modern low emissions combustion technologies for aero gas turbine engines. *Progress in Aerospace Sciences*, *94*, 12–45. https://doi.org/10.1016/j.paerosci.2017.08.001

Lobo, P., Rye, L., Williams, P. I., Christie, S., Uryga-Bugajska, I., Wilson, C. W., Hagen, D. E., Whitefield, P. D., Blakey, S., Coe, H., Raper, D., and Pourkashanian, M. (2012). Impact of alternative fuels on emissions characteristics of a gas turbine engine - part 1: Gaseous and particulate matter emissions. *Environmental science & technology*, *46*(19), 10805–10811. https://doi.org/10.1021/es301898u

Lukachko, S. P., and Waitz, I. A. (1997). Effects of engine aging on aircraft NOx emissions. *Volume 1: Aircraft Engine; Marine; Turbomachinery; Microturbines and Small Turbomachinery*. https://doi.org/10.1115/97-GT-386

Malte, P. C., and Pratt, D. T. (1975). Measurement of atomic oxygen and nitrogen oxides in jet-stirred combustion. *Symposium (International) on Combustion*, *15*(1), 1061–1070. https://doi.org/10.1016/S0082-0784(75)80371-7

Mann, H. B., and Whitney, D. R. (1947). On a test of whether one of two random variables is stochastically larger than the other. *The Annals of Mathematical Statistics*, *18*(1), 50–60. https://doi.org/10.1214/aoms/1177730491

Maughan, J. R., Luts, A., and Bautista, P. J. (1994). A Dry Low NOx Combustor for the MS3002 Regenerative Gas Turbine. *Volume 3: Coal, Biomass and Alternative Fuels; Combustion and Fuels; Oil and Gas Applications; Cycle Innovations*. https://doi.org/10.1115/94-GT-252

Moore, R. H. (in preparation). Sustainable aviation fuel effects on engine particle and trace gas emissions measured behind the 2021 Boeing ecoDemonstrator.

Moore, R. H., Thornhill, K. L., Weinzierl, B., Sauer, D., D'Ascoli, E., Kim, J., Lichtenstern, M., Scheibe, M., Beaton, B., Beyersdorf, A. J., Barrick, J., Bulzan, D., Corr, C. A., Crosbie, E., Jurkat, T., Martin, R., Riddick, D., Shook, M., Slover, G., . . . And Anderson, B. E. (2017). Biofuel blending reduces particle emissions from aircraft engines at cruise conditions. *Nature*, *543*(7645), 411–415. https://doi.org/10.1038/nature21420

Nicolet, M. (1964). Reactions and photochemistry of atoms and molecules. introduction to chemical aeronomy. *Discussions of the Faraday Society*, *37*, 7. https://doi.org/10.1039/df9643700007

Penner, J. E. (Ed.). (1999). *Aviation and the global atmosphere: A special report of ipcc working groups i and iii in collab. with the scientific assessment panel to the montreal protocol on substances that deplete the ozone layer* (1. publ) [ISBN: 978-0-521-66300-7]. Cambridge University Press.

Pitari, G., Cionni, I., Di Genova, G., Søvde, O. A., and Lim, L. (2017). Radiative forcing from aircraft emissions of NOx: Model calculations with ch4 surface flux boundary condition. *Meteorologische Zeitschrift*, *26*(6), 663–687. https://doi.org/10.1127/metz/2016/0776

Prinn, R. G., Weiss, R. F., Miller, B. R., Huang, J., Alyea, F. N., Cunnold, D. M., Fraser, P. J., Hartley, D. E., and Simmonds, P. G. (1995). Atmospheric trends and lifetime of CH3CCI3 and global OH concentrations. *Science (New York, N.Y.)*, *269*(5221), 187–192. https://doi.org/10.1126/science.269.5221.187

Saluja, H. S. (2021). *Sensitivity study of engine design parameters to climate impact* [Master's thesis, Delft University of Technology]. http://resolver.tudelft.nl/uuid:32f7c2a2-607d-408d-beb3-70d16366712d

Saravanamuttoo, H. I. H., Rogers, G. F. C., Cohen, H., Straznicky, P., and Nix, A. (2017). Gas Turbine Theory [299-310]. Pearson.

Schlager, H., Konopka, P., Schulte, P., Schumann, U., Ziereis, H., Arnold, F., Klemm, M., Hagen, D. E., Whitefield, P. D., and Ovarlez, J. (1997). In situ observations of air traffic emission signatures in the north atlantic flight corridor. *Journal of Geophysical Research: Atmospheres*, *102*(D9), 10739–10750. https://doi.org/10.1029/96JD03748

Schulte, P., and Schlager, H. (1996). In-flight measurements of cruise altitude nitric oxide emission indices of commercial jet aircraft. *Geophysical Research Letters*, *23*(2), 165–168. https://doi.org/10.1029/95GL03691

Schulte, P., Schlager, H., Ziereis, H., Schumann, U., Baughcum, S. L., and Deidewig, F. (1997). NOx emission indices of subsonic long-range jet aircraft at cruise altitude: In situ measurements and predictions. *Journal of Geophysical Research: Atmospheres*, *102*(D17), 21431–21442. https://doi.org/10.1029/97JD01526

Schumann, U. (1997). The impact of nitrogen oxides emissions from aircraft upon the atmosphere at flight altitudes—results from the aeronox project. *Atmospheric Environment*, *31*(12), 1723–1733. https://doi.org/10.1016/S1352-2310(96)00326-3

Shahabuddin, M., Alam, M. T., Krishna, B. B., Bhaskar, T., and Perkins, G. (2020). A review on the production of renewable aviation fuels from the gasification of biomass and residual wastes. *Bioresource technology*, *312*, 123596. https://doi.org/10.1016/j.biortech.2020.123596

Stevenson, D. S. (2004). Radiative forcing from aircraft NOx emissions: Mechanisms and seasonal dependence. *Journal of Geophysical Research: Atmospheres*, *109*(D17). https://doi.org/10.1029/2004JD004759

Stevenson, D. S., and Derwent, R. G. (2009). Does the location of aircraft nitrogen oxide emissions affect their climate impact? *Geophysical Research Letters*, *36*(17). https://doi.org/10.1029/2009GL039422

Stickles, R., and Barrett, J. (2013). *TAPS II Combustor Final Report* (tech. rep.) (Not available online). FAA.

Stocker, T., Qin, D., Plattner, G.-K., Alexander, L., Allen, S., Bindoff, N., Bréon, F.-M., Church, J., Cubasch, U., Emori, S., Forster, P., Friedlingstein, P., Gillett, N., Gregory, J., Hartmann, D., Jansen, E., Kirtman, B., Knutti, R., Krishna Kumar, K., ... And Xie, S.-P. (2014). Technical summary. In Intergovernmental Panel on Climate Change (Ed.), *Climate change 2013 - the physical basis* (pp. 31–116). WMO IPCC. https://doi.org/10.1017/CBO9781107415324.005

Stratmann, G. (2013). *Stickoxidmessungen in der Tropopausenregion an Bord eines Linienflugzeugs: Großräumige Verteilung und Einfluss des Luftverkehrs* [Doctoral dissertation, Technical University of Munich]. https://elib.dlr.de/89732/

Teoh, R., Schumann, U., Voigt, C., Schripp, T., Shapiro, M., Engberg, Z., Molloy, J., Koudis, G., and Stettler, M. E. J. (2022). Targeted use of sustainable aviation fuel to maximize climate

benefits. *Environmental science & technology*, *56*(23), 17246–17255. https://doi.org/10.1021/acs.est.2c05781

Undavalli, V., Gbadamosi Olatunde, O. B., Boylu, R., Wei, C., Haeker, J., Hamilton, J., and Khandelwal, B. (2023). Recent advancements in sustainable aviation fuels. *Progress in Aerospace Sciences*, *136*, 100876. https://doi.org/10.1016/j.paerosci.2022.100876

Warnatz, J. (2001). *Combustion: Physical and chemical fundamentals, modeling and simulation, experiments, pollutant formation* (3rd Edition). Springer. https://doi.org/10.1007/978-3-662-04508-4

Welch, B. L. (1938). The significance of the difference between two means when the population variances are unequal. *Biometrika*, *29*(3-4), 350–362. https://doi.org/10.1093/biomet/29.3-4.350

Wilcoxon, F. (1992). Individual comparisons by ranking methods. In S. Kotz and N. L. Johnson (Eds.), *Breakthroughs in statistics* (pp. 196–202). Springer New York. https://doi.org/10.1007/978-1-4612-4380-9{\textunderscore}16

Wolfrum, J. (1972). Bildung von Stickstoffoxiden bei der Verbrennung. *Chemie Ingenieur Technik - CIT*, *44*(10), 656–659. https://doi.org/10.1002/cite.330441004

Wuebbles, D., Gupta, M., and Ko, M. (2007). Evaluating the impacts of aviation on climate change. *Eos, Transactions American Geophysical Union*, *88*(14), 157. https://doi.org/10.1029/2007EO140001

Zeldovich, Y. B. (1992). The oxidation of nitrogen in combustion and explosions. In E. Jackson, G. I. Barenblatt, J. P. Ostriker, R. A. Siuniaev and I. A. B. Zeldovich (Eds.), *Chemical physics and hydrodynamics* (pp. 364–403). Princeton University Press. https://doi.org/10.1515/9781400862979.364

Ziereis, H., Stock, P., and Schlager, H. (2012). Measurements of nitrogen oxides and related trace gases. In U. Schumann (Ed.), *Atmospheric physics* (pp. 261–276). Springer.

A

Fuel Type versus Nitrogen Oxide Emissions: Additional Analyses

Jet A-1 and HEFA SPK Blends

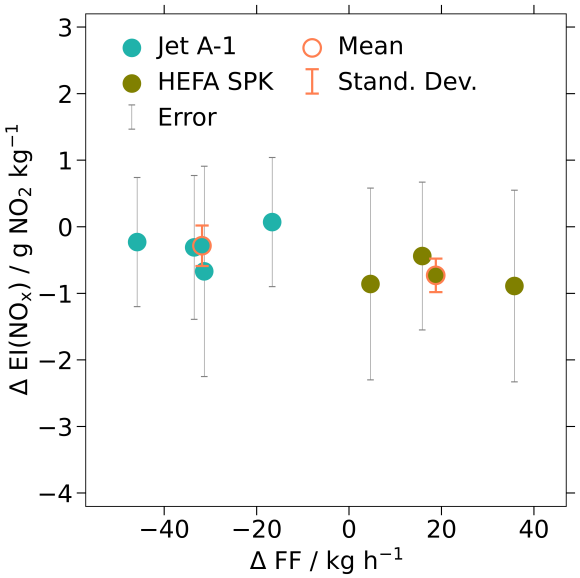

Figure A.1: Normalized nitrogen oxide emission indices $\Delta EI(\mathrm{NO_x})$ for Jet A-1 and HEFA SPK blends at mid T3 setting in forced pilot-only combustion mode during Flight 1 (02/28/2023), including individual measurement errors $Error$, as well as the mean emission index $\overline{\Delta EI(\mathrm{NO_x})}$ and the standard deviation s for each fuel.

Table A.1: Comparison between Jet A-1 and HEFA SPK blends at mid T3 setting in forced pilot-only combustion mode during Flight 1 (02/28/2023), including the number of samples n, normalized mean emission indices $\overline{\Delta EI(\mathrm{NO_x})}$, absolute mean emission index errors $\overline{Error}$, absolute standard deviations of the sample groups s, the absolute difference between normalized mean emission indices of the sample groups Δ, the p-value resulting from the T-test p_t and the p-value resulting from the Mann-Whitney U rank test p_{MW}.

Fuel	n / -	$\overline{\Delta\mathrm{EI}(\mathrm{NO_x})}$ / g $\mathrm{NO_2}$ $\mathrm{kg^{-1}}$	$\overline{\mathrm{Error}}$ / g $\mathrm{NO_2}$ $\mathrm{kg^{-1}}$	s / g $\mathrm{NO_2}$ $\mathrm{kg^{-1}}$	Δ / g $\mathrm{NO_2}$ $\mathrm{kg^{-1}}$	p_T / -	p_{MW} / -
Jet A-1 Dominant	4	-0.29	1.15	0.30	0.45	0.089	0.114
HEFA Dominant	3	-0.73	1.33	0.25			

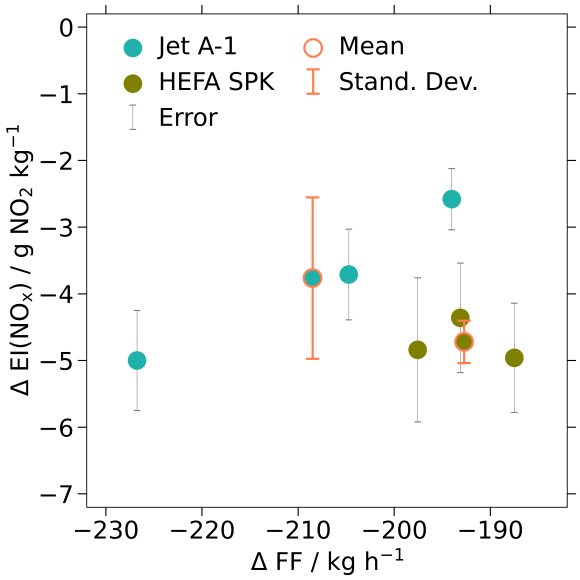

Figure A.2: Normalized nitrogen oxide emission indices $\Delta EI(\mathrm{NO_x})$ for Jet A-1 and HEFA SPK blends at low T3 setting in forced pilot-only combustion mode during Flight 1 (02/28/2023), including individual measurement errors $Error$, as well as the mean emission index $\overline{\Delta EI(\mathrm{NO_x})}$ and the standard deviation s for each fuel.

Table A.2: Comparison between Jet A-1 and HEFA SPK blends at low T3 setting in forced pilot-only combustion mode during Flight 1 (02/28/2023), including the number of samples n, normalized mean emission indices $\overline{\Delta EI(\mathrm{NO_x})}$, absolute mean emission index errors $\overline{Error}$, absolute standard deviations of the sample groups s, the absolute difference between normalized mean emission indices of the sample groups Δ, the p-value resulting from the T-test p_t and the p-value resulting from the Mann-Whitney U rank test p_{MW}.

Fuel	n / -	$\overline{\Delta\mathrm{EI(NO_x)}}$ / g NO_2 kg^{-1}	$\overline{\mathrm{Error}}$ / g NO_2 kg^{-1}	s / g NO_2 kg^{-1}	Δ / g NO_2 kg^{-1}	p_T / -	p_{MW} / -
Jet A-1 Dominant	3	-3.76	0.63	0.99	0.96	0.303	0.700
HEFA Dominant	3	-4.72	0.91	0.26			

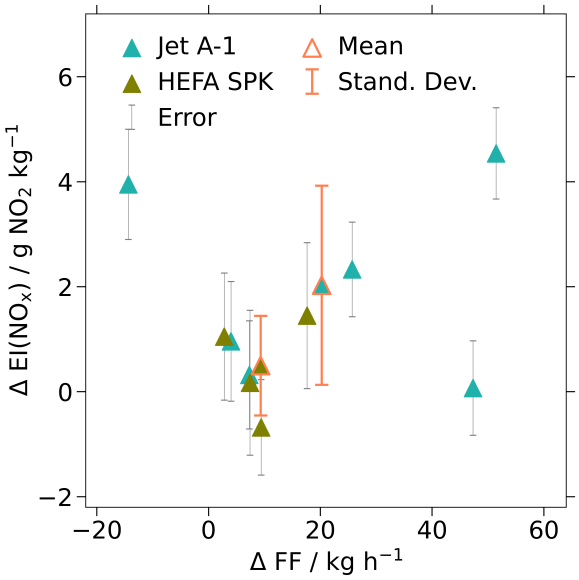

Figure A.3: Normalized nitrogen oxide emission indices $\Delta EI(\mathrm{NO_x})$ for Jet A-1 and HEFA SPK blends at mid T3 setting in pilot+main combustion mode during Flight 1 (02/28/2023), including individual measurement errors $Error$, as well as the mean emission index $\overline{\Delta EI(\mathrm{NO_x})}$ and the standard deviation s for each fuel.

Table A.3: Comparison between Jet A-1 and HEFA SPK blends at mid T3 setting in pilot+main combustion mode during Flight 1 (02/28/2023), including the number of samples n, normalized mean emission indices $\overline{\Delta EI(\mathrm{NO_x})}$, absolute mean emission index errors $\overline{Error}$, absolute standard deviations of the sample groups s, the absolute difference between normalized mean emission indices of the sample groups Δ, the p-value resulting from the T-test p_t and the p-value resulting from the Mann-Whitney U rank test p_{MW}.

Fuel	n / -	$\overline{\Delta EI(NO_x)}$ / g NO_2 kg^{-1}	$\overline{Error}$ / g NO_2 kg^{-1}	s / g NO_2 kg^{-1}	Δ / g NO_2 kg^{-1}	p_T / -	p_{MW} / -
Jet A-1 Dominant	6	2.03	0.98	1.90	1.53	0.132	0.352
HEFA Dominant	4	0.50	1.22	0.95			

HEFA SPK+LA

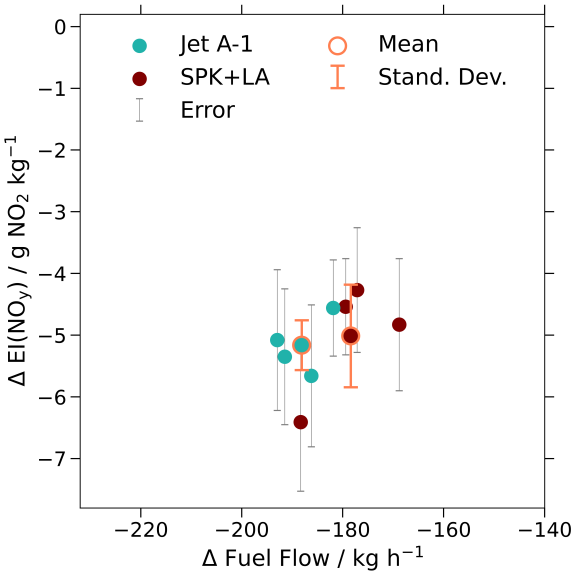

Figure A.4: Normalized nitrogen oxide emission indices $\Delta EI(\mathrm{NO_x})$ for Jet A-1 and HEFA SPK+LA at low T3 setting in forced pilot-only combustion mode during Flight 2 (03/11/2023), including individual measurement errors $Error$, as well as the mean emission index $\overline{\Delta EI(\mathrm{NO_x})}$ and the standard deviation s for each fuel.

Table A.4: Comparison between Jet A-1 and HEFA SPK+LA at mid T3 setting in forced pilot-only combustion mode during Flight 2 (03/11/2023), including the number of samples n, normalized mean emission indices $\overline{\Delta EI(\mathrm{NO_x})}$, absolute mean emission index errors $\overline{Error}$, absolute standard deviations of the sample groups s, the absolute difference between normalized mean emission indices of the sample groups Δ, the p-value resulting from the T-test p_t and the p-value resulting from the Mann-Whitney U rank test p_{MW}.

Fuel	n / -	$\overline{\Delta\mathrm{EI(NO_x)}}$ / g NO_2 kg^{-1}	$\overline{\mathrm{Error}}$ / g NO_2 kg^{-1}	s / g NO_2 kg^{-1}	Δ / g NO_2 kg^{-1}	p_T / -	p_{MW} / -
Jet A-1	4	-5.16	1.04	0.47	0.15	0.791	0.486
HEFA	4	-5.01	1.00	0.96			

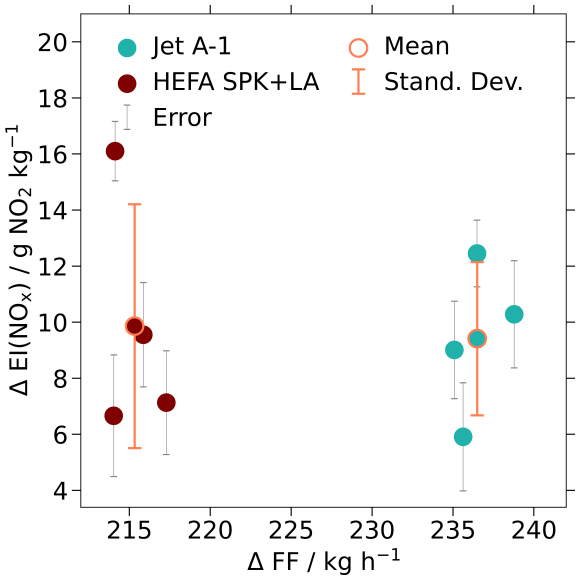

Figure A.5: Normalized nitrogen oxide emission indices $\Delta EI(\mathrm{NO_x})$ for Jet A-1 and HEFA SPK+LA at high T3 setting in forced pilot-only combustion mode during Flight 2 (03/11/2023), including individual measurement errors $Error$, as well as the mean emission index $\overline{\Delta EI(\mathrm{NO_x})}$ and the standard deviation s for each fuel.

Table A.5: Comparison between Jet A-1 and HEFA SPK+LA at high T3 setting in forced pilot-only combustion mode during Flight 2 (03/11/2023), including the number of samples n, normalized mean emission indices $\overline{\Delta EI(\mathrm{NO_x})}$, absolute mean emission index errors $\overline{Error}$, absolute standard deviations of the sample groups s, the absolute difference between normalized mean emission indices of the sample groups Δ, the p-value resulting from the T-test p_t and the p-value resulting from the Mann-Whitney U rank test p_{MW}.

Fuel	n / -	$\overline{\Delta EI(\mathrm{NO_x})}$ / g NO_2 kg^{-1}	$\overline{Error}$ / g NO_2 kg^{-1}	s / g NO_2 kg^{-1}	Δ / g NO_2 kg^{-1}	p_T / -	p_{MW} / -
Jet A-1	4	9.41	1.69	2.73	0.45	0.868	1.000
HEFA	4	9.86	1.74	4.35			

HEFA SPK+HA

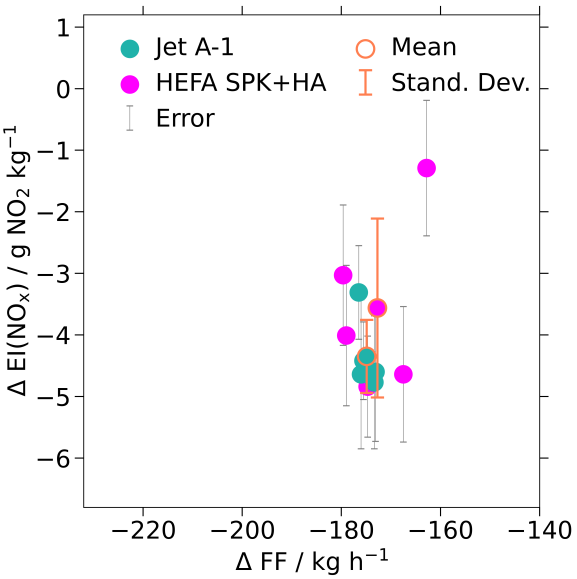

Figure A.6: Normalized nitrogen oxide emission indices $\Delta EI(\mathrm{NO_x})$ for Jet A-1 and HEFA SPK+HA at low T3 setting in forced pilot-only combustion mode during Flight 3 (03/16/2023), including individual measurement errors $Error$, as well as the mean emission index $\overline{\Delta EI(\mathrm{NO_x})}$ and the standard deviation s for each fuel.

Table A.6: Comparison between Jet A-1 and HEFA SPK+LA at low T3 setting in forced pilot-only combustion mode during Flight 3 (03/16/2023), including the number of samples n, normalized mean emission indices $\overline{\Delta EI(\mathrm{NO_x})}$, absolute mean emission index errors $\overline{Error}$, absolute standard deviations of the sample groups s, the absolute difference between normalized mean emission indices of the sample groups Δ, the p-value resulting from the T-test p_t and the p-value resulting from the Mann-Whitney U rank test p_{MW}.

Fuel	n / -	$\overline{\Delta\mathrm{EI(NO_x)}}$ / g NO_2 kg^{-1}	$\overline{\mathrm{Error}}$ / g NO_2 kg^{-1}	s / g NO_2 kg^{-1}	Δ / g NO_2 kg^{-1}	p_T / -	p_{MW} / -
Jet A-1	5	-4.35	0.96	0.59	0.79	0.311	0.600
HEFA	5	-3.56	1.06	1.45			

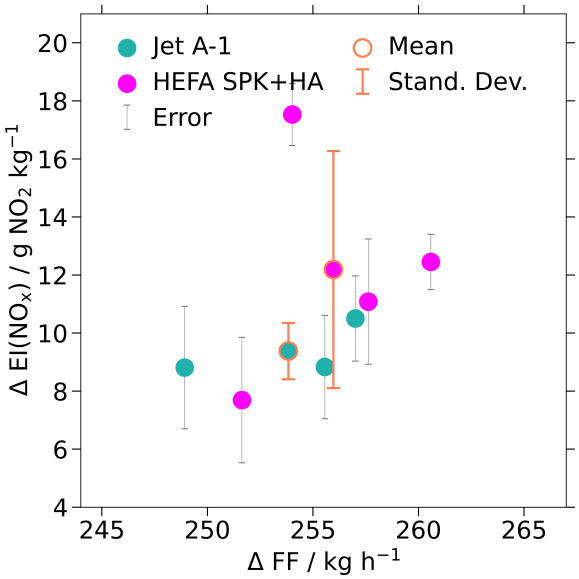

Figure A.7: Normalized nitrogen oxide emission indices $\Delta EI(\mathrm{NO_x})$ for Jet A-1 and HEFA SPK+HA at high T3 setting in forced pilot-only combustion mode during Flight 3 (03/16/2023), including individual measurement errors $Error$, as well as the mean emission index $\overline{\Delta EI(\mathrm{NO_x})}$ and the standard deviation s for each fuel.

Table A.7: Comparison between Jet A-1 and HEFA SPK+HA at high T3 setting in forced pilot-only combustion mode during Flight 3 (03/16/2023), including the number of samples n, normalized mean emission indices $\overline{\Delta EI(\mathrm{NO_x})}$, absolute mean emission index errors $\overline{Error}$, absolute standard deviations of the sample groups s, the absolute difference between normalized mean emission indices of the sample groups Δ, the p-value resulting from the T-test p_t and the p-value resulting from the Mann-Whitney U rank test p_{MW}.

Fuel	n / -	$\overline{\Delta EI(\mathrm{NO_x})}$ / g NO_2 kg^{-1}	$\overline{Error}$ / g NO_2 kg^{-1}	s / g NO_2 kg^{-1}	Δ / g NO_2 kg^{-1}	p_T / -	p_{MW} / -
Jet A-1	3	9.38	1.79	0.97	2.81	0.266	0.400
HEFA	4	12.19	1.56	4.09			